UNIVERSIDADE D
COIMBRA

Pedro José da Silva Carreira

Processing NiTi Shape Memory Alloy Powder by Material Extrusion (MEX)

Tese no âmbito do Doutoramento em Engenharia Mecânica, área de Sistemas Avançados de Produção orientada pela Professora Doutora Maria Teresa Freire Vieira e pelo Professor Doutor Nuno Manuel Fernandes Alves e apresentada ao Departamento de Engenharia Mecânica da Faculdade de Ciências e Tecnologia da Universidade de Coimbra.

Dezembro de 2021

• U C •
FCTUC FACULDADE DE CIÊNCIAS
E TECNOLOGIA
UNIVERSIDADE DE COIMBRA

PROCESSING NiTi SHAPE MEMORY ALLOY POWDER BY MATERIAL EXTRUSION (MEX)

Pedro José da Silva Carreira

A thesis presented for the degree of Doctor in Mechanical Engineering, Advanced Production Systems

Supervisor

Professor Maria Teresa Freire Vieira

Professor Nuno Manuel Fernandes Alves

Department of Mechanical Engineering

Faculty of Science and Technology

University of Coimbra, Portugal

December 2021

1 2 9 0

UNIVERSIDADE D
COIMBRA

To my little star, Petra…

Acknowledgements

My deepest thanks are to:

Professor Teresa Vieira for all the help, knowledge and advice.

Professor Nuno Alves and Professor Artur Mateus, for the friendship, trust and for allowing me to work in something that really inspires me.

To all members of CDRSP, IPL and CEMMPRE who somehow helped me complete this work.

To all my friends.

To my family, especially my parents and my sister who have always been part of my life.

To Cristiana, for all the support, understanding and for helping me give the first step.

And to Petra, for shining every day ...

Many thanks to you all!

Abstract

This research was performed to investigate the direct (powder bed fusion) and predominantly indirect additive manufacturing of NiTi shape memory alloys. During the last decennia, selective laser melting has been the technology of additive manufacturing more studied to improve the quality of NiTi 3Dobjects. Nevertheless, NiTi powder type (elemental or prealloyed) due to process parameters readily undergo chemical and phase modifications, which can induce variations in the properties of the alloy and consequently poor application performance. This research explores the potential usefulness of NiTi and its limitations when processed by one of the most promising indirect additive processes – material extrusion. Whatever the powder selected, different steps must be optimized to avoid secondary phases formation, however in this study, the prealloyed powder used, particularly with other common materials, $NiTi_2$ and Ni, was the primordial selection. The study highlighted the role of $NiTi_2$, which has a melting temperature lower than the temperature of sintering in the liquid phase, in promoting the reaction of $NiTi_2$ with Ni, $NiTi_2$ and NiTi. The reaction mainly contributes to the formation of the brittle phase Ni_3Ti, particularly around the boundaries of NiTi and $NiTi_2$ phases and precipitates inside the primary phase, influencing the final properties of the 3Dobject. These intermetallics are similar to those observed in selective laser melting essentially when using elemental powder. Thus, two main targets should be attained in the sintering step associated with the decrease in sintering temperature. One is to reduce production costs, by evaluating the lowest temperature and dwelling time necessary to produce effective sintering, and the other is to add other material to decrease the presence of intermetallics other than NiTi. The study has shown the role of TiH_2 when mixed with virgin prealloyed NiTi powder. The non-formation of Ni_3Ti is clear for a specific composition. H_2 was always used during debinding and sintering as a reductive atmosphere to avoid contamination and the consequent formation of other secondary phases. Other feedstocks with a balancing addition of Ni revealed the priority in Ni_3Ti formation, highlighting the role of loose Ni in the virgin powder. Another complementary contribution was the evaluation of NiTi critical powder volume content to process high-quality filaments for material extrusion. A typical 3D filament before (green) and after debinding & sintering were used as a homothetic of a 3Dobject, where the strand (layer) is also characterized as green. This methodology allowed the extensive study of all stages depending on the filament, because is known that 3Dobjects defects can be inherit from filament and/or strand. Finally, a case study highlights the combination of additive manufacturing with the unusual behaviour of NiTi shape memory alloy, which can be a solution for demoulding undercuts in the injection moulds industry.

KEYWORDS: Nickel–Titanium; Shape Memory Alloys; Material Extrusion; Direct/Indirect Additive Manufacturing; Metallic Powder Filaments; Shaping, Debinding and Sintering; NiTi prealloyed powder.

Resumo

Este estudo foi realizado para investigar a fabricação aditiva direta (fusão em cama de pó) e predominantemente a fabricação aditiva indireta das ligas de memória de forma NiTi. Durante a última década, a fusão seletiva por laser foi a tecnologia de fabrico aditivo mais estudada na otimização da qualidade de objetos 3D em NiTi. No entanto, seja qual for o tipo de pó de NiTi (elementar ou pré-ligado) devido aos parâmetros do processamento, sofre facilmente modificações químicas e de fase, o que pode causar alterações nas propriedades da liga e consequentemente induzir a um desempenho indesejado durante a aplicação. Esta trabalho de investigação explora a utilidade potencial do NiTi e as suas limitações quando processado por um dos mais promissores processos aditivos indiretos - extrusão de material. Independentemente do pó selecionado, as diferentes etapas do processo devem ser otimizadas para evitar a formação de fases secundárias, porém neste estudo, a seleção primordial do pó pré-ligado foi efetuada com a presença de $NiTi_2$ e Ni na sua composição. O estudo destacou o papel do $NiTi_2$, que apresenta uma temperatura de fusão mais baixa que a temperatura de sinterização durante a fase líquida, na promoção da reação do $NiTi_2$ com Ni, de $NiTi_2$ e de NiTi. A reação contribuiu para a formação de uma nova fase frágil, o Ni_3Ti, principalmente em torno dos limites das fases NiTi e $NiTi_2$, mas também com ocorrências no interior da fase primária. Estes intermetálicos são semelhantes aos observados em fusão seletiva por laser principalmente quando é utilizado pó elementar. Desta forma, associado à diminuição da temperatura, dois objetivos principais devem ser atingidos na etapa de sinterização. Sendo o primeiro a redução dos custos de produção, pela avaliação da temperatura mínima e tempo de estágio necessários para produzir uma sinterização eficaz, e o segundo é a adição de outro material de forma a diminuir a presença de intermetálicos além de NiTi. O estudo mostrou também o papel do TiH_2 quando misturado com pó pré-ligado virgem de NiTi. A não formação de Ni_3Ti é clara para uma composição especifica. O H_2 foi sempre utilizado durante o ciclo térmico como atmosfera redutora para evitar contaminação e a consequente formação de outras fases secundárias. Algumas composições com a adição de equilíbrio de Ni revelaram prioridade na formação de Ni_3Ti, evidenciando o papel do Ni livre no pó inicial. Outra contribuição complementar foi a avaliação do teor de volume crítico de pó de NiTi no processamento de filamentos de alta qualidade para utilização em extrusão de material. Um filamento 3D típico antes (verde) e depois da remoção do ligante/aditivos e sinterização foi utilizado como homotético de um objeto 3D, onde o fio extrudido (camada) é caracterizado como verde. Esta metodologia permitiu o estudo extensivo de todas as etapas do processo em função do filamento, pois é sabido que os defeitos no objeto 3D podem ser herdados do filamento. Por fim, um caso de estudo destaca a combinação do fabrico aditivo com o comportamento incomum do NiTi, que pode ser uma solução para desmoldar negativos na indústria de moldes para injeção.

PALAVRAS-CHAVE: Níquel– Titânio; Ligas com Memória de Forma; Extrusão de Material; Fabricação Aditiva Direta e Indireta; Filamentos Baseados em Pó; Impressão, Remoção de Ligante e Sinterização; Pó de NiTi pré-ligado.

Abbreviations

3Dobject – Part/System/Device
Af - Austenite finish
AM - Additive Manufacturing
As – Austenite start
ASTM - American Society for Testing and Materials
BSE - Backscattered Electrons
BJT – Binder Jetting
CIP - Cold Isostatic Pressing
CPVC – Critical Powder Volume Content
DDM - Direct Digital Manufacturing
EBM – Electron Beam Melting
EBSD - Electron Backscattered Diffraction
EDS - Energy Dispersive Spectroscopy
ESB - Energy selective Backscattered
FDC – Fused Deposition of Ceramics
FDM - Fused Deposition Modelling
FDMet – Fused Deposition of Metals
FFF – Fused Filament Fabrication
HIP - Hot Isostatic Pressing
ICDD - International Centre for Diffraction Data
IP - Isostatic Pressing
LDS - Laser Diffraction Spectrometry
LENS - Laser Engineered Net Shaping
MEX – Material Extrusion
Mf – Martensite finish
MIM – Metal Injection Moulding
Ms – Martensite finish
PBF - Powder Bed Fusion PEP – Powder Extrusion Process
PIM – Powder Injection Moulding
PM – Powder Metallurgy
PP – Powder Pressing
PSD - Particle Size Distribution
RM – Replicative Manufacturing
RP - Rapid Prototyping
SE - Secondary Electrons
SLM - Selective Laser Melting
SDS – Shaping, Debinding, Sintering
SME – Shape Memory Effect
SSA – Specific Surface Area
TGA - Thermal gravimetric analysis
WEDM – Wire Electric Discharge Machine
XRD - X-ray Diffraction
XRF – X-ray Fluorescence

List of figures

List of tables

Content

INTRODUCTION

The world is constantly evolving, grasping for trends to create new products suitable to application, and strategies to improve customer satisfaction. The challenge is demanded by the consumer who search the best quality, associated to sustainability, and by entrepreneurs who seek to improve their technologies in order to attain more and more the highest productivity/competitivity. Current and future directions, concerning advanced materials and processing technologies, have a main role in the worldwide market, whatever the application.

Shape Memory Alloys (SMA) is a class of materials, which are defined as any metallic material, with the ability to restore its previously defined shape when exposed to an appropriated stimulus, as specific thermal cycle, hydrostatic pressure or magnetic field, through either the Shape Memory Effect (SME) and/or superelasticity [1-3].

In general, these materials are used for engineering and medical applications and recently have been expanded to other industrial fields. However, they are extremely difficult to process whatever the technology selected [4].

Among the various intermetallic SMA, nickel-titanium alloy (NiTi) is known due to its unique characteristics. NiTi has an equiatomic composition of nickel and titanium, corresponding in weight content (wt%) to 55 of nickel and 45 of titanium. This intermetallic was patented in 1965 by W. Buehler and F. Wang from the Naval Ordnance Laboratory [1], and its common name is Nitinol. This intermetallic is mainly used in the development of thermostatic and electromechanical actuators, to perform mechanical actions assisted by temperature change phenomena, via electric current, for different applications. Actuators and sensors based on NiTi have been found to be possible, suggesting being of enormous interest for advanced technologies. Recently, new studies tried also to highlight the role of the intermetallic NiTi as sensors of cracks in aluminum alloys for aeronautical applications (i.e. *4DComposite, **Crack free projects).

Processing based on NiTi as the master material is quite difficult due to the difference between elements density, presence of microstructural defects and variation in the chemical composition, which can modify its transformation temperatures significantly [4, 5]. For instance, the nickel content deviation in NiTi of 1 at% gives rise to an Ms deviation of 100°C [6]. These modifications typically occur as a result of the presence of impurities, the formation of new intermetallic phases and/or environmental conditions during production or application.

*4DComposite Project: POCI-01-0247-FEDER-033758 - Intelligent molding of 4D components based on shape memory alloys embedded in carbon pre-impregnated with thermoplastic.

**Crack free: POCI-01-0145-FEFER-029101 - Towards self-repairing metallic alloys.

Up to now, the most produced shapes of NiTi using conventional technologies are limited to basic shapes like rods, wires, bars, tubes, sheets, strips, and springs. This fact is due to Ni-Ti, difference of density, high reactivity and ductility, resulting in processing and machining difficulties [7]. Powder technologies could be the solution to produce 3Dobjects of NiTi. Nevertheless, the replicative processes like Powder Injection Molding (PIM/MIM) as industrial manufacturing have not yet the expectable application in macro and micro 3Dobjects, despite of the number of publications in the domain.

Additive manufacturing (AM) could be "the elective processing technology for 3D near-net-shape objects directly from computer design", mainly due to its geometric flexibility, quick design and manufacturing, with the possibility to be applied to any metallic powder. AM could be the challenging solution to produce geometries based on NiTi.

In the last decennium, AM technologies, particularly Selective Laser Melting (SLM), have been applied in the direct production of complex geometries of NiTi. Nevertheless, the critical steps towards a successful manufacturing, such as powder preparation, optimum deposition parameters, and fabrication conditions are not yet well established. The more present AM technology for processing NiTi powder particles is SLM. Although, the high temperatures produce a melt pool that is very susceptible to contamination and formation of undesired phases during rapid and uncontrolled cooling. High temperatures in the melt pool can induce nickel evaporation, causing an unbalance in the NiTi chemical composition and/or phases present, consequently changing the phase transformation temperatures [8-11]. A variant of SLM is Selective Laser Sintering (SLS) that present as the main advantage, the capability to produce porous products that are of enormous interest to biomedical applications. Nevertheless, a weak surface finish (powdery surface) and post-processing treatments are required to increase product density and improve mechanical properties [12-14].

A new AM process is necessary to obtain the primordial target, the production of 3Dobjects, whatever the geometry. In general, they should have a thickness lower than 5 mm, and in according to some authors less than 10 mm [15]. However, is expected that this limitation will be overcome soon, based on new developments about inner channels design.

The indirect additive process of Material Extrusion (MEX) based on the additive manufacturing initially of polymers, Fused Deposition Modeling (FDM) and powder extrusion process/injection molding (PEP/PIM), could be the solution. MEX [16] is the terminology adopted for FDM, which is a trademark of Stratasys [17]. Although both names relate to the same technology, MEX was adopted in according the nomenclature of ASTM standard [16]. In these technologies, an optimized feedstock, in which metal powder particles are the raw material, are mixed with polymers (binder and additives). The advantage of this technology, in the context of NiTi, is that the maximum temperature attained in the manufacturing is lower than the melting temperatures of Ni, Ti and NiTi (reached in SLM), and the distance between

powder particles is controlled. This indirect process (SDS) has three main different steps, shaping (S), debinding (D) and sintering (S), needed for final product consolidation [18, 19]. Also, a controlled feedstock, in order to guarantee the minimum distance between powder particles, is necessary. This methodology is applied in feedstocks for PIM. Although other difficulties must be overcome, the use of MEX can resolve some problems associated with direct processing, including nickel evaporation.

Enhancing the reduction behavior of the environmental atmosphere and decreasing the temperature and holding time of the sintering stage, may also improve the implementation of the MEX process, when the raw material is a prealloyed NiTi powder. The temperatures used during debinding and sintering may cause an unbalance in Ni:Ti ratio that contributes to secondary phase formation. Ni content above 50.5 at% promotes the formation of Ni-rich phases, which shift Ni:Ti ratio. Moreover, the presence of impurities, particularly oxygen from the atmosphere and carbon from ustulation of polymeric binder, promotes the formation of undesired phases, such as $Ni_2Ti_4O_x$ and TiC [19-23], changing the Ni:Ti ratio and, consequently, the transformation temperatures.

Until now, no methodology was able to retain NiTi as a single phase. Different types of powder particles and binders/additives, temperatures, holding times and environmental atmospheres of debinding and sintering were unsuccessfully used.

The main objective of the present study is to produce 3Dobjects from prealloyed NiTi powder particles with and without addition of other materials.

3Dobjects were built layer-by-layer deposition using MEX, from optimized compositions of NiTi prealloyed powder-based filaments. Thermal debinding and sintering were processed at the lowest temperatures in a H_2 atmosphere. Also, this study highlights the effect of a reducing atmosphere (H_2) and low temperature sintering in the final phase composition of NiTi 3Dobjects. Finally, the role of Ni and TiH_2 powder in the final phasic composition was also highlighted.

The big challenges of the present study are as follows:

- Optimization of feedstock composition.
- Application of microtomography to highlight the defects in green filaments.
- Production of filaments with mechanical properties to withstand the printing process, homogeneous distribution of constituents and dimensional accuracy to fit in a common 3D printer.
- Definition of optimal set of parameters for printing, debinding and sintering.
- Role of prealloyed powder in the final phase composition after sintering.
- Achieving 3Dobjects with a phasic composition suitable to the application.

- Contribution to overcome the downsides of MEX using microtomography (printing defects, limitation of mechanical strength).

The thesis has four main chapters. After the introduction, chapter I starts with a description of the state of the art about additive manufacturing and powder technologies. In Chapter II, materials, processing methodologies and characterization techniques selected for this study were described. Chapter III exhibits the results and discussion of all the critical stages of MEX, from mixing up to sintering, for the compositions selected. Chapter IV describes a possible solution for demolding undercuts in injection molding, using SMA replacements of sliders produced by MEX. The thesis finish highlighting the main conclusions and pointing to future works.

CHAPTER I

State of the art

1.1 NiTi shape memory alloys

SMA is a class of materials, which are defined as any material, with the ability to restore its previously defined shape when exposed to an appropriated stimulus, as specific thermal cycle, hydrostatic pressure or magnetic field, through either the SME and/or superelasticity [1-3].

Nickel-titanium was identified as SMA and named Nitinol (Nickel–Titanium Naval Ordnance Laboratory) at the United States Naval Artillery Labs [1, 24]. The behaviour of NiTi is due to the reversible and without diffusion change, between the martensitic phase, at lower temperature, and austenitic phase, at high temperature, and can be denominated SME (pseudoplasticity) or by the superelasticity effect [20]. The martensitic phase has a low symmetry and complex twinned monoclinic B19' structure (Figure 1a)) and the austenitic phase has a highly symmetric and ordered body centered cubic structure, known as B2 (Figure 1b). The martensite phase has a needle-like structure arrayed in a herringbone shape (mosaic like pattern) and has high ductility; the austenite phase is hard and stiff. A third phase can be present during transition from austenite to martensite denoted as R-phase, which has a rhombohedral structure. The R-phase is more common in Ni-rich alloys which were submitted to aging or cold working processes, in some compositions due to precipitates and due to any alloy elements.

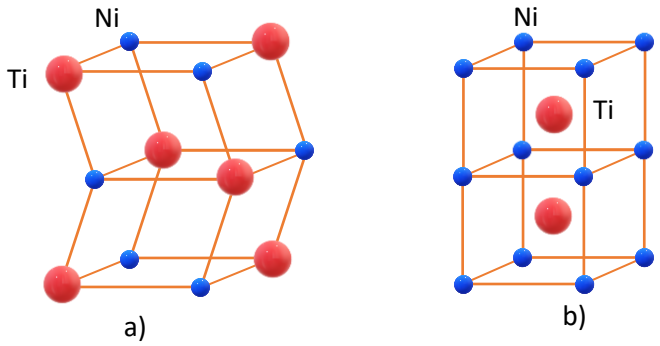

Figure 1. Crystal structure phases of NiTi a) B19' Martensite b) B2 Austenite.

The SME is characterized by reverting an actual geometry into the primordial with the use of temperature. The effect of superelasticity occurs when the alloy is totally in the austenitic phase at high temperatures, and by the action of an external force is transformed into the martensitic phase, changing its shape, after the release of the external force, the alloy recovers the austenitic phase, and the original geometry [25]. Figure 2 depict the SME phases based on transformation temperature. At low temperature the alloy will be in the twinned martensite phase (B). Applying a deformation will cause the lattice structure to change to a detwinned martensite (C) by the reorientation of the twin boundaries in order to better accommodate the

load. When heated above (As) austenite start to be present (E) until finish its transformation from martensite (Af, F) [26].

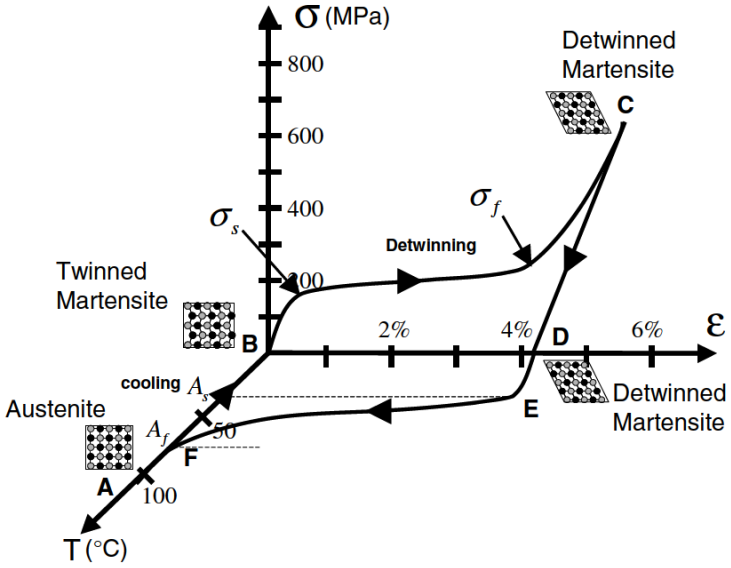

Figure 2. Stress-strain-temperature illustration showing NiTi SME [27].

Martensitic transformation, or the temperature range that it occurs, determines the behaviour of SME and superelasticity effect, which are very important to practical applications [28]. As referred, transformation temperatures are very sensitive to chemical composition of Ni-Ti and alloying elements. This means that a very rigorous control of chemical composition and alloying elements is necessary, in order to achieve the desired properties or transformation temperatures. In the present study there are no alloy elements added to the matrix only additives (TiH_2 and Ni). Therefore, chemical composition deviation is the most important influence on transformation temperatures.

Figure 3, in the NiTi phase domain, Ti-rich side is almost vertical, showing almost no solubility, meaning that tuning transformation temperatures is very hard by chemical composition changes. Nevertheless, on the Ni-rich side, solubility of Ni in NiTi changes with temperature, which makes possible to study the influence of Ni in the martensitic transformation temperatures. The alloy can dissolve some excess Ni but cannot dissolve the excess Ti, so the Ti-rich alloys show a behaviour similar to equiatomic ones. Generally, a Ni-rich alloy exceeds the limit of Ni solubility, and, therefore, the extra Ni tends to form Ni-rich precipitates such as Ni_4Ti_3, Ni_3Ti_2, and Ni_3Ti which results in the depletion of Ni from the NiTi matrix. Ni-rich precipitates formation together with Ni evaporation leads to a high Ti contents within NiTi matrix, and therefore the transformation temperatures increase significantly [29].

In present work the NiTi is enriched in Ni element. Thus, increasing Ni content causes a drastic decrease in martensitic transformation temperature.

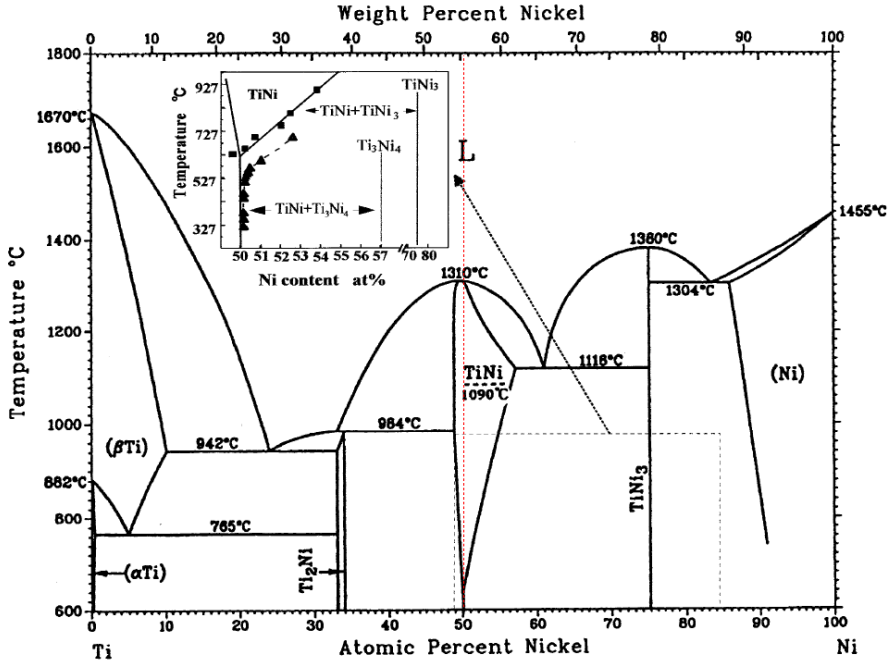

Figure 3. NiTi Phase diagram with phase equilibrium between NiTi (B2) and Ti_3Ni_4 [28].

Figure 4 shows the martensite start temperature (M_S) as function of the Ni at%. M_S drops from approximately 50°C for a concentration of 50 at% Ni to sub-zero temperatures for a concentration of 51 at% Ni. An alloy with 49 to 51 at% of Ni has a window of temperature of transformation between -50 to 100°C with a transformation hysteresis of approximately 30°C [30].

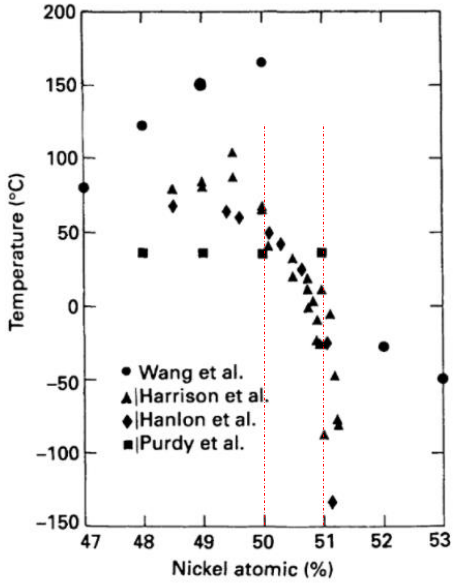

Figure 4. M_S temperature of NiTi as function of Ni at% [31].

Whatever the technology used for processing NiTi, shows a quantity of problems, since any microstructural defect or a small variation in chemical composition can change the transformation temperatures significantly [4, 5]. For example, changing the nickel concentration in NiTi by 1 at%, the martensitic transformation temperature may shift 100°C approximately [6]. Although, the martensitic transformation that occurs in NiTi shape memory and superelastic behaviours is diffusionless, the control of such behaviour can be done by a diffusional precipitation reaction [28]. Aging treatments can be also used to change transformation temperatures [32] by attaining the equilibrium between the NiTi and metastable phases (Ni_4Ti_3) [33, 34].

In the recent past the manufacturing technologies used in the production of 3D objects in NiTi were essentially foundry and powder technologies based on the pressing, followed by sintering. However, both are associated to the appearance of impurities in the metal matrix, in the casting process due to the high temperatures, and in the powder technologies due mainly to the great specific area of the particles, where a tendency to react with of carbon and oxygen is enormous [12]. In recent years some research work was done essentially using for additive manufacturing of NiTi, based on direct process, particularly SLM[26, 35-38]. The AM allows the final product to be obtained directly from the manufacturing technology without further operations. In this way, it is possible to combine the unique characteristics of NiTi with the freedom of shape of the specimens obtained by AM. Although SLM has been the most used AM technology to process NiTi, many problems are associated with it. In this work, MEX will be approached as an alternative method of processing NiTi. The extrusion of high-loaded polymeric filaments (loads above 45 vol %) arose mainly for two classes of materials, metallic [39, 40] and ceramic [41-43]. The major difficulty in filament production is due mainly to the high concentration of fillers. It is important to mention that filaments, to be used in MEX, require a good relation between resistance and flexibility, in order to be extruded without breaking, which would stop the production, meaning that the part being produced would be damaged. Depending mainly on size and printing parameters, some productions could take hours or even days to finish.

The existent literature refers mainly works on 316L stainless steel [39, 40, 44-48], on 17-4PH stainless steel [44, 49], Neodymium alloy [50] and iron carbonyl [48]. Up to date there are no references in literature of any work using MEX to process NiTi alloys.

1.2 Powder Processing Technologies for NiTi

Up to last decennia, the most common metallic powder processing technologies studied are those based on replicative manufacturing (RM), like powder pressing (PP) and PIM,

depending on the geometrical complexity. Both are suitable for high series production, and one use dies and punches and the other moulds, like those used in polymer 3Dobject production. The use of moulds allows to produce parts/systems/devices with complex geometries associated to high dimensional precision and surface quality, denominated net-shape processes in opposition to AM which products are usually denominated as near-net-shape.

Nowadays, AM, has being a contributor to overcome new challenges to produce new geometries independent of mould limits. Free geometries are possible to be produced and new technologies are developed to attain this target. AM technologies can be characterized as direct or indirect, depending on the technic and methodology selected. Although there are many AM processes with the ability to process metal powders, the most widely used and that have been the target of more study are: SLS, Laser Engineered Net Shaping (LENS), Electron Beam Melting (EBM) and SLM [51]. Unlike most metal alloys, there is still no fully effective method capable of guaranteeing reproducibility and especially of producing components free of impurities and intermetallic phases that affect the behaviour of the NiTi alloy. In AM the impurities are originated in the production of the powder and during the processing of it, due to the parameters and the atmosphere of production. Although SLM has been the most used AM technology to process NiTi from powders in one step, many problems are associated with it. In this work, MEX will be approached as an alternative method of processing NiTi and could be an excellent solution to overcome the problems highlighted by SLM. MEX is an indirect process that requires additional steps than direct processes, like debinding and sintering. In fact, the shaping stage is the same of polymers. The difference is in the feedstock that in metallic powder technologies is a mixing between polymer materials (binder and additives) and metallic powder.

In consequence, the state of art is organized firstly by the revision of RM process of metallic powder particles for complex geometries (PIM), followed by AM research studies. Both have as *leitmotiv* NiTi.

1.2.1 Replicative Manufacturing

a. Metal Injection Moulding

PIM is a replicative technology where powders of metal (MIM) or ceramic (CIM) are injected in a mould like a polymer. This technology allows to manufacture complex geometries in high series of parts. This is a process with three stages: Shaping, Debinding and Sintering, in general denominated as SDS [18, 19]. Each of these steps is optimized through its control parameters, in order to optimize the final product.

The technology follows the same principles of polymer injection, where a polymer at the processing temperature is forced into a mould, acquiring its shape upon cooling, *i.e.*, depends on the moulding of a polymeric binder, composed of polymers, waxes, plasticizers, etc., loaded with metal particles.

In order to mimic a polymer, the metallic/ceramic powders must be "coated" with a polymer or a mixing of polymers, to create a homogeneous feedstock. This feedstock must have the higher quantity of metallic powders without losing flowability, similar to polymers. The binder must be adequate, depending on the metal powder characteristics and geometry of the parts.

After shaping, the green must be submitted to a chemical and/or heat treatment to eliminate the binder without loss of shape (debinding). After sintering of the "brown" part (without binder), the metallic particles are consolidated (bulk), and a significant dimensional contraction (15 to 20%) is observed, with significant values, when compared to the injection of polymers (0.5 to 3.0%). After cooling, the density of parts is close to the bulk material. During the injection, the control parameters of both the raw material and the mould are mainly related to pressure and temperature. During the decomposition of the binder, each technique has its own method, however it is intended that the binder is completely removed, without contamination of the metal particles. In what concern sintering, it must be carried out at temperatures close to the melting point of the metallic material [52]. The metallic products made by MIM can be competitive with other technologies, as they have good mechanical properties and good dimensional tolerances. Moreover, powder injection technology, has a very good reproducibility [52, 53]. The size of the products that can be obtained by MIM varies from 2 to 50 mm and up to 1 kg of weight [29].

Since MIM is a technology well stablished in industrial world, it has a well-defined standardization [54]. The ecosystem that surrounds it is very vast and information and research regarding the binomial technology/material is significant. The most common metallic materials processed by MIM are steels, titanium and titanium alloys, nickel alloys, copper, cobalt-chromium alloys, tungsten, etc. The emergence of new materials and improvements in processing reflects the requirements of new products for the automotive, aerospace and medical markets[54].

The processing of NiTi alloys by MIM was studied by several authors, and the change in chemical composition during processing, was identified as the main obstacle to the normal behaviour of the SMA. *Schöller et al.* carried out one of the first characterization studies of prealloyed NiTi powders processed by MIM [20]. Using prealloyed NiTi powders, the chemical analysis revealed that into all the specimen, the content of contaminants increased during processing when compared to the initial powder. The authors refer that the precipitation of $NiTi_2$ is due to nickel content to be lower than titanium, and also the presence of $Ni_2Ti_4O_x$, a very

common precipitate due to the presence of oxygen and low solubility of this element in NiTi. Also, they identified TiC mainly by the darker colour of the precipitates (SEM micrographies). During post-processing the formation of a double layer on the surface was observed, which is resulting from the different affinity of nickel and titanium to oxygen. The outer layer mainly formed by Ti-rich precipitates ($Ni_2Ti_4O_x$) causes the Ti depletion in the lower layer leading to Ni_3Ti precipitation, highlighting that this is a common phenomenon in NiTi alloys, in high temperature processes, in the presence of oxygen. Due to the Ni concentration being greater than 50.5 at%, there was also precipitation of Ni_4Ti_3 during cooling after sintering. The R-phase is associated with the appearance of the Ni_4Ti_3 phase. However, the author could not find a direct correlation between sintering temperatures, level of impurities and the phase transformation phenomena. *Köhl et al.* also detected the increase in oxygen and carbon content during debinding and sintering, which led to the precipitation of the Ti-rich intermetallics TiC and $Ni_2Ti_4O_x$. The increase of the nickel content in the NiTi Matrix, causes a change in the transformation temperatures to lower values and a decrease of the mechanical properties, because these intermetallic are quite fragile [21]. The uptake of oxygen is more propitious during the debinding process however its concentration tends to decrease during sintering and carbon uptake tends to increase due to the combustion of the binder [22]. *Bram et al.* detected the precipitation of the intermetallic phases TiC and $NiTi_2$ ($Ni_2Ti_4O_x$) due to the increase of carbon and oxygen content respectively during processing, due to the very low solubility of both oxygen and carbon in the NiTi matrix, and Ni_4Ti_3 during cooling after sintering [55]. The formation of titanium-rich intermetallic phases increases the concentration of nickel, which influences the transformation temperatures. In the mechanical characterization of fatigue, it was detected the appearance of cracks in the $NiTi_2$ precipitates because these are known to be quite fragile [56]. The sintering of NiTi alloys should be done below the melting temperature of the alloy (Tm ≈ 1310°C), between 1230 and 1265°C and for at least 5 hours, in order to obtain a theoretical density above 90% (ρ = 6.45 g/cm^3). After sintering, during slow cooling in alloys exceeding 50.5 at% of nickel, the formation of Ni-rich phases is almost impossible to avoid, in the temperature ranging between 350 and 630^{o}C. The author observed that the Ni_4Ti_3 intermetallic phase can be dissolved in the matrix by quenching at 1000^{o}C for one hour followed by rapid cooling in water [55, 57]. *Bidaux et al.* studied superelastic NiTi alloys processed by MIM. They observed also that Carbon, Oxygen and Nitrogen are practically insoluble in NiTi, resulting in the formation of intermetallic phases. The increase of the oxygen concentration is resulting of the reaction with the stearic acid and possible residues in the sintering atmosphere, which caused the precipitation of $Ni_2Ti_4O_x$ (concentrations higher than 0.045 at% oxygen) and carbon by direct contact or incomplete debinding, originating the precipitation of TiC. As expected, there was precipitation of Ni_4Ti_3 in concentrations of Nickel that exceeds 50.5 at% during cooling of thermal processes over 700^{o}C. The significant presence of Ni_4Ti_3 is one of the factors for the appearance of the R-phase [23].

Muhhamad et al. detected the presence of the Ni_3Ti phase, that has a high predominance at low temperature sintering of 950°C and tends to be dissolved in the matrix at high temperature sintering of 1250°C. For all temperatures tested, the NiTi phase present is predominantly austenitic B2, with some incidence of low temperature martensitic NiTi B19', which also tends to decrease, with increasing of sintering temperature. The authors concluded that in order to maximize the formation of NiTi and avoiding the formation of phases such as $NiTi_2$ and Ni_3Ti, the sintering temperature should be higher than 1050°C, in order to allow sufficient interdiffusion. However, to minimize the size and the quantity of porous, the best observed temperature was 1250°C [58].

The use of NiTi alloys by MIM is quite common and successfully established. However, problems associated with replicative processing could be similar to those existing in AM processing. Whatever the manufacturing process, the problems associated to contamination and precipitation of intermetallics continue to be the main cause of chemical composition variation and consequent modification of the transformation temperatures. By other hand, for instance in MEX, besides the difference of the shaping step, the other steps (debinding and sintering) are quite similar to the steps of MIM.

1.2.2 Additive Manufacturing

AM is defined by the American Society for Testing and Materials (ASTM) as a "process of joining materials to make parts from 3Dmodel data, usually layer upon layer, as opposed to subtractive and formative manufacturing methodologies". ASTM F2792 [59] defined standardized terminologies for AM which in 2015 was replaced by ASTM52900:2015 [60] and more recently by ASTM52900:2021 [16]. The main advantage of AM is the possibility of producing almost all shapes and geometric details [61].

Rapid Prototyping (RP) applied in general to polymers can be considered the genesis of the AM, where the objective was to produce prototypes for demonstration and aiding to the development of new products. Since it allowed a quick way to have a physical product, that could be analysed and modified at low cost, when compared to the technologies available at the time (Figure 5) [62].

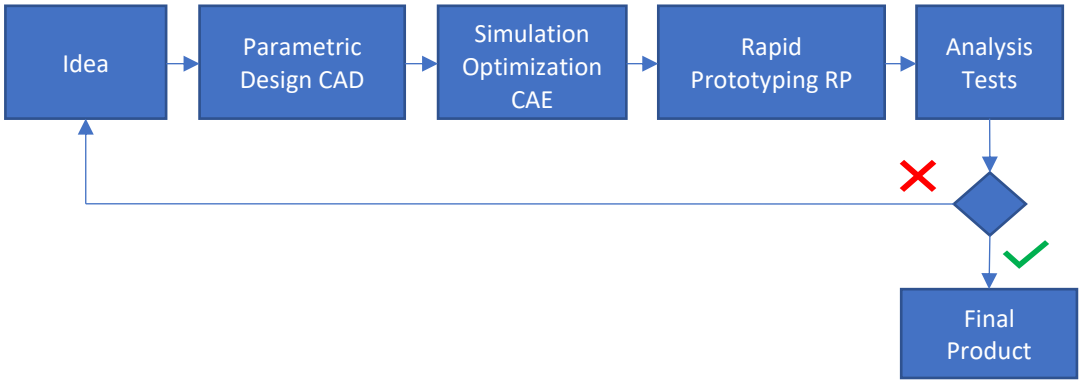

Figure 5. Product conception timeline (1991) [62].

With RP it was possible to obtain functional 3Dobjects, capable of human interaction, at low cost, in a relatively short period of time and the possibility of creating almost all geometric forms [63].

For some authors, additive fabrication, additive process, additive technique, additive layer manufacturing, layer manufacturing, solid free form manufacturing are alternative designations for additive manufacturing [64]. Moreover, Frazier [65] states that direct digital manufacturing (DDM) and free form fabrication (FFF) have the same designation as additive manufacturing. However, the term 3D Printing, that according to the ASTM is: "making objects by depositing a material using a printhead, nozzle or other printing technology", remains the most widely used, regardless its category [64]. A search on Google by the term “ADDITIVE MANUFACTURING” finds 134 million references while the term “3D PRINTING” finds 2150 million references supporting the last assertion. In the present study, the definition proposed by ASTM will be adopted. Thus, the production of a physical 3Dobject, by the successively deposition of layers of inorganic materials, including NiTi powder with or without other materials, from a virtual model, and the terminology used will be AM.

In 2018 the markets that more recurred to AM for producing 3Dobjects were the Industrial/Business machines, Automobile and Aerospace (Figure 6).

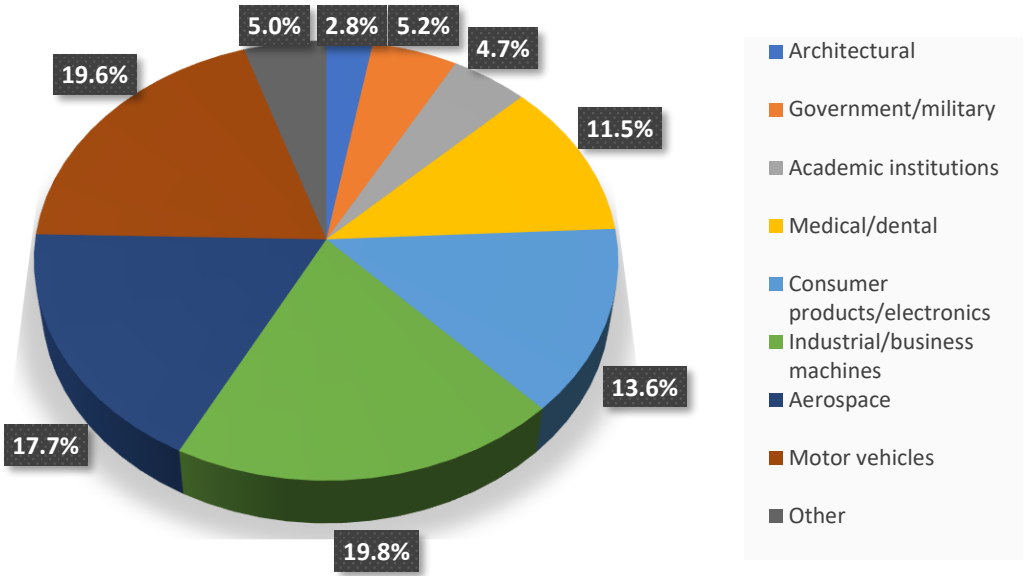

Figure 6. Use of AM per market sector in 2018 [66].

In financial terms, the AM market in 2018 handled about 8 thousand million euros and is estimated to reach 21.5 thousand million in 2022, which shows the growth of this market when compared to the first 20 years to reach the first million. Between 2020 and 2023*, the global AM market is expected to grow by 17%/year. The rising number of application areas is expected to drive industry direction, with the production of tooling components and patterns for metal castings, being the most promising fields of growth. The market for AM products and services is predicted to almost triple between 2020 and 2026*[67].

Regarding materials applied in AM, in 2016 approximately 620 million euros were handled, and in 2018 approximately 1.5 thousand million. Where 26.9% represents the commercialization of polymeric particles, 20.6% represents the commercialization of filaments, 17.4 % represents the commercialization of metallic powder particles and others 35.1% (Figure 7). In 2016 the business volume of metal powders was 14%, which highlighted the evolution in powder metallic materials and AM processing technologies. The large slice represented by the filaments is due to the appearance of many inexpensive equipment that uses this type of feedstock. This equipment is not only used in industrial environment, but also by the common user, which has led to the mass production of FDM equipment. The most of this equipment use any type of filament, not requiring the use of filament of the own brand, which promoted the appearance of many filament producers. The thermoplastic filaments for FDM handled about 254 million euros in 2018. Although the 3D printing materials market is currently dominated by plastics, metallic materials are projected to spur market growth.

* The predicted data presented, were collected without considering the impact of the pandemic situation experienced worldwide.

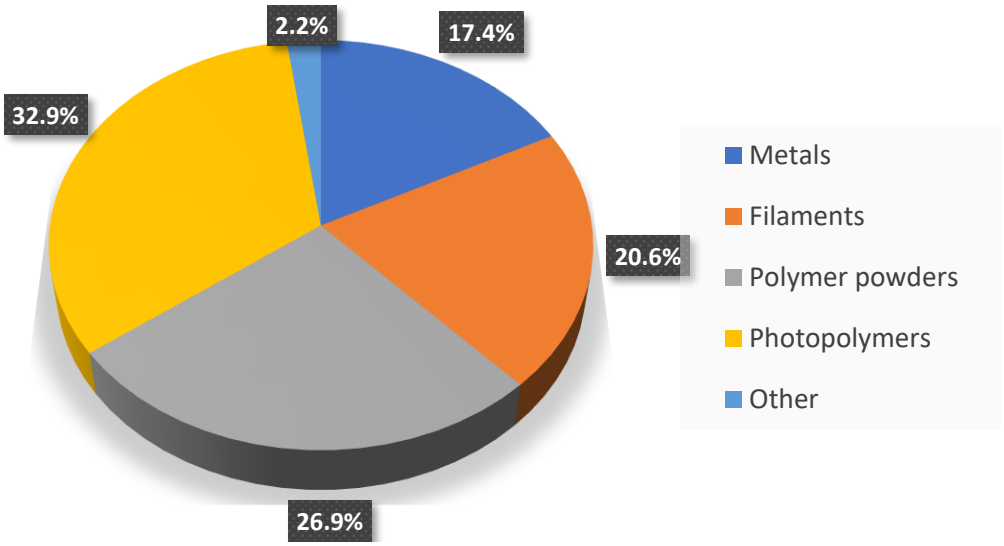

Figure 7. Feedstock for AM in 2018 [66].

The metallic materials remain the most required, representing this sector in 2018 a volume of business of about 185 million euros [66].

In 2019, the global metal AM market were valued at 2.02 thousand million euros including system, material and service bureau part sales and it is expected to grow to 6.92 thousand million euros until 2024*. Also, in 2019, the powder bed fusion technologies (PBF) generated 85% of the revenue of the system suppliers (more 5% compared to 2018). Direct energy deposition (DED) technologies took a market share of global system sales revenue of 8.3%, while metal extrusion, binder jetting (BJT) and other technologies sum up to about 7% (Figure 8). While the market share from PBF is expected to drop, the market share from DED is expected to grow to 11.1%. And more important, the sinter-based technologies like MEX and binder jetting are projected to grow from 5% to 13% market share in 2024*. As expected, and also a key target in the present study is finding solutions and establish a production strategy for the debinding and sintering steps that will be critical to the success of these technologies.

* The predicted data presented, were collected without considering the impact of the pandemic situation experienced worldwide.

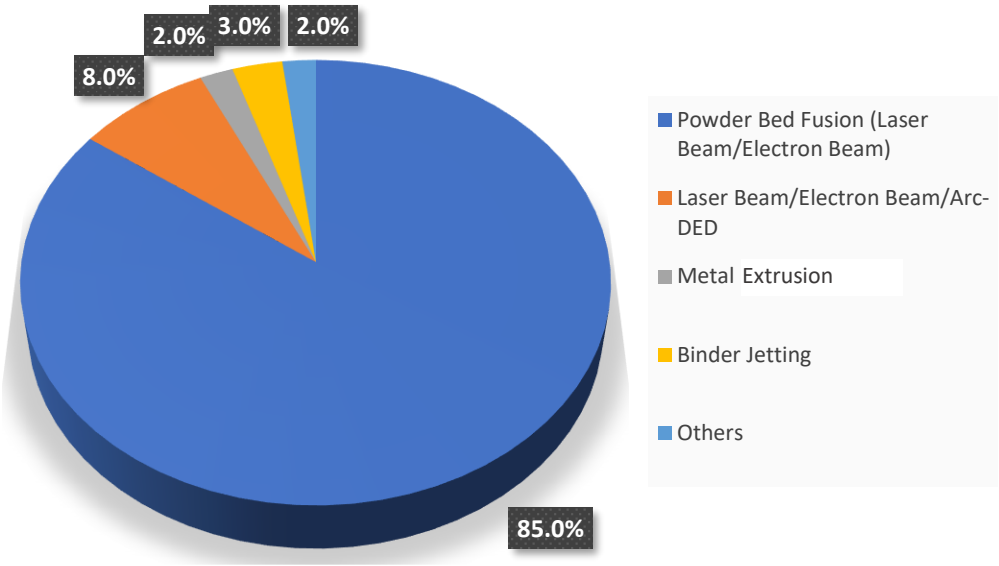

Figure 8. Sales revenue from metal additive manufacturing technologies in 2019 [68].

The aerospace, turbine and helicopter industries have the highest revenue in system sales in 2019 increasing almost 80% from 2018 and it is estimated to triple its revenues until 2024*. The medical and dental industry doubled the revenues in one year and is expected to grow its sales revenues 19% until 2024*, however it is the third technology in the sales revenue. Although the automotive sector is placed in second, compared to 2018 the machine sales revenues were reduced by 10%. The 5-year supplier forecast predicts a growth of 40% in this sector. For the remaining sectors an annual revenue growth exceeding 30% is predicted by the system suppliers (Figure 9) [68].

Nowadays, there are equipment suitable to produce 3Dobjects near-net-shape, or even net-shape. This concept is not only related to functionality and geometry, but also with other characteristics like surface finishing, gradient of materials, resolution, precision, etc. In 2016, 19 of 97 manufacturers of industrial AM equipment, sold more than 100 machines and in 2018 the total sale raised to 20 000 machines [64].

* The predicted data presented, were collected without considering the impact of the pandemic situation experienced worldwide.

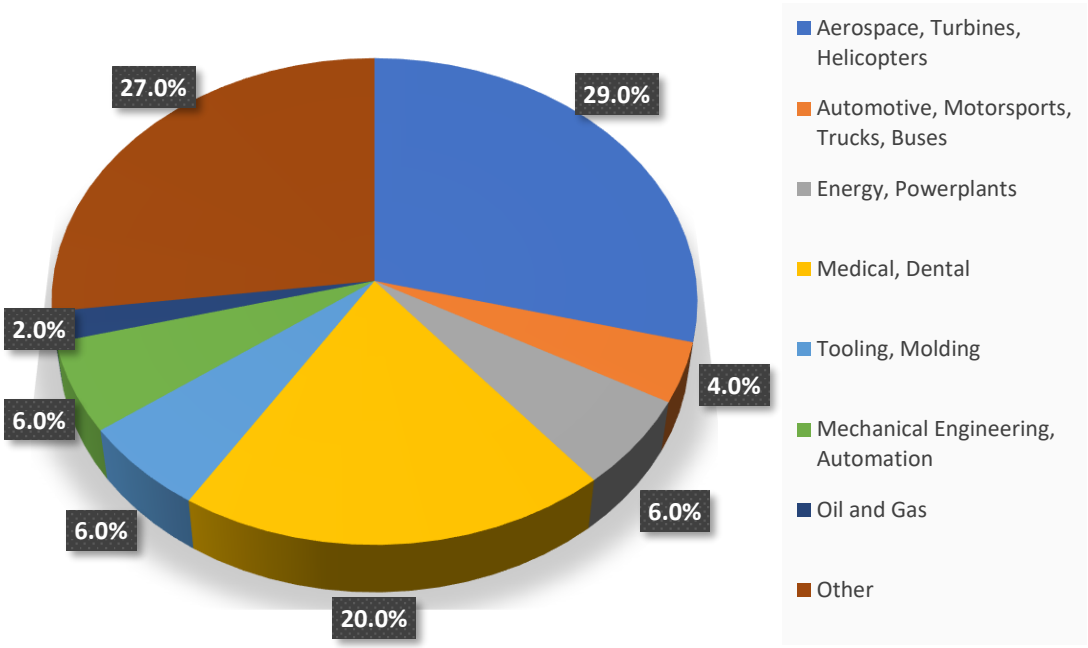

Figure 9. Sales revenue from metal AM technologies by industry in 2019 [68].

Among the fastest-growing services for a specific material type are metals and metal alloys. Besides metal AM technology to be relatively recent, many major breakthroughs take place every year. Nevertheless, AM of powder metals are generally more expensive. This application is generally a slower process and the machinery itself is in some cases more expensive [67].

Regardless the technology used and the material to be processed, direct AM follows, from the virtual concept to the physical product, the same steps to achieve the final part. (Figure 10). There are numerous computational applications suitable to produce three-dimensional models, with more or less modelling capability, commercial or with free access, the only requirement is that they can convert the 3D model to a STL (stereolithography file) [69]. During product development, depending on the technology to be used, there are rules that must be considered, such as placement of supports, 3Dobject position, draft angles, etc. These parameters directly influence the quality of the manufactured part [70-72]. Converting the part to an STL file (triangle model), usually causes errors, among others, mismatched faces or the normal of the triangle inverted, that must be repaired. The use of supports and its location can be selected by the user or by the software itself. Depending on the technology selected, the supports can have various functions. For instance, in SLM, the supports have also the function of dissipating the heat to the building platform, since it is the remaining powder itself that supports the construction. Against MEX, where the supports only aid on the building. However, regardless the technologies, the supports must always be removed, fact that affect the surface quality of the 3Dobjects. The position of the part on the table strongly influences the final quality

of the outer surfaces but also the mechanical properties of the 3Dobject. After positioning the part, the ideal processing parameters are selected, and the slicing is performed. This step defines what the AM equipment does in each layer, meaning that the software defines the external contour as the production limit and everything inside it is considered 3Dobject. Each layer is then translated into a language that the equipment interprets and transforms into trajectories, for example in G-Code (MIT, 1950), and the production is performed. After production, the removal of the part, depending on the technology, may be as simple as taking the part off the platform, like in MEX, but in technologies that use total fusion like SLM, it is necessary milling or wire electric discharge machines (WEDM), since the part becomes “welded" to the building platform. In post-processing, cleaning tasks are necessary, for example, in powder bed technologies like SLM, it is necessary to remove the excess of powder and the supports.

The surface finish and the quality of the 3Dobject can be improved, by milling or by other post-processing. This can also include heat treatments to control the final microstructure of the 3Dobject, and to contribute for decreasing the residual porosity. Hot Isostatic Pressing (HIP) or Cold Isostatic Pressing (CIP) could be the solution [72].

Figure 10. Direct AM workflow (adapted from [72]).

The ASTM F42 committee that regulates AM has defined in the ISO/ASTM52900:2021 [16] the additive Manufacturing Standards Structure. Figure 11 is the adaptation of the general schema presented in [64] for AM process whatever the material, to the main topics studied in the present thesis. Besides the main technology used is preferably oriented to the "Material Extrusion" category, the group of the "Powder Bed Fusion" in particularly SLM will also be approached.

In the present work SLM it was the first technology selected, however, due to different problems results, particularly high temperature of processing, led to a bad quality of the final product. Thus, it was replaced by MEX, due to be the possible technology to overcome the technical problems of SLM.

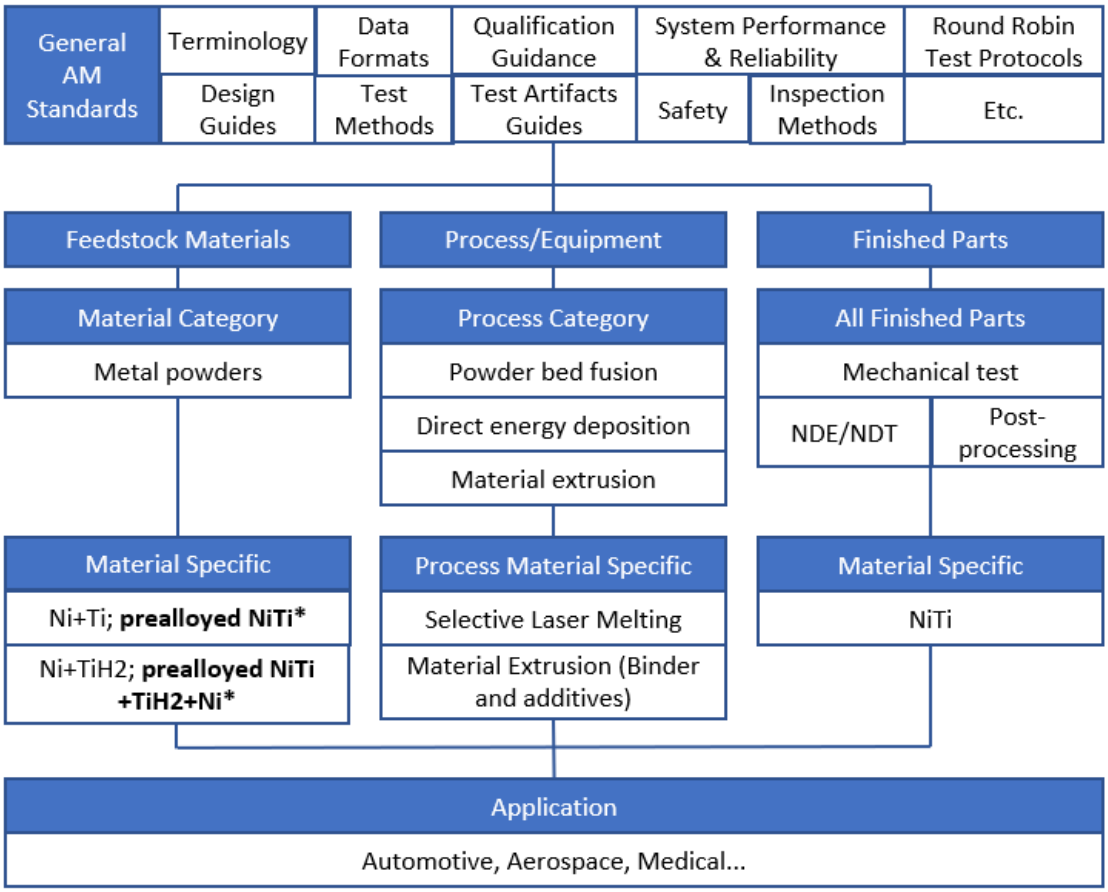

Figure 11. Additive Manufacturing Standards Structure adapted from (Wohlers, T.) [64].

*Specific material studied in this PhD thesis.

In consequence, two different items in state of art, concerning the AM of NiTi, are detailed: SLM and MEX. SLM is an AM technology integrated in the denominated direct processes, meaning, shaping and consolidation in the same step. Against MEX where two different steps are required to attain the final 3D object. First step shaping and second debinding and sintering (consolidation), denominated by indirect processes.

a. Selective Laser Melting - Direct Process

The SLM technology resulted from a partnership between *M. Fockele* and *D. Schwarze* with the Fraunhofer Institute for Laser Technology in 1999 in Germany [73]. The technology uses the total melting of the metal and ceramic powders as a bonding method, in order to produce parts with high precision, complexity and density [74]. SLM is one of the denominated powder bed technologies, where each powder layer is placed before the laser scanning, *i.e*. the first layer is deposited on the building platform (bed), usually of the same material to be processed, followed by the laser scan that completely melts the 3Dobject area. The same procedure is executed, layer by layer, until the 3Dobject is complete. The process takes place in a dynamic or static controlled atmosphere, that can be inert (Argon or Argon+Nitrogen) or reactive atmosphere. In the dynamic atmospheres, the fluid circulates and can also assume the role of cleaner.

The technology needs large concentrations of energy to melt the powder particles. The volumetric energy density (VED) is provided by the laser and can be expressed by the following expression:

$$VED = \frac{P_{ef}}{v_s \cdot \Delta h_s \cdot d_t}$$

Where P_{ef} is the effective power of the laser, v_s is the scanning speed, Δhs is the spacing between passages (hatch) and d_t is the layer thickness [11, 75, 76]. In this compromise between parameters, there is no effective way to control melt temperature, which makes it difficult to process alloys such as NiTi that are extremely sensitive to impurity pickup and to other intermetallic phases formation. Although SLM is one of the most used AM technologies to process NiTi 3Dobjects, many problems are inherent to it, mainly due to the volumetric energy density, which is dependent on the processing parameters. The energy density in SLM is one of the most studied parameters in the specific bibliography since it influences many factors during processing. A high VED increases impurities pickup [77] and a very large melt area with uneven surfaces that can compromise the subsequent layer topography, as it can cause the collapse of the deposition system against the last solidified layer. Size of Ni_4Ti_3 precipitates gradually increase with the increase of VED, and tend to change from dispersion to agglomeration [38]. Due to the high temperatures reached in the melt pool, the evaporation of Ni (Ni=2913^{o}C, Ti=3287^{o}C) causes an unbalance in the NiTi intermetallic compound, creating an excess of Ti, which significantly changes the processing temperatures [8-11]. For each 15 Jmm^{-3} of energy density the NiTi transformation temperatures increase about 8°C [78]. Energy density is also related to structural defects, such as balling [10, 79] and grain size, both of which increase with

increasing energy density [10]. Although a low VED can be effective in supressing cracks [80] if too low, a continuous strip of melt may not be formed, which compromises adhesion to the substrate making impossible to produce a fully dense 3Dobject [76].

As mentioned before, another source of the NiTi matrix unbalance is the precipitation of undesired phases. The time of laser interaction is directly related to the cooling time that could contribute to the observation of secondary phases including the R-phase [81, 82].

One way to revert the intermetallic phases back to the NiTi matrix, is to promote the adequate heat treatment, where the most effective is quenching due to rapid cooling rate [83]. By the other hand, annealing treatments also promote the formation of undesirable precipitates [82]. Being the SLM parts related to high stress, due to rapid heating and cooling, an adequate study most be performed before thermal treatments.

The atmosphere of processing is another cause of contamination and alteration of NiTi composition. During cooling, elements and powder particles of the atmosphere can be retained in the melt pool [83].

In conclusion, processing intermetallics of NiTi by SLM, mainly due to the high temperatures, makes it difficult to control the elemental content, which is reflected directly in the transformation temperatures. Other technologies where the maximum temperature attained is lower are imperative. Thus, MEX as an indirect process can accomplish the main objective of the present study to produce NiTi by AM.

b. Metal Extrusion - Indirect Process

In FDM the filament is forced, by a system formed by a pulley and a sprocket, through a hot zone that heats the feedstock to the processing temperature, and it is deposited in a plate by a nozzle (strand), layer by layer. After each layer, there is an increase in the distance between the previous layer and the deposition system, which is equivalent to the height of the layer, and to the resolution of the final surface. This technology is quite versatile, easy to use and since the expiration of the Stratasys patent, have arisen in the market equipment with features and prices that satisfy both corporate and personal users. It allows to produce dense or hollow parts, the latter with supporting internal structures. One of the main disadvantages of MEX is the resolution in the height direction, typically the Z axis, that defines the surface finish quality. In order to improve the surface quality, the step in the Z axis must be as small as possible, which increases the production time significantly. The pristine technology FDM allows to process many polymers, like Polylactic Acid (PLA), Polycarbonate (PC), Polyamides (PA), Polystyrene (PS), Polyethylene (PE), Polypropylene (PP), and Butadiene Acrylonitrile Styrene (ABS) [84-87]. In case of metallic powder, it is necessary to resort to organic materials addition, one with the role of

binder and the other one as reinforcement material (additive) in order to manipulate and produce strands from metallic based filament.

The concept of extrusion of polymeric based filaments with other class of materials in a significant content (≥ 45 vol%), was presented in the 90's giving rise to the technology denominated by Fused Deposition of Metals (FDMet) [39, 40] and Fused Deposition of Ceramics (FDC) [41-43]. Nowadays, the denomination for metal filament processing, regardless of the material, is MEX [16]. This technology, also based on PIM, after production of feedstock filaments [88, 89], follows three steps: Shaping (S) (green), heat treatment - to remove binder and additive materials (Debinding (D)), and in order to consolidate the metallic powder particles (Sintering (S)). This sequence of steps is denominated by SDS [90].

In present study, only filaments with high concentrations of fillers will be addressed (concentrations higher than 45 vol% of powder particles). Since the appearance of this technology that many authors have produced and analysed filaments with different types of metallic particles [39, 40, 44-48, 91].

Wu et al. produced filaments based on 17-4 PH steel (58 vol%), concluding that this kind of filaments induce 3Dobjects with good geometrical accuracy and reproducibility. However, it is necessary to develop new methods for removing the supports, in order to improve the surface finish [39, 40]. For the same steel, *Gutierrez et al.* used a lower concentration of metallic powder (55 vol%), having obtained filaments with good geometric shape, but with inside defects as pores. After sintering, the printed products exhibit a linear contraction of 19% [44]. Filaments also with 55 vol% of 316L stainless steel were produced, having observed the same preservation of geometry and porosity inside the filament and 3Dobject, however the linear contraction was 15% [44, 45]. *Kukla et al.* produced filaments with 55 vol% of 316L stainless steel with various binder combinations. They observed that the mechanical properties of some filaments are not suitable for MEX, having concluded that is the binder, for the same concentration of metallic powder, that confers the desired properties. The filaments that were possible to process, presented also linear contraction of 15% [91]. *Cruz et.* al used several iron carbonyl concentrations in order to test various types of binder, having concluded that the best concentration of metal filler was 61 vol%, for the binder composition selected. The authors did not perform any test of printing, only produced the filament [48]. *Kukla et al.* also studied the influence of particle size in printing quality. Two average particle sizes (D_{50}≈5.5 e D_{50}≈8.6 µm) of 316L was selected at metallic powder concentration of 55 vol%, and the only feedstock suitable to be printed is the constituted by the lowest size of powder steel. The increase in mean particle size caused a decrease of viscosity, which could be beneficial for printing, but also contributes to a decrease in elongation and Young modulus, which are detrimental factors. Thus, they concluded that it is apparently more important to preserve a high modulus and elongation than a low viscosity [46]. The same authors, performed another study with 316L steel (D_{50}≈6.5 µm)

and of NdFeB (D_{50}≈1.35 μm), both with 55 vol% of metallic powder, where the filaments were produced and used for 3D printing. Although the concentration of powder in feedstock to be the same, the elongation until break is much higher in the 316L (40%) than in NdFeB (3%). In spite of NdFeB particles to be smaller than 316L ones, the mechanical properties of the 316L are more suitable for printing than NdFeN, having concluded that the nature of powder particles also has a significant role on printing process. *Burkhardt et al.* used the same 55 vol% of 316L powder particles to produce filaments for printing. The authors concluded that due to stresses caused by rapid cooling the parts warped, and it was necessary to control the temperature of the production atmosphere in order to make the printing properly. Pores were observed in the green parts that may be associated with low deposition pressure in printing process, inducing a lack of contact between stands in the same layer and a coarse finish both between layers and in the last layer, which may be associated also to processing parameters. A comparative study of surface finishing by sandpaper, sandblasting and laser polishing was performed, where the most effective was the laser treatment. With this type of polishing, the polymer surface is re-melted, which attenuates the effect of the layer separations. After sintering, the parts had a linear contraction of 19% [47].

In conclusion, MEX encompasses five main steps, each one has its own set of optimal parameters that dictate the quality of the final product. Thus, it is crucial to deep study each one of them. Mixing, where a methodology similar to PIM was used; extrusion to produce the filament; printing, to shape the 3D object; debinding, to ustulate all the binder and additives and sintering to consolidate the metallic particles and get a bulk product. In this work, where the material being processed is NiTi, a sixth step could be made, training, where the shape memory or superelastic behaviours are tested. Figure 12 depicts the workflow of MEX of NiTi.

Despite the enormous importance that could be the production of 3Dobjects from NiTi powder, the state of art highlights the absence of any research work concerning the optimization of MEX applied to the NiTi powder (shape memory alloy). In particular, due to the enormous difficult of manufacturing NiTi from bulk (replicative (foundry, plastic deformation), subtractive (machining)) and powder.

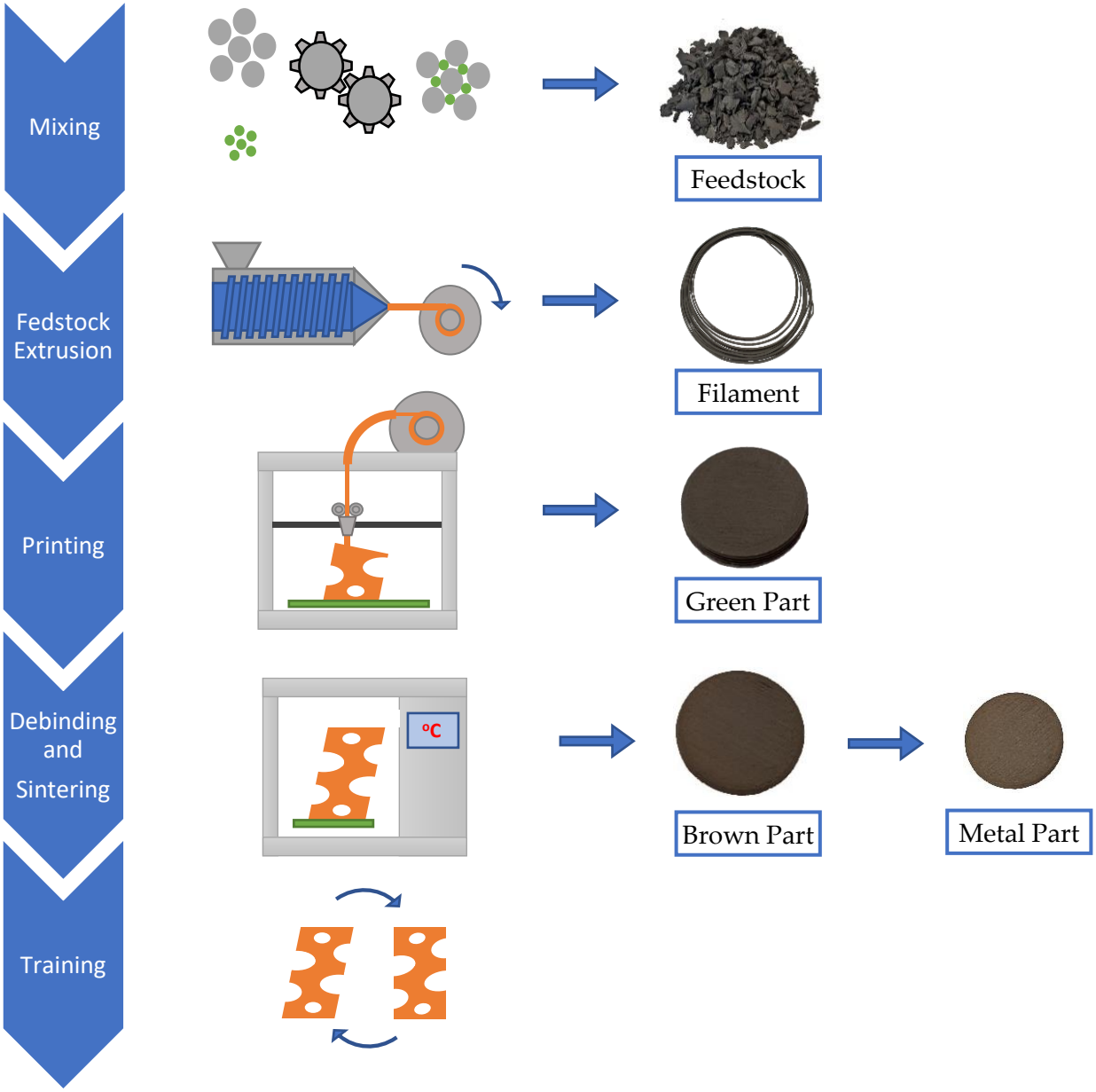

Figure 12. Workflow of metal extrusion of NiTi .

CHAPTER II

Experimental Techniques and Methods of Analysis

In the present study two main technologies of AM were selected. The first one based on the experience developed up to now in direct processes (SLM). The second one is a new approach to produce 3Dobjects using indirect AM technology based on NiTi powder (MEX), the main objective of this study.

In section 2.1 the techniques selected to the present study are described.

2.1 Selected processing technologies

a. Selective Laser Melting

In this work an SLM125HL from SLM Solutions (D) was the equipment available (Figure 13).

Figure 13. SLM 125HL.

There is a vast literature regarding the optimization of SLM parameters, in what concerns the processing of NiTi powders [76, 80, 92]. The sets of parameters found in literature were used, none was suitable to process the NiTi powder using SLM 125HL. However, it is important to highlight that anyone used the same equipment. Table 1 summarizes the parameters selected to this study.

Table 1. SLM parameters.

Parameters	Value
Size build [mm]	125 x 125 x 125
Laser Type	Fibber Laser: Yb
Laser Power [W]	400 (max)
Scan Speed [mm·s^{-1}]	100-2000
Laser Thickness [mm]	0.02-0.04
Hatch Space [mm]	0.07-0.15
Beam Laser [mm]	0.070-0.100
Inert Gas along the build [m^3·s^{-1}]	8.33×10^{-6} (Ar/N2)
Inert Gas to start the build [m^3·s^{-1}]	1.67×10^{-4} (Ar/N2)

b. Metal Extrusion

The indirect additive process designated by MEX is constituted by five steps as follows: mixing, filament extrusion, shaping, debinding and sintering.

b.1 Mixing

The optimization of the binder and additive contents performed for the NiTi filament production is based on the methodology used to produce feedstocks for PIM. This methodology allows the precise evaluation of the critical powder volume concentration (CPVC) [89, 93, 94]. This correspond to the best viscosity of the feedstock that by one hand enables the injection and by other allows the interaction between particles, after debinding [95, 96]. CPVC is defined as the ratio of the volume of solid particles to the total volume of binder and metallic particles [97]. The concentration of the binder/metallic particles can occur in three different outcomes. When the concentration of binder is excessive there are no interaction between the solid particles (Figure 14a), when the critical powder volume concentration is achieved there are interaction between the particles and all the voids between particles are filled with binder (Figure 14b), finally, when the binder is insufficient there are the formation of voids and the viscosity of the flow suffers a drastic raise (Figure 14c) [97].

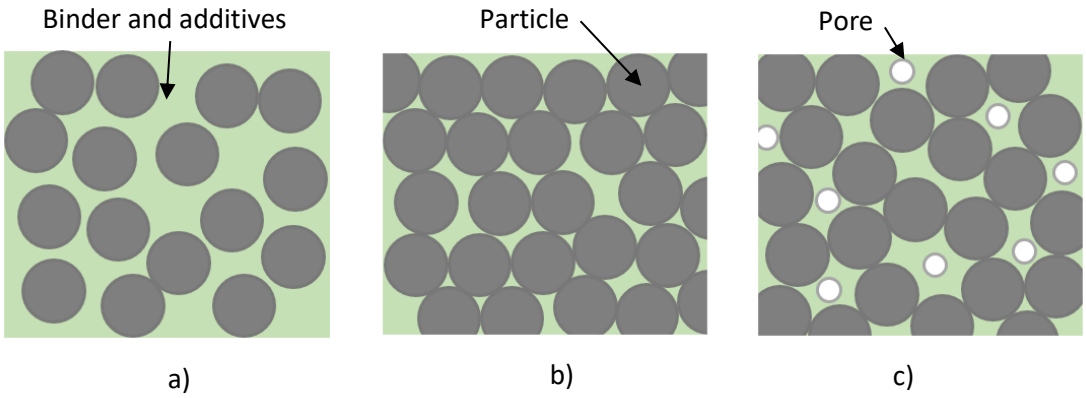

Figure 14. Mixture Binder & additives and Particles a) excessive concentration of binder and additives b) critical concentration of binder and additives c) insufficient concentration of binder and additives (adapted from [96]).

In order to evaluate the CPVC of NiTi powder mixture a torque rheometer (Plastograph Brabender GmbH & Co.) with a selected rotation speed of the blades (30 rpm) and a temperature of 180°C is used (Figure 15). This equipment is constituted by a processing chamber with mixing blades(Figure 15b), an oil temperature controller, and an accessory to control and register data (Figure 15a). The temperature is set by an oil circuit and controlled by a thermocouple placed between the blades. The primary physical property measured in this equipment is the torque, that means the resistance of material to the rotating movement of the blades, during the mixing process. The blades are attached to a dynamometer that measures torque as a function of time. The resulting diagram illustrates the relationship between torque (viscosity) and temperature over the measuring time [98].

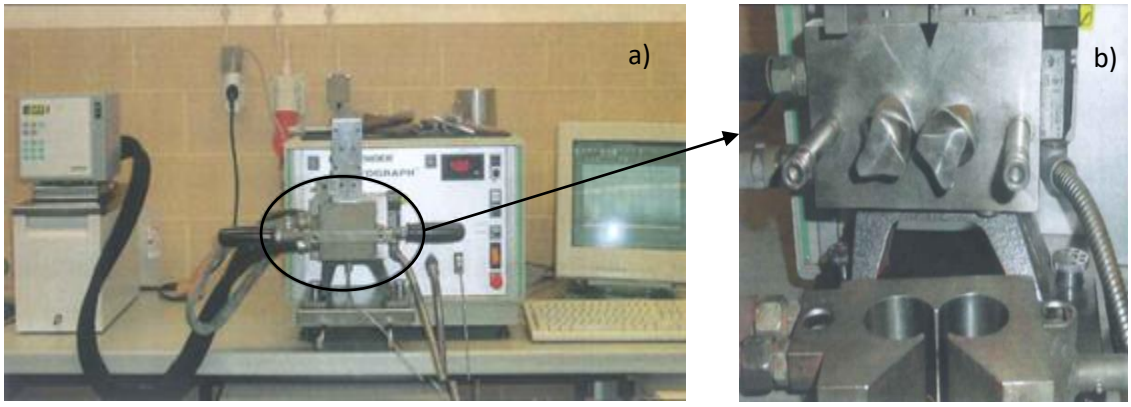

Figure 15. Torque Rheometer Plastograph Brabender GmbH & Co. KG a) full set b) chamber and blades [97].

b.2 Filament production

Figure 16a show the extruder selected to make filaments. The granulated prepared according to b.1 is the feedstock to a single screw extrusion equipment (Brabender GmbH & Co. E 19/25 (D), without calibration system). Where the nozzle has a diameter of 1.75 mm (Figure 16a) (typical diameter in the most used filaments of MEX) and the chamber temperature of 180°C, in according to the temperature for which the torque values of the feedstock were evaluated (b.1).

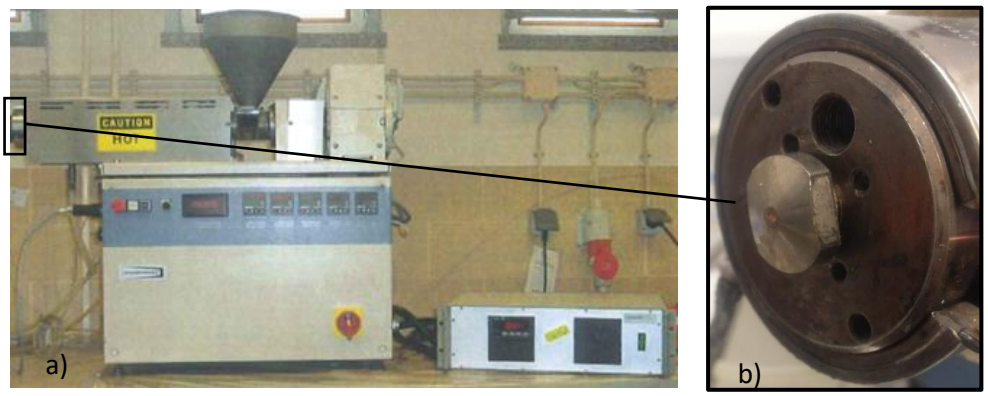

Figure 16. Brabender GmbH & Co. Extruder a) full set b)nozzle detail: diameter of 1.75mm

b.3 Shaping

Shaping is the step where the virtual model is materialized in a 3Dobject. The filament is stored in a coil, that during shaping is pushed through a heated zone in order to create a strand (Figure 17).

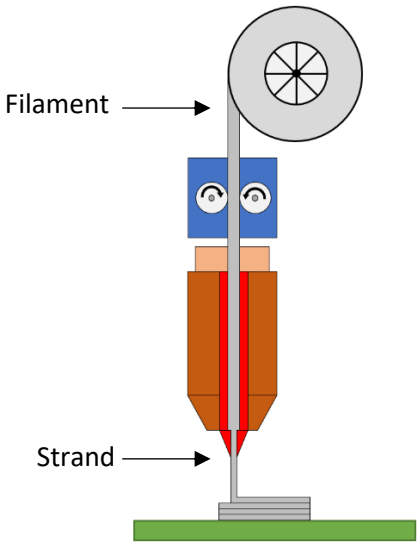

Figure 17. MEX typical equipment.

A successfully shaped 3Dobject (green), oblige to the optimization of the process parameters, in order to ensure quality, dimensional precision and enhance productivity rates reducing production time and costs [99]. This diagram established for FDM can be considered to MEX (Figure 18).

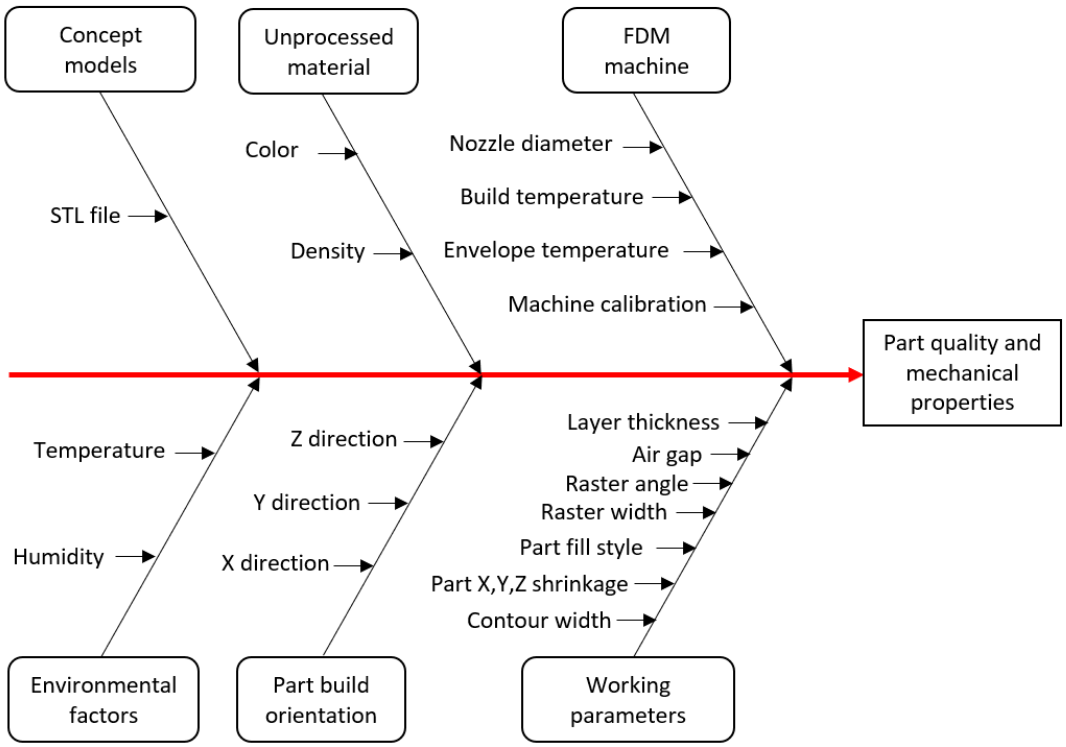

Figure 18. Diagram of FDM process parameters (adapted from [99]).

The selection of the optimal process parameters is a hard and iterative process and are function of many factors like the geometry of the model, the material, the machine, etc.

In the present work NiTi 3Dobjects, are formed layer-by-layer from filaments, were three-dimensionally modelled and translated into an STL file using Solidworks software from Dassault Systèmes [100], and the G-Code was created using the CURA software from Ultimaker B.V. [101]. The printer (Hephestos2 from BQ) had different nozzle diameters: 0.2, 0.4 and 0.8 mm (Figure 19).

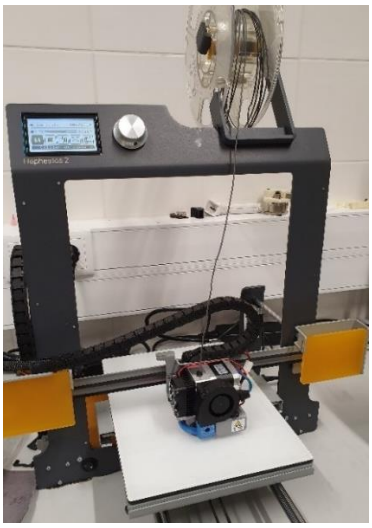

Figure 19. Printer Hephestos 2 shaping NiTi 3Dobjects (green).

b.4 Isostatic Pressing

After shaping, the 3Dobject (green) can be submitted to high pressure conditions in order to decrease the space interlayers. The Isostatic Pressing (IP) was applied in a homemade equipment, working with Argon as the pressure fluid at 200 MPa. The green part was protected with a hermetic and flexible container.

b.5 Debinding

Debinding is the production step where all binder and additives are eliminated from the green parts, creating the brown parts. Depending on the species of the binder and additives [102], several methods can be used to perform the debinding process, being the most actually used the thermal treatment. This step is very important, because any binder residue will act as a contaminant, which could lead in case of NiTi to the precipitation of undesired phases during the sintering stage. Typical binders to process NiTi by PIM are composed by different materials which could be eliminated using more than one debinding process or if thermal debinding, different temperatures (Table 2).

Table 2. Debinding conditions of prealloyed NiTi powders processed by PIM.

Binder/ Space Holder [wt %]	1st debinding step	2nd debinding step	3rd debinding step	Ref.
• 60 Wax • 40 polymer	Capillary force Al_2O_3 150°C 5h	Thermal debinding 480°C 30 min	-	[19]
• 60 Wax • 40 polymer	Capillary forceAl_2O_3 180°C 5h	Thermal debinding 480°C 30 min	-	[20]
• PMMA • NaCl	Thermal debinding 150°C air	NaCl distilled water bath 8h	Thermal debinding 500°C 2h	[21]
• PE Wax • Amide wax • NaCl	Thermal debinding 150°C air	NaCl distilled water bath 8h	Thermal debinding 500°C 2h	[22]
• 55 Parafin • 35 LDPE • 10 SA	Thermal debinding at 230°C 2h Argon	Thermal debinding at 440°C 2h Argon	-	[23]

In the present study the debinding is performed in a MIM3002T from ELNIK Systems furnace (Figure 20). This equipment is the same for sintering. It has 50 litres of volume capacity (retort) and is suitable to operate under primary vacuum (1 Pa) and secondary vacuum (10^{-4} Pa), in an atmosphere of pure H_2, N_2, Ar or mixtures. The furnace has an all-refractory metal hot-zone for a high purity atmosphere and a low temperature distribution of +/- 3°C under gas. In sintering stage, the work temperatures can attain 1500°C.

Figure 20. Sintering/Debinding Furnace [103].

As referred the thermal cycle of the debinding must eliminate all the organic binder and additives. However, this elimination should be step by step to not disturb the geometry selected. In consequence, it is necessary to evaluate the temperatures corresponding to loss of weight

due to degradation/ustulation of different feedstock components. The thermal treatment used in debinding is previously established from the results of thermal gravimetric analysis (TGA). The atmosphere must be similar to the debinding step. Nevertheless, it was not possible to have access to a TGA equipment that could operate with hydrogen. Concerning the heating rate, parameter very important to an effective debinding, 10°C·min^{-1} was selected. The maximum temperature is normally less than 800°C. The debinding finish starts the sintering cycle.

b.6 Sintering

Sintering is the phenomenon resulting from the tendency of the particulate systems to decrease their free energy [104]. It is a spontaneous process, but it is accelerated by increasing temperature. The sintering step is where the powder particles of the brown parts, mainly by diffusion mechanisms but also by other atomic transport mechanisms, are bonded together, resulting in a theoretical dense object [29]. The finer the particle powder the faster is the kinetic rate of sintering [55, 105]. Because temperature is involved, grain growth also has a role on the sintering properties. Powders with a narrower starting particle size distribution exhibited a lower sintering rate prior to the occurrence of grain growth, but a higher densification rate after the grain growth took place [106]. Small particles are desirable to allow sinter densification[102]. Also regarding densification, shape factor of 1 is preferable, in other words, the more spherical the particles, the more dense parts are after sintering [107].

When sintering NiTi, which are very sensitive, there are some precautions to consider. During the cooling stage, after sintering, as it usually is a slow process depending on the size and properties of either the furnace or 3Dobjects, the passage through the range of 650 to 630 °C is very slow. This temperature window is known because is where the precipitation of Ni_4Ti_3 occurs, and in this case unavoidable. However, NiTi objects can be post annealed at defined temperatures in order to reset the elements to the metallic matrix [55]. In addition, the transformation can be into two steps, on cooling or on heating, because an intermediate R phase transformation can occur. The R phase results from the presence of precipitates in the as-sintered part. NiTi with Ni content exceeding 50.5 at% decomposes when slowly cooled from high temperature or during aging below 700°C [108]. During furnace cooling, this critical temperature region is probably passed through slowly enough to allow precipitation. The presence of a fine distribution of coherent Ni_4Ti_3 precipitates is known to be one of the factors to origin R phase in NiTi.

The sintering atmosphere is also very important, since it performs two major roles, protecting the NiTi from reacting with other elements and removing the burnout products by sweeping them away [109]. Contaminants present during sintering, like oxygen, carbon and nitrogen that are almost insoluble in NiTi could lead to the formation of other phases. Oxygen

contents higher than 0.045 at% lead to the formation of the $Ti_4Ni_2O_x$ oxides, giving rise to embrittlement of NiTi. Three atmospheres are more commonly used for sintering: vacuum (oxygen and nitrogen very low content), argon or hydrogen. None was identified as being the most suitable atmosphere to use in NiTi, although, using vacuum in MEX shaped 3Dobjects could lead to layer detachment. Argon is also used, and since it is inert it will prevent the formation of precipitates. On the other hand, studies show that it retards sintering densification, as it fills the pores and compromises to attain the highest densification [109]. No previous studies about sintering NiTi with a total atmosphere of hydrogen were found in literature. In the present work, as a novelty, debinding and sintering will be performed in a 100% hydrogen atmosphere.

In Table 3 is listed the latest sintering and post processing conditions for NiTi from elemental powder mixing, and the final phases achieved.

Table 3. Sintering and post processing conditions of elemental NiTi powder and final phases.

Temp [°C]	Holding time [h]	Atmosphere [Pa]	Post-processing	Binder/space holder [wt%]	CPVC binder [vol%]	Phases	Ref.
800	1	Vacuum (3×10^{-5})	-	-	-	• NiTi • Ni+Ti • $NiTi_2/Ni_2Ti_4O_x$ • Ni_3Ti • Ni_4Ti_3	[110]
900 950 1000 1100 1200	2		-			• NiTi • $NiTi_2/Ni_2Ti_4O_x$ • Ni_3Ti	
1100 1200			1000°C 6h vacuum				
750	6	Vacuum (1.3×10^{-5})	-	-	-	• $NiTi_2/Ni_2Ti_4O_x$ • Ni+Ti	[111]
850						• $NiTi_2/Ni_2Ti_4O_x$ • Ni_3Ti • NiTi • Ni+Ti	
950						• $NiTi_2/Ni_2Ti_4O_x$ • Ni_3Ti • NiTi • Ni	
1080						• $NiTi_2/Ni_2Ti_4O_x$ • Ni_3Ti • NiTi	
1050	0.5	Vacuum (3×10^{-5})	-	-	-	• NiTi • Ni_3Ti • Ni_3Ti_2 • Ni_4Ti_3	[112]
	4						
	0.5		• Heated 1050°C 2h • Water quenching			• NiTi • Ni_4Ti_3 • Ti_2Ni	
	4						
980	9	Vacuum ($1.2\text{-}2.8 \times 10^{-4}$)	-	NaCl	50	• NiTi • $NiTi_2/Ni_2Ti_4O_x$ • Ni_3Ti • Ni_4Ti_3	[113]
1020	1		• Heated 1000°C 1h • Iced Water quenching • Aging 400°C 1h • Water quenching				

When using elemental powders to obtain NiTi, usually no binder is used, although for specific applications additives can be used (e.g. space holders to create porosity [113]), since its

components could react with the elemental Ni-Ti and consequently lead to the formation of secondary phases. By the other hand, when using NiTi prealloyed powders, binder and additives are commonly used. In Table 4 are the latest sintering and post processing conditions, as well as the final phases achieved, when the starting powder is a prealloyed NiTi.

Table 4. Sintering and post processing conditions of prealloyed NiTi powder and final phases.

Temp [°C]	Holding time [h]	Atmosphere [Pa]	Post-processing	Binder/space holder [wt%]	CPVC binder [vol%]	Phases	Ref.
1250	10	Vacuum (1×10^{-2})	-	• 60 Wax • 40 polymer	• 35	• NiTi • $NiTi_2/Ni_2Ti_4O_x$ • TiC	[19]
1270	5	Argon Flow	HIP 1050°C 3 h 195 MPa				
1100	5	Vacuum (-)	• Solution treatment 850°C 1 h • Annealing 550°C 1 h • Water quenching	• 60 Wax • 40 polymer	-	• NiTi • $NiTi_2/Ni_2Ti_4O_x$ • TiC • Ni_3Ti • Ni_4Ti_3	[20]
1200							
1270							
1100		Argon Flow (-)					
1200							
1270							
1250	10	Vacuum (-)	-			• NiTi • $NiTi_2/Ni_2Ti_4O_x$ • Ni_4Ti_3	
1250	10	Vacuum (1×10^{-3})	-	• PMMA • NaCl	• 20-25	• NiTi • $NiTi_2/Ni_2Ti_4O_x$ • TiC	[21]
1250	10	Vacuum (1×10^{-3})	-	• PE Wax • Amide wax • NaCl	• 25-28	• NiTi • $NiTi_2/Ni_2Ti_4O_x$ • TiC	[22]
1265							
1260	4	Argon Flow (-)	-	• 55 Parafin • 35 LDPE • 10 SA	-	• NiTi • $NiTi_2/Ni_2Ti_4O_x$ • TiC • Ni_4Ti_3	[23]

In this work, after debinding, the brown is sintered in a hydrogen atmosphere at different temperatures and holding times (1100°C (1h), 1165°C (1h and 5h) and 1270°C (5h)). The sintering is performed with a heating and cooling rate of $5°Cmin^{-1}$.

2.2 Characterization from powder to final NiTi 3Dobject

The NiTi powder can be made using elemental (Ni, Ti) powder mixtures or prealloyed one. Ni and Ti powder could be desirable due to their low prices and also the possibility during

process to change the content of each element and therefore the final properties [34]. Although, it is much more difficult to control the composition changes during processing. Moreover, in MEX elemental powder is much more susceptible to reaction with the binder/additives and environmental atmosphere. The prealloyed powder has already a defined composition and some problems can be avoided with its use. In the present study prealloyed powder was selected.

a. NiTi powder mixture

NiTi prealloyed powder could be used without other powder additions. However, as in elemental powder (Ni+Ti) the presence of TiH_2 and/or Ni could be also used as an adjustment of the chemical composition, in order to avoid the formation other phases rather than NiTi.

a.1 NiTi master powder

NiTi is a binary intermetallic compound (SMA). Several methods are used to produce prealloyed NiTi powder particles, such as mechanical attrition, hydriding, water/gas/plasma atomization, induction (EIGA), etc [12].

In the present study two different powders are available, the first (LPW) resulting from atomisation and a second one (AE) that the process was not provided by the supplier (confidential). The characteristics of powder (LPW) and (AE) were evaluated concerning the 4Ss (particle size, particle size distribution, shape, structure). Table 5 summarize the chemical composition of the supplied powders.

Table 5. Chemical composition of NiTi powder LPW [114] and powder AE [115].

	Powder LPW	Powder AE
Element	[wt%]	
Ni	57.141	55.957
Ti	41.602	43.065
Al	0.746	0.724
Mg	0.261	-
Si	0.102	0.104
Cr	0.065	0.066
Co	0.044	0.047
Fe	0.035	0.033
Zr	0.004	0.004

The density of the powder LPW was 6375 kgm^{-3} (after magnetic separation due to presence of Ni particles (8908 kgm^{-3})), and its specific surface area was 293.4 m^2kg^{-1} (Table 6). By one hand the highest values of specific surface area means the best sintering kinetics, high density after sintering [55] and good surface finish [102]. On the other hand, the powder is more susceptible to impurity pickup [12]. The bulk density attributed to NiTi is 6450 kgm^{-3}, this difference of powder densities may result from the variable content of one or more phases in the prealloyed powder, which can include a secondary intermetallic phase that may occur during the synthesis of NiTi. The density of the powder B was 6194 kgm^{-3} and its specific surface area was 3633 m^2kg^{-1} (Table 6). In fact, structural analysis by X-ray diffraction of the prealloyed powder LPW revealed other phases other than NiTi and Ni; it also included $NiTi_2$ (5640 kgm^{-3}) (Figure 21), against powder AE where NiTi is the unique phase (Figure 22).

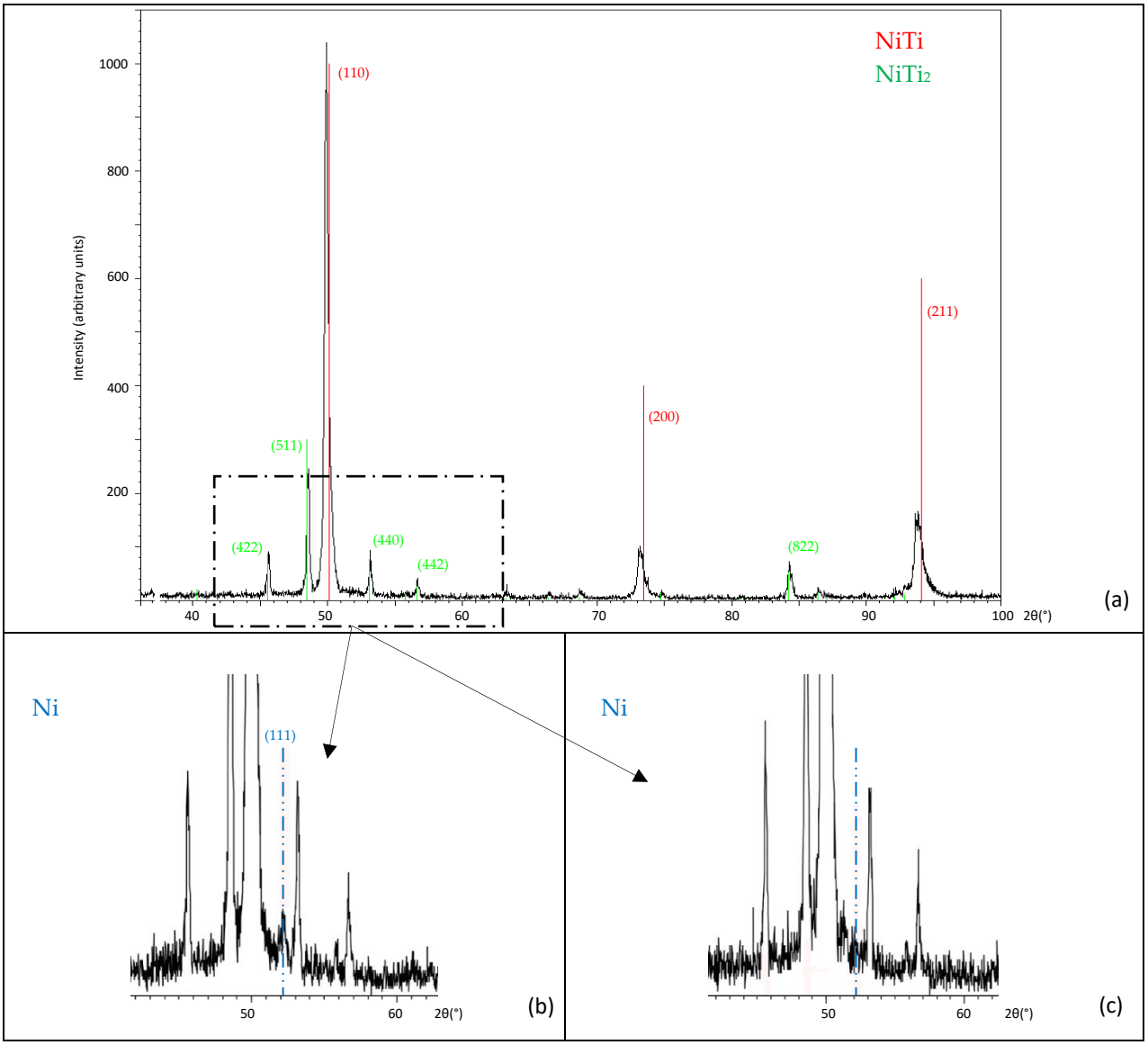

Figure 21. X-ray diffractogram of prealloyed NiTi powder LPW containing a) NiTi and $NiTi_2$ b) Ni c) Ni after magnetic separation.

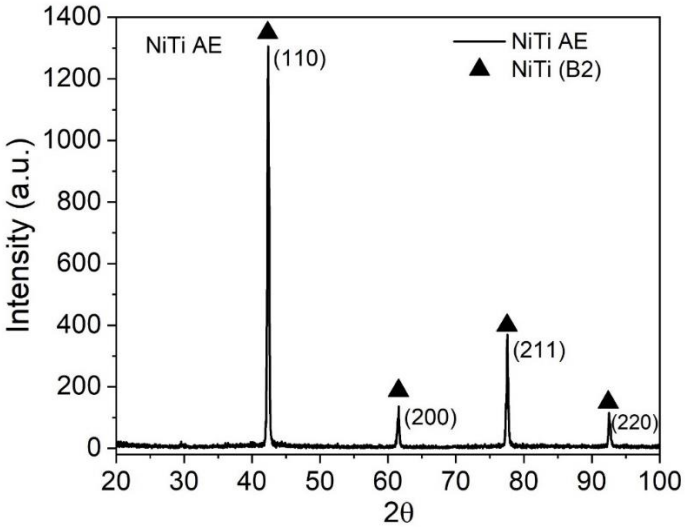

Figure 22. X-ray diffractogram of prealloyed NiTi powder AE.

Table 6, Figure 23 and Figure 24 show the powder particle size, particle size distribution, specific surface and density of powder LPW and AE.

Table 6. NiTi prealloyed powder particle size, particle size distribution, specific surface area (SSA) and density of powder LPW and AE.

	Powder LPW	Powder AE
Density [$kg \cdot m^{-3}$]	6375±139	6194±46
D_{10} [µm]	13.4	0.8
D_{50} [µm]	22.1	2.7
D_{90} [µm]	34.7	7.6
SSA [$m^2 \cdot kg^{-1}$]	293.4	3633.0

* Specific surface area (**SSA**) is a property of solids defined as the total surface area of a material per unit of mass.

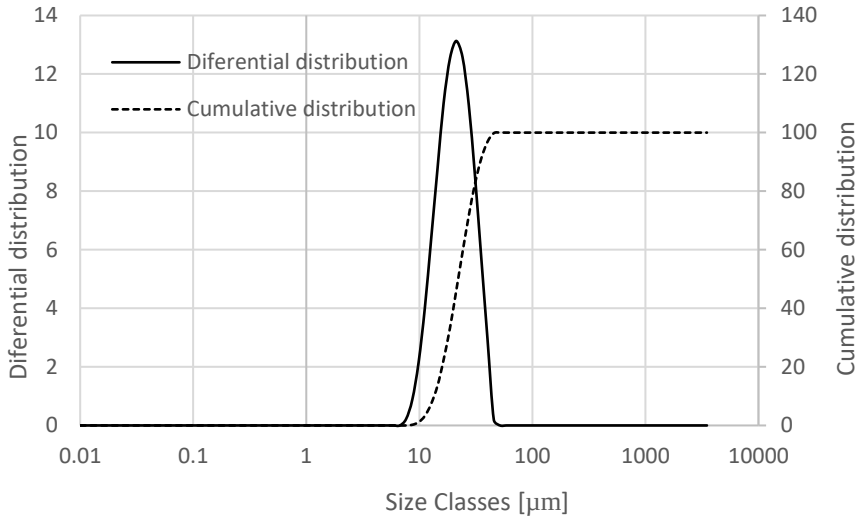

Figure 23. Powder particle size and particle size distribution of NiTi powder LPW.

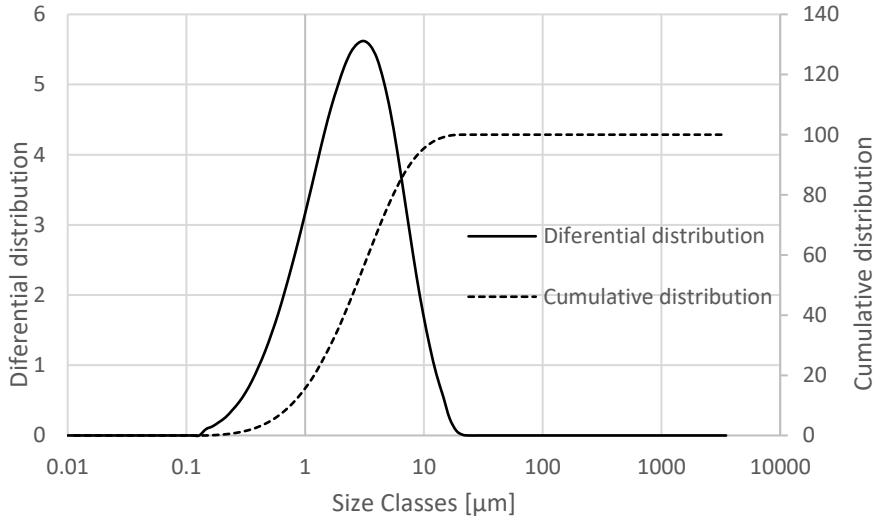

Figure 24. Powder particle size and particle size distribution of NiTi powder AE.

Regarding powder LPW, from the cumulative distribution is observed that the biggest particles are lower than 51.8 µm and from the differential distribution that 50% are inferior to 22.1 µm. About powder AE, from the cumulative distribution is observed that the biggest particles are inferior in size than 24.1 [µm] and from the differential distribution that 50% are inferior to 2.7 [µm]. Particle distribution has a high impact on the sintering stage. The D_{50} gives the information that less than half of the particles in the lot have 22.1 µm. The above-mentioned sizes of particles of the powder LPW are typical for direct additive manufacturing processes (*i.e.,* SLM, EBM). The powder AE could be used only in indirect process, but the particles are very small and could induce agglomeration that is not adequate to mixing and sintering stages.

Figure 25 depicts the particles shape of powder LPW (a,b) and AE (c,d), which are apparently spherical, with a shape factor close to 1. Spherical particles are preferable to obtain

high densification after sintering [107], and have better rheological behaviour compared to irregular particles [116].

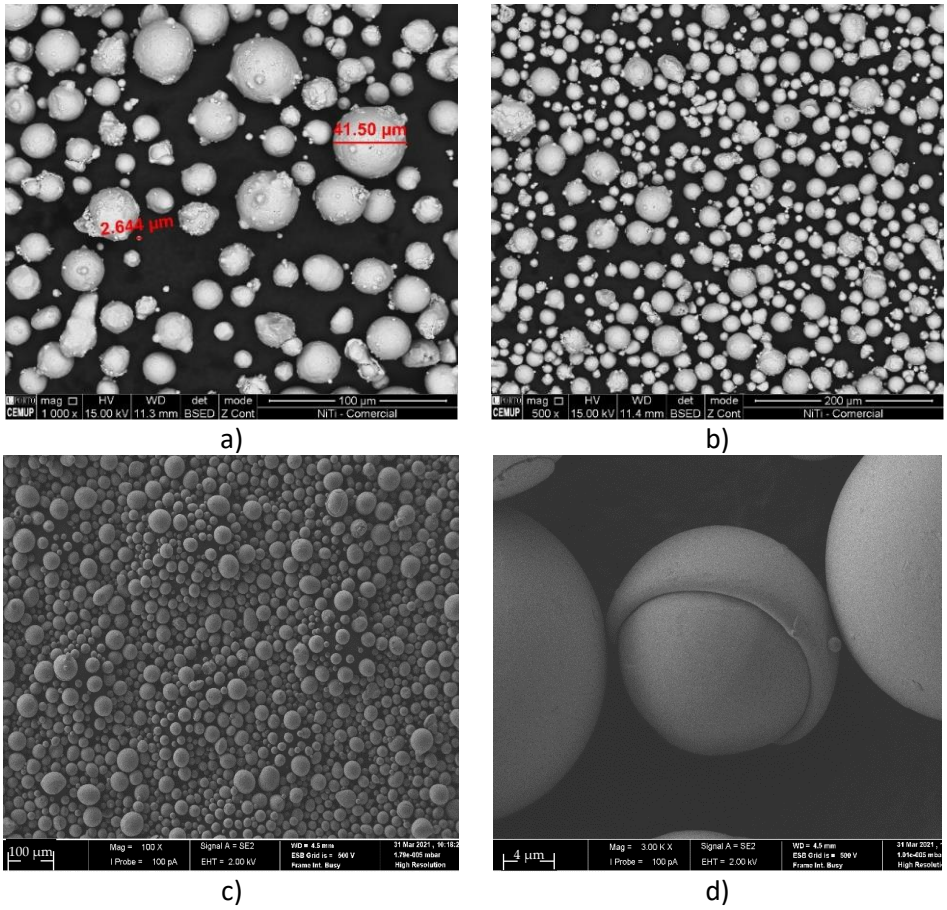

Figure 25. Shape of prealloyed NiTi powder particles a) b) powder LPW c) d) powder AE.

Aside with the presence of other elements and/or phases causing deviation in the density, are hollow particles (Figure 26). These particles can be formed during molten metal atomization due to the atmosphere of processing that could be captured in the liquid drops, usually Ar is used. During the throwing process of the liquid drops, argon will expand until the drops solidify, and then the hollow powder particles are formed. In 3Dobject where high density is a priority these particles are a clear disadvantage. Nevertheless, if properties like low density, good energy absorption, thermal exchange capability, and a high ratio of strength to weight is required, hollow particles should be an advantage [117].

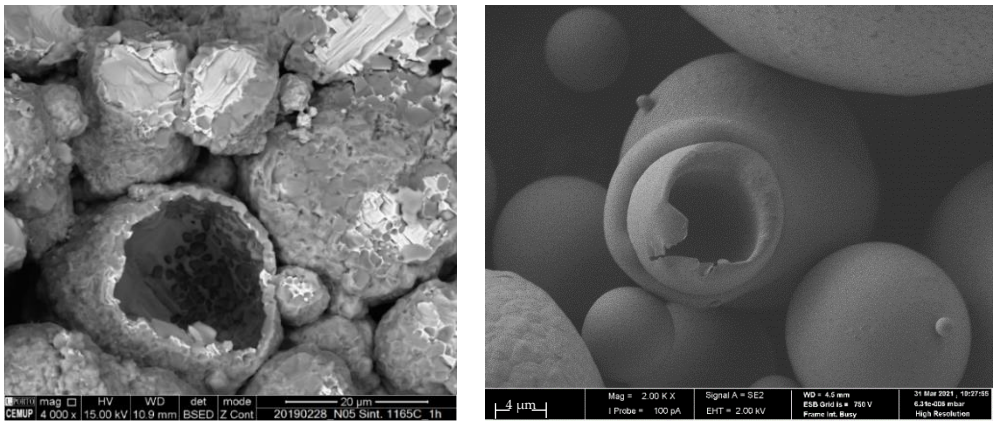

a) b)

Figure 26. NiTi hollow particles a) powder LPW b) powder AE.

Particle size and distribution showed that powder LPW with particle sizes around 45 µm is more suitable for SLM processing [118]. However, powder AE which present smaller particles, and high SSA in according to other studies is expected to be more adequate for MEX, in particularly during the sintering stage. Moreover, the structural analysis reveal that powder AE only show the presence of NiTi B2, while powder LPW showed other secondary phases.

Consolidation of sintered 3Dobjects can be achieved by HIP, which causes compressive distortions of the thin-walled hollow powder particles, by vacuum sintering, which needs a prolonged high-temperature treatment to achieve strong particle–particle bond or by liquid-phase sintering which is the preferential method [119] or can be separated from the dense particles by the floatation method [120].

In MEX technology, against all expectations, preliminary tests with filaments made from powder LPW showed better results than powder AE. 3Dobjects made from powder AE showed a lack of contact inter-particles, becoming fragile. Although powder AE was apparently the best candidate for production 3Dobjects by MEX, those resulting from powder LPW showed the best integrity and mechanical properties. Therefore, powder LPW was selected to highlight the role of MEX in AM of NiTi by SDS.

a.2 Other additions: Titanium Hydride (TiH_2) and Nickel (Ni)

Two different powder particles (TiH_2 and Ni) were added to the NiTi prealloyed powder to balance its chemical composition avoiding the formation of unsuitable phases. Figure 27 and Table 7 show the phase composition (X-ray diffractograms) and other characteristics of the powder TiH_2 and Ni, respectively.

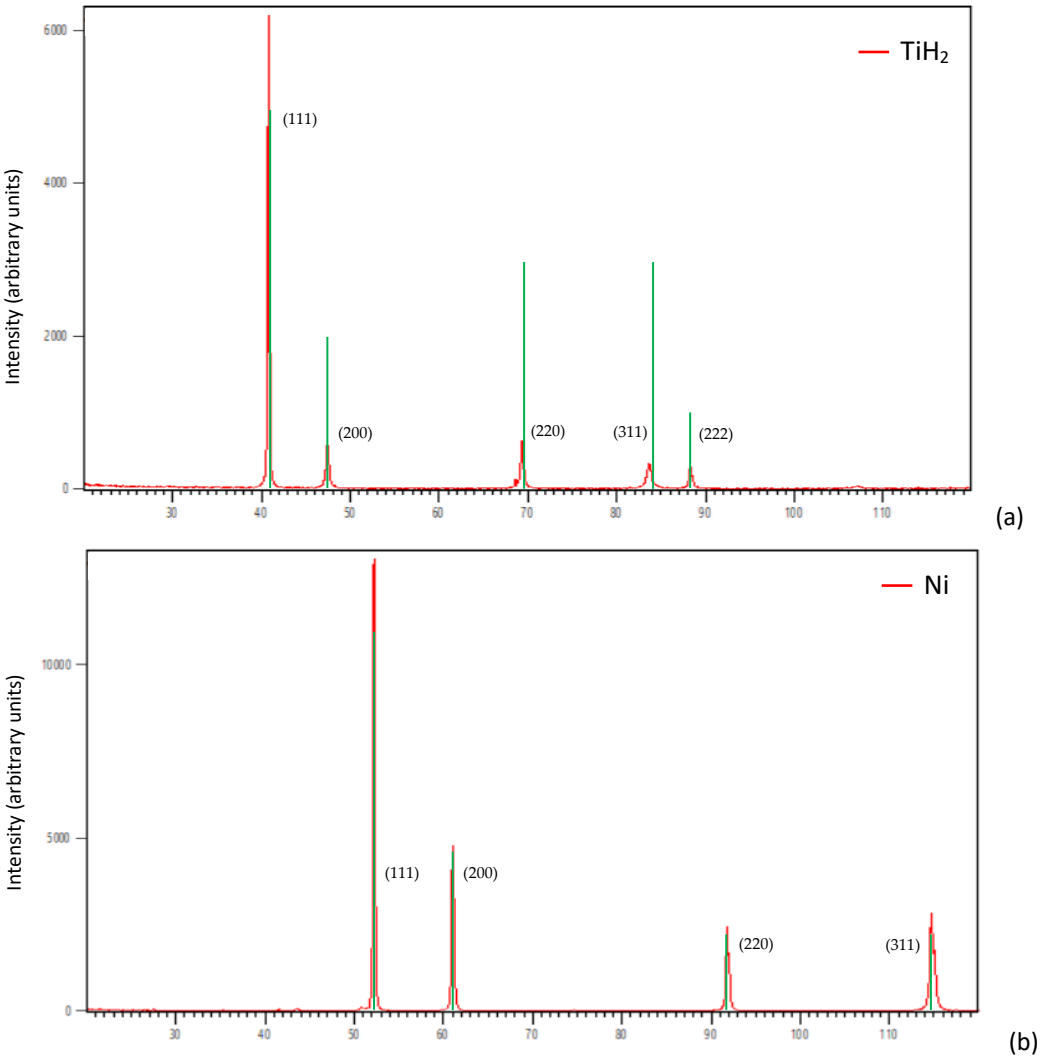

Figure 27. X-ray diffractograms of powders a) TiH_2 b) Ni.

Table 7. TiH_2 and Ni powders particles size, particle size distribution and specific surface area (SSA).

	TiH2	Ni
D_{10} [µm]	3.44	21.4
D_{50} [µm]	15.3	30.0
D_{90} [µm]	35.7	41.2
SSA [m^2kg^{-1}]	750.2	207.7

b. Binder and additives

First of all, it will be defined the concept associated to binder and additive. Master binder is a mixing of different polymer, with or without other organic materials (paraffin, stearic acid, etc) used to improve the connection between metallic or ceramic powder particles in green

bodies. On the other hand, additive is the denomination associated to the improvement of some properties of the mixing (toughness, stiffness, etc) essentially to handling, *i.e.,* filaments. The optimization of the NiTi filament master binder and additive content (feedstock) was performed using the same methodology for PIM feedstocks preparation, by evaluating the CPVC. Previous tests were already performed where the powder was stainless steel reinforced with carbon nanotubes and unenforced [89, 104, 121]. All feedstocks used as master binder M1 trademark from Atect® Company, Higashiomi, Japan. Moreover, in order to achieve suitable filament toughness and flexibility for storage and use in the MEX, polymeric additives were added to the filament feedstock, including a thermoplastic elastomer (TPE) and a plasticizer (P). The new metallic powder and additives oblige to new research concerning the evaluation of CPVC, and a detail analysis concerning inside homogeneity before and after extrusion (filament and strand to produce the 3Dobject layer by layer).

In Table 8 is described the volume content of each main components in the feedstock.

Table 8. Feedstock composition (vol%) [89].

		Binder mixture [vol%]	Feedstock [vol%]
	NiTi (LPW+AE)		60
	Binder + additives		40
Binder mixture	M1 (polyolefin waxes and ethylenic polymers)	77.5	31
	Elastomer (TPE)	17.5	7
	Plasticizer	5	2

The master binder used in this work has a density of 969 kgm^{-3}, and any thermal process up to 600°C is enabled to remove it completely [104, 121]. Polyolefin waxes and ethylenic polymers are responsible for connecting the metallic particles powder holding the shape of 3Dobject. Dispersant agents, compatibilizers, and stabilizers can be used, to disperse the metallic particles in the polymeric binder, preventing agglomeration and phase separation [122]. If the feedstock has high viscosity, stearic acid (SA) can integrate the chemical composition of the feedstock. SA is very used in PIM feedstocks, as a dispersant, once it reduces inter-particle forces and lubricate the powder [89, 97], and can be removed by thermal debinding [123]. Although total ustulation is expected during debinding of master binder at 600°C, this temperature is not suitable for total elimination of the residues of the SA, that can act as a contaminant of the metallic powder. The solution could be to improve debinding temperature (950°C) [121]. The binder and additives greatly influences the production process and the quality of the sintered parts, even though, it should be completely removed during the debinding step [122] and without carbon residue [89]. If binder removal is incomplete, the trapped polymeric

residues will be a contamination source [124]. This must be a condition to fully be fulfilled because the affinity of carbon to titanium will lead to the precipitation of TiC. The feedstock selected to produce filaments of stainless-steel powder was tested and it was evident that all the organic components from master binder and additives disappeared at debinding temperature (600°C)[89]. The thermal analysis is crucial to understand the thermal behaviour of the binder and additives. They must be completely removed in order to obtain total density of the metal powder and to prevent contamination from carbon residue. The TGA highlights the different kinetics of the debinding of binder (M1) and additives (TPE, P).

In general, the filament has Ø1.75 mm and is supplied in standard coil that fit in every MEX equipment. The filament has to present suitable mechanical toughness, to allow it to be rolled and unrolled from the coil, and during processing to withstand the pull from the deposition system and the push against the nozzle. There must be also a homogeneous distribution of powder particles and the binder and additive components in order to minimize the segregation of powder during processing, which could lead to visual defects, excessive porosity, warpage and cracks and anisotropic shrinkage after debinding and sintering [125].

2.3Characterization Techniques

The different characteristics and properties of the material selected, during different steps of additive manufacturing are evaluated using different equipment. The description of the techniques and methodologies adopted are described below.

a. Chemical composition

The powder chemical composition was evaluated by x-ray Fluorescence (XRF). The method is fast, accurate and non-destructive. The precision and reproducibility of XRF analysis is very high if good standard specimens are available but also in applications where no specific standards can be found, the concentration range goes from sub-ppm levels to 100%. Elements with high atomic numbers have better detection limits than lighter elements. The system used in present work was a Panalytical AXIOS-Advanced WDXRF (wavelength dispersive) spectrometer (UK) fitted with an SST-MAX x-ray source (rhodium target) with a 4kW output and operating at 160 mA. The AXIOS uses SuperQ software for standard-based analysis and has a standard-less software module called OMNIAN capable of giving the complete composition and quantification of most types of materials.

b. Density

The real or theorical density is defined as mass per unit volume of a material, excluding open and closed pores. The equipment used to measure the density of the metallic powders was a Pycnometer, Micromeritrics Accupyc 1330 (USA). This equipment uses the gas displacement technique, helium. The pressure observed upon filling the chamber and then discharging it into a second empty chamber allow computation of the solid phase volume. Helium molecules rapidly fill the tiniest pores of the body and only the solid phase displaces the gas. The mass is measured on a high-quality scale and is registered by the pycnometer software, that together with the measured volume, gives the density.

c. Particle size distribution

The powder Particle Size Distribution (PSD) was evaluated by Laser Diffraction Spectrometry (LDS) on a Malvern Instruments Mastersizer 3000 (UK). By focusing a laser beam on a particle, the diffracted spectrum is analysed by a receiver and by using the suitable theory, particle size distribution can be achieved. The Fraunhofer diffraction theory, states that the angle of diffraction of light scattered by a particle is inversely proportional to the particle size [104]. This technique uses a dispersion media, in the present work water was used. The distributions are quantified in D_{10}, D_{50} and D_{90}, meaning that 10, 50 and 90% of the particles have size inferior to this measure.

d. Specific surface area

The specific surface area per unit weight (SSA), is a characteristic that help to understand powder reactivity. The value of SSA depends on the characteristics of the powder particles, like size, shape and porosity. For the same volume of solids, small particles have a higher SSA than larger ones. This gives an indirect information for instance, about reactivity and powder ability to sinter. A very large specific surface is more propitious to attain the high sintering density [55], meaning that the process will be faster [104, 105] and the 3Dobject will have low porosity [102, 106].

e. Phase composition

X-ray diffraction (XRD) is a technique for characterizing crystalline materials. It provides information on structure, phase, crystal orientation and other structural parameters, such as

crystallinity, strain, and crystal defects. X-ray diffraction peaks are produced by constructive interference of a monochromatic beam of X-rays scattered at specific angles from each set of lattice planes. The peak intensities are determined by the atomic positions within the lattice planes [126]. The information is represented in a diffractogram that follows the Bragg equation:

$$n\lambda = 2d_{hkl} \sin\theta$$

where n is an integer number representing the diffraction order, λ is the wavelength of the anticathode, d_{hkl} is the interplanar spacing of the analysed crystal and θ is the angle of the diffraction (Bragg angle) [104]. The diffractogram is then compared with a database (International Centre for Diffraction Data - ICDD) in order to identify the phases, present in the material.

In this work a Philips X'Pert diffractometer (UK) was used with cobalt anticathode with wavelengths $\lambda(k_{\alpha 1})$ = 1.78897 nm and $\lambda(k_{\alpha 2})$ = 1.79285 nm. The potential to accelerate the electrons was 40 kV with a current intensity of 35 mA and according to the Bragg-Brentano geometry $(\theta - 2\theta)$. The scanning range was from 20° to 100° in steps of 0.25° with acquisition time of 1 second in each step.

f. Microstructure

Two kinds of microscopy were used in the present study, optical (OM-Leica ICC50 W(D)) and scanning electron microscopy (SEM- FEI Quanta 400 FEG ESEM /EDAX Genesis (USA), (CEMUP). This technology with better resolution than optical one, has as electron beam with a spot size of less than 10 nm and a depth of 1 μm that applied on the surface of a specimen generates the signals able to produce high magnification images. The beam electron–specimen interactions produce the backscattered electrons (BSE), secondary electrons (SE), and x-rays that are collected by proper detectors, and convey information about the specimen, such as topographic features (SE), composition (BSE) and crystal structure. The use of SEM allowed assessing the particle morphology and microstructural details of different stages of the processing of NiTi specimens. Electron Backscattered Diffraction (EBSD) images and Energy Dispersive Spectroscopy (EDS) elemental maps were some of the functionalities capable to obtain extra information about the chemical composition and phase distribution.

g. X-ray microcomputed tomography (Micro-CT)

Microtomography is an X-ray technique in which shadows of superimposed structures are blurred out by a moving X-ray tube [127]. An X-ray generator emits the X-rays that travel through the 3Dobject and are recorded by a detector to produce radiographs. By an iterated

process, the 3Dobject is rotated by a fraction of degree and another projection image is taken at the new position until it completes 180 or 360°, producing a series of projection images. These are then processed using computer software to show the internal structure of the 3Dobject non-destructively. The reconstructed images can then be used to build a 3D volumetric object for quantitative analysis or visualization [128].

The filament was micro-CT scanned using a Bruker SkyScan 1275 (Bruker, Kontich (B)). An acceleration voltage of 80 kV and a beam current of 125 µA was set while using a 1 mm aluminium filter and step-and-shoot mode. Pixel size was set to 6 µm, and random mode was used. The images were acquired at 0.2° angular step with 5 frames average per step using an exposure time of 46 ms. The micro-CT images were reconstructed with the dedicated manufacturer software.

Figure 28. Micro-CT (X-ray microcomputed tomography) equipment.

h. Thermal Analysis

TGA was performed in master binder, M1, plasticizer and elastomer, individually. Also, to the feedstock, already with the metallic particles was thermo analysed. TGA is essential to define the thermal cycle for debinding. TGA works by detecting weight changes resulting from decomposition, vaporization, sublimation, chemical reactions, etc. The equipment used was a Setaram Setsys Evolution(F) (sensibility of 0.1 mg), with an Al_2O_3 crucible in an Ar+H_2 or Nitrogen atmosphere.

i. Mechanical Characterization

The mechanical characterization was performed by tensile, flexural tests and hardness on 20 filament specimens. Tensile and flexural tests had 25 mm in length, that they were randomly removed from the filament coil. The filaments were mechanically tested with a TA.XTplusC analyser (Stable Micro Systems, Godalming, UK (Figure 29) at a speed of 0.5 mms^{-1} at room temperature (22°C).

(a) (b)

Figure 29. TA.XTplusC analyser a) flexural test (3-point bending) b) tensile test.

Tensile and flexural ultimate strengths were measured and used to calculate the Weibull index, and the tensile stress/strain curve was evaluated to define the Young's Modulus, between 25 and 50 % of ultimate strength value, applied to filaments.

Microhardness equipment from Fisher Instruments (Fischerscope H100, Massachusetts, EUA) was used to evaluate the hardness after sintering. A nominal load of 98.07 mN was applied during 15s. The indenter was a Vickers. The indentation depth was measured using a capacitance displacement gauge with an accuracy of 2 nm. During the test, the load was increased in steps until the nominal test load was reached. The number of steps and the time between them were selected before the test; the first load step was always equal to 0.4 mN. Each specimen was tested 40 times. The mean hardness (MH) and standard deviation (SD) were the values included in the tables. Comparing with microhardness, the same mechanisms of evaluation are used, however, the applied force is very low [104]. Microhardness was performed in highlight polished surfaces*.

*Surfaces resulting from grinding and polishing. The equipment used was a Planopol polisher from Struers. Planopol is a machine for production of plane specimen surfaces by means of mechanical grinding and polishing. A turntable accommodates horizontally rotating exchangeable polishing discs, moved by a two-speed motor. The last polishing was of a suspension of abrasive material, with a D_{50} = 5 and 1 µm.

CHAPTER III

Results and discussion

In the present study, NiTi 3Dobjects are additive manufactured by a direct (SLM) and indirect process (MEX). Two very different technologies to accomplish one goal, to produce 3Dobjects with a unique phase of NiTi. State of the art highlights the difficulties in both technologies. In SLM, due to uncontrolled phenomenon that occurs in the melting pool, resulting from the VED, and in the indirect process (debinding step), mainly due to the conditions in the processing chamber.

Due to the difficulty of maintaining the NiTi characteristics during processing, especially when using subtractive technologies, NiTi bulk is supplied in strips, wires, and ingots. Moreover, the last one is essentially used to make powder particles.

In the additive processes, the main problems associated to SLM, are due to the high values of VED, that can cause evaporation phenomenon and warping with consequential detachment of the 3Dobject from the building platform. In SDS productions, the problems arise from the difficulty of performing an efficient debinding and sintering. Therefore, the focus of the present study is to produce 3Dobjects with small dimensions.

3.1 Ni-Ti processed by SLM

Although SLM has been the most studied technology to make 3Dobjects from powder, layer by layer, the present study starts by evaluating the quality of SLM NiTi 3Dobjects by optimizing the processing parameters. The amount of energy deposited (VED) in the powder bed is meticulously studied, based on the vast number of technical and scientific papers as a starting point. Specimen with Ø10x10 [mm] was produced by SLM equipment described in chapter II (Figure 30).

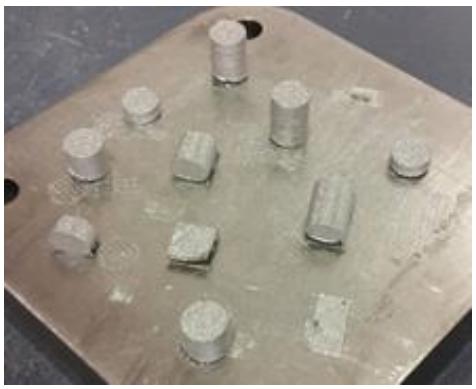

Figure 30. 3Dobjects produced by SLM.

During processing, an energy density of 35 Jmm^{-3} was the best for powder LPW. High values of VED caused the modification of powder particles properties and lower values resulted in an inefficient bound to building platform.

Table 9 summarizes the set of parameters optimized in the study.

Table 9. SLM parameters.

Energy density (VED) [Jmm^{-3}]	Laser Power (P_{ef}) [W]	Scan Speed (v_s) [mms^{-1}]	Hatch Spacing (Δh_s) [mm]	Layer thickness (d_t) [mm]	Spot diameter [mm]
35	50	400	0.12	0.03	0.087

The first layer was most of the time unattached to the powder bed, due to the inexistence of a platform of similar material. Two solutions were adopted to overcome the mismatching between powder bed material (steel or titanium) from the SLM equipment, and NiTi powder.

In fact, this difficulty identified by the tendency of SLM 3Dobjects to warp, gives rise to a lot of distortion in first solidified layers, that have direct contact with the building platform. This phenomenon has direct influence on the construction of the 3Dobject, compromising the correct deposition of remaining layers or even leading to the detachment from the table. Different temperatures between the powder bed and the melting pool are the cause of a continuous flow of heat through the contact area. The solution could be the heating of the platform in order to relieve stress. However, the high diffusion coefficient of titanium in the NiTi phase are responsible for the formation of a layered interface enriched in $NiTi_2$, hindering the use of heated platforms, when they are based on Ti. The solution experienced is only applied to steel platforms.

A new design of the powder bed system was optimized in order to minimize the stress between platform and 3Dobject. The system has its own heater and is built with insulating materials to shield the SLM equipment from the heat (Figure 31a,b).

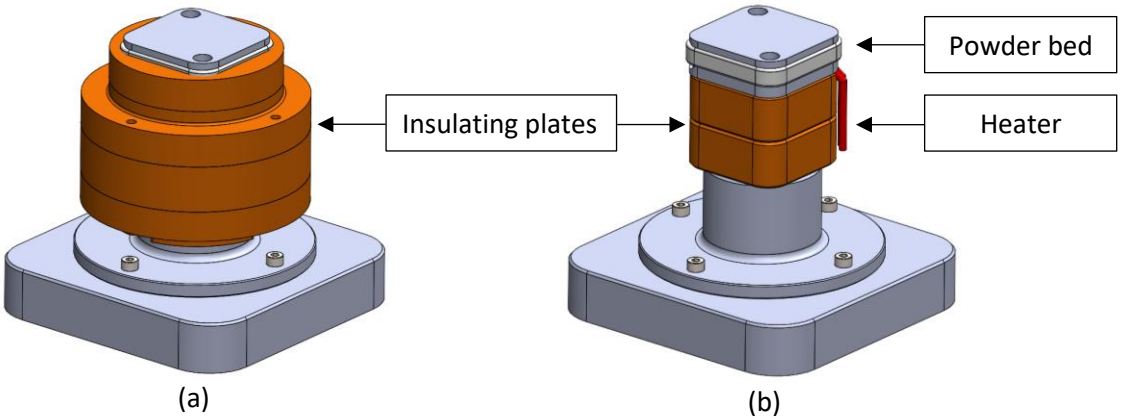

Figure 31. New design for a heated platform a) full set b) inside detail.

With the use of a heater placed inside the powder bed, the heat flow should be minimized, increasing the time of cooling of the first layers, and consequently preventing its warpage. The system was assembled and tested in the SLM equipment (Figure 32).

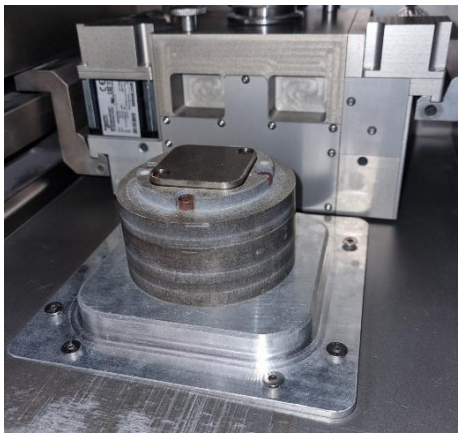

Figure 32. Heated powder bed assembled in SLM equipment.

When the powder bed cannot be heated, due to possible diffusion, a second approach is to change the interface between powder bed material and NiTi. In fact, as refereed the Ti has an enormous tendency to diffuse in NiTi, depending on the temperature and time. In this case, the solution can be the use of an interface, that has properties similar to Ti, but with lower diffusion coefficient.

The tests were performed using a building platform of Ti, NiTi powder particles (sample A), and Ti_6Al_4V as the interface between NiTi and the Ti platform (sample B). The Ti_6Al_4V was proved to be efficient in promoting adhesion between 3Dobjects and building platform. However, some contamination of NiTi was detected (Figure 33).

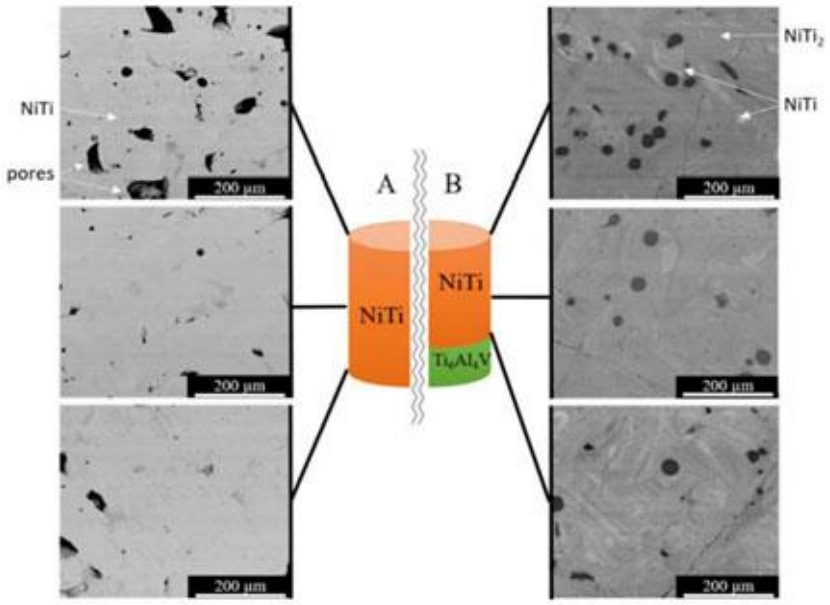

Figure 33. Micrographies of samples produced by SLM.

In both cases, some porosity is visible. Besides porosity in sample B there are some cracks. This behaviour could be attribute to the presence $NiTi_2$. The XRD of both samples shows that $NiTi_2$ is only visible in the sample B. The X-ray diffractograms confirm the presence of NiTi as the main phase in both samples. Only in sample B, $NiTi_2$ was detected. The presence of $NiTi_2$ is explained by Ti diffusion from the interface of Ti_6Al_4V, but not from the Ti of bed powder [8-11]. Although the Ti_6Al_4V interface has resulted as a method to promote adhesion, also induces the formation of the fragile phase $NiTi_2$ [poster awarded with 1st place at the 4th International Conference on Titanium Powder Metallurgy & Additive Manufacturing, 2017, Xian-China].

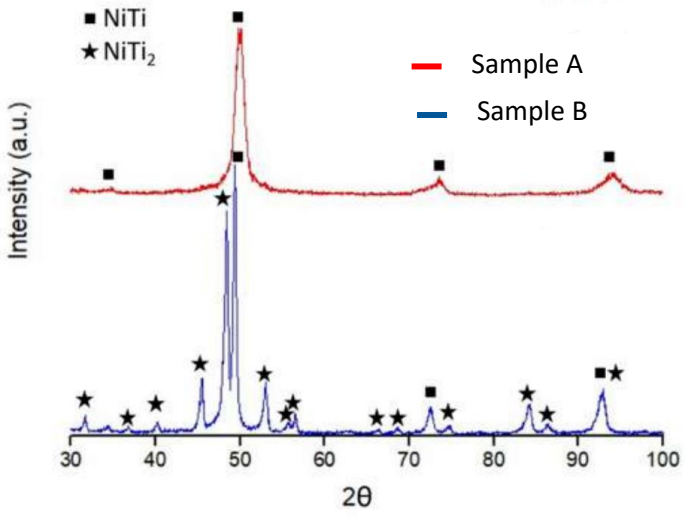

Figure 34. X-ray diffractogram of NiTi 3Dobjects produced by SLM.

In conclusion the solution envisaged to optimize the interface conditions and the reduction of 3Dobjects warpage and stresses, is not of great interest.

The experiments performed showed that fabrication of 3Dobjects in NiTi by SLM is an extremely difficult task. With the use of low VED was possible to produce solid samples, however, many pores and cracks were detected. Moreover, also originated objects contaminated ($NiTi_2$), with poor interlayer adhesion and with poor adhesion to the powder bed. On the other hand, the use of high VED caused the destruction of the 3Dobjects, particularly when producing small features, due to the difficult to control the VED in the melt pool.

Also, the impossibility to control the melt pool temperature, which rises above the melting temperature of the NiTi elements, could unbalance the Ni:Ti ratio by evaporation phenomena.

In conclusion, due the difficulties described above, and due to the low dimension of the 3Dobjects, SLM technology was replaced by a new promising technology inspired in PIM and FDM, denominated by MEX.

3.2 Ni-Ti processed by MEX

According to the state of art concerning MEX/FFF/FDMET, papers about NiTi (SMA) processing, up to now, only two very recent papers (2020, 2021) are published. One from the author *et al*, based on part of the results of this thesis [88] and the other partially based on it [129].

Besides the shaping process being different between PIM and MEX, the feedstocks can present similitudes, in what concern binder and debinding & sintering steps. From Table 4 (Chapter II) it is evident that no optimal route was established to produce NiTi 3Dobjects. Whatever processing parameters selected, the final product has phases other than NiTi, resulting mostly from environmental and sintering conditions.

Nevertheless, it is important to mention, that the feedstock for PIM, in general has no additives. The filament to be processed needs to present adequate mechanical properties to be rolled/unrolled from the coil and to be 3D printed without breaking. As mentioned, the feedstock for MEX needs additives (other polymers), and the rheological behaviour needs to be studied.

3.2.1 Fabrication of Filament

a. Feedstock production

Filament production with A composition (prealloyed NiTi powder + binder (PIM) + additives) was made with a feedstock containing 60 vol% of NiTi powder, with 40 vol% of binder and additives (elastomer and plasticizer) (Figure 35). The relationship comes from the CPVC typical of PIM feedstocks. In fact, the evolution of torque with time, at similar temperature (180°C), shows an evolution and maximum values of torque similar to those of PIM feedstocks. The process started by adding the binder to the chamber, raising the torque up to 3.3 Nm which stabilized after 6 minutes at 2.0 Nm. The additives are added in different contents in order to attain a steady state, with a torque value close to 4.0 Nm, value consider to be ideal to process the mixture by extrusion or by PIM.

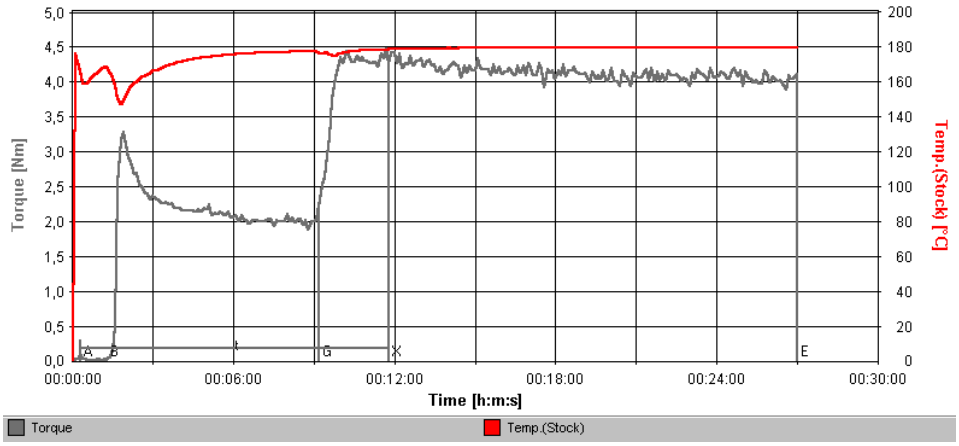

Figure 35. Torque evolution with time during mixing at 180°C (CPVC=60vol%).

The pre-selection of CPVC of 60 vol% results from the best compromise between NiTi powder content in the organic feedstock and torque value [89, 93, 94].

After mixing, in order to produce the feedstock for extrusion, the feedstock prepared in the Z blade was pelletized into small granules (Figure 36).

Figure 36. Pellets of NiTi feedstock.

b. Filament extrusion

The NiTi filament was successfully produced with suitable flexibility and stiffness values needed to be processed by a 3D printer (Figure 37a). Some predictable geometrical deviations were observed in the filament because of the absence of a calibration system (Figure 37b). Most diameter measurements were in the range between 1.72 and 1.74 mm. Nevertheless, diameter value variation did not inhibit the shaping process quality.

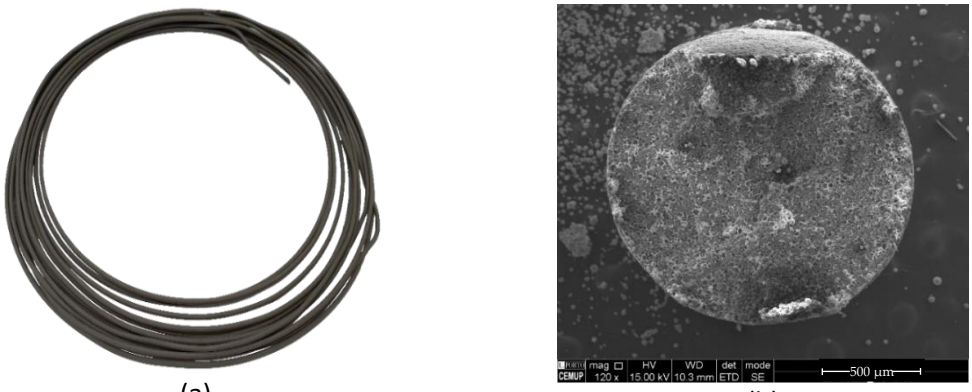

(a) (b)

Figure 37. NiTi filament a) coil b) cross section.

In the filament, NiTi powder particles were homogeneously dispersed throughout the binder and additives (Figure 38a). A homogeneous distribution of powder particles and binder components help to minimize the segregation of components (powder, binder and additives) during the shaping process, and later to obtain isotropic shrinkage after debinding and sintering [122]. For high magnifications is perceptible the multiplicity of particle sizes and satellites (Figure 38b), that in according to some authors, can promote the densification during the sintering process [102].

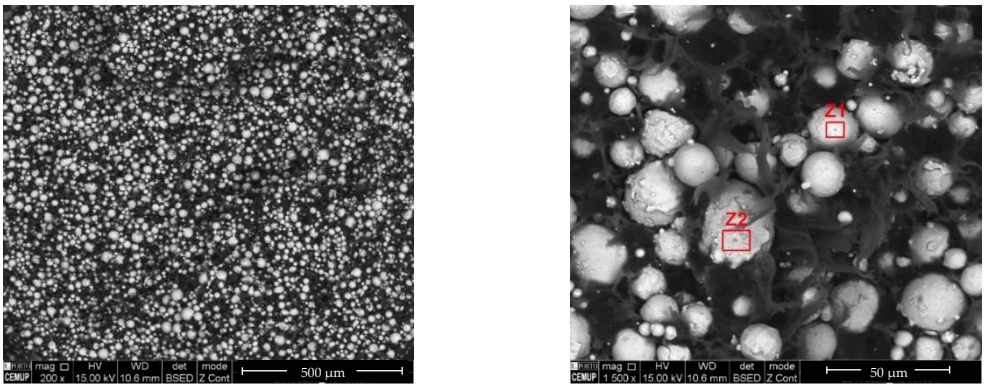

(a) (b)

Figure 38. Metallic particles in filament of mixing A a) general distribution b) EDS analysis.

The powder chemical composition in the green (Z1 and Z2, Figure 38b) suggests that there was no change in the Ni:Ti (Table 10).

Table 10. Ni:Ti of the green filament (Figure 38b).

Ni:Ti (at%)	
Z1	Z2
1.1	1.1

Tensile and bending tests were performed to confirm the mechanical homogeneity of the filament, and the results were evaluated using the Weibull modulus (*m*) (Figure 39). The *m* value is essential to confirm the reproducibility of the mechanical strength, which is a function of the powder/binder homogeneity of the filament. Values of *m* greater than 10 indicate significant reproducibility, particularly if the test is a bending test.

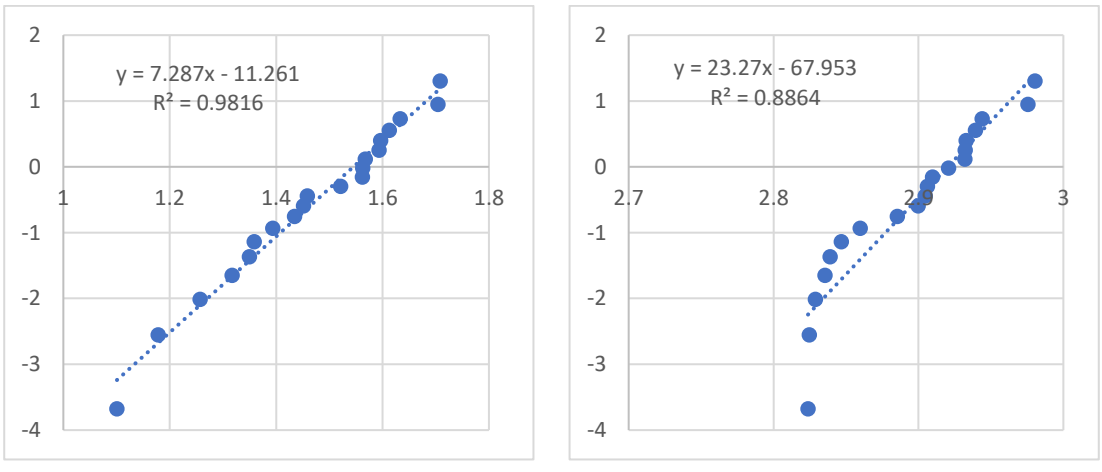

a) b)

Figure 39. Weibull modulus plots of filament A a) tensile test b) 3 point bending test.

The tensile test of mixing A shows a Weibull modulus *m*=7. Against, the bending test that revealed, as expected, a Weibull modulus of *m*=23. These results are consistent with the selected tests (tensile and flexural). In powder technologies, the *m* values concerning tensile stress versus the inverse of failure probability usually are lower than those resulting from the flexural strength. In fact, the sections submitted to maximum load in the tensile test is the whole specimen, resulting in values that are significantly lower than those in the bending test, in which the maximum load is applied to only a very thin cross-section of the specimen. In reality, the probability of defects is enormous in tensile test comparing to the flexure ones. However, the analysis of the Weibull modulus, resulting from 3-point bending test, revealed a significant level of homogeneity in the filament.

The mean value of the Young's Modulus of the green filament was 258±11 MPa (Figure 40).

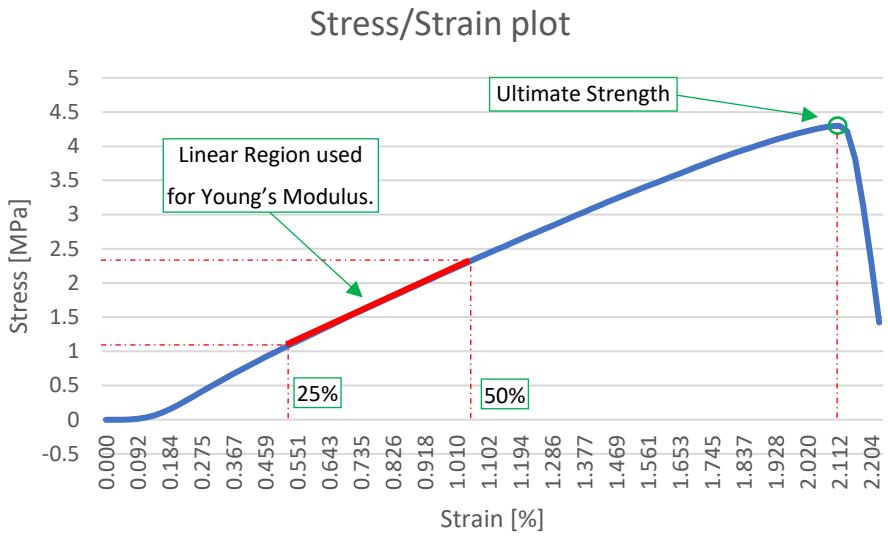

Figure 40. Stress/Strain plot of the green filament.

3.2.2 Shaping

During shaping three different nozzles diameters were tested (0.2, 0.4 and 0.8 mm) in order to evaluate the process and the quality of the final surface (Figure 41). The 0.8 mm nozzle improved the filament flowability, but the dimensional variations and the surface quality of the filament were poor. The use of a nozzle with a diameter of 0.4 mm resulted in some difficulties concerning the filament flowability. The 0.2 mm nozzle produced a material with the best surface quality. However, throughout the process, the nozzle was continuously obstructed.

Thus, a nozzle diameter of 0.4 mm was selected. This was the same diameter used in the MEX of another metal studies [39, 40, 89, 130].

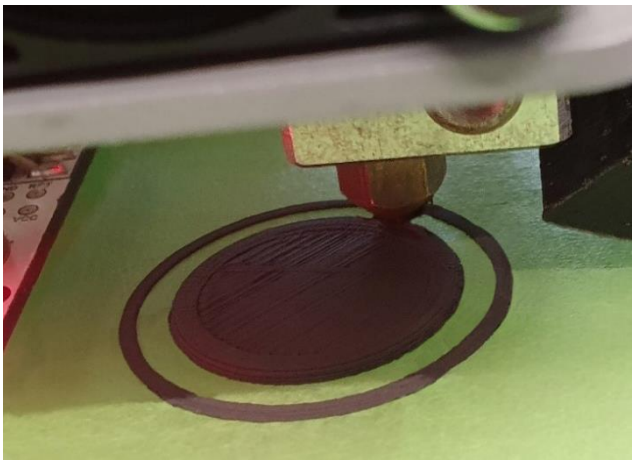

Figure 41. Shaping NiTi 3Dobjects.

The shaping parameters strongly influence the quality of the 3Dobjects and were tested exhaustively until the right set was found. Table 11 summarize the parameters of the 3D printer.

Table 11. MEX 3D printer parameters ($Ø_{nozzle}$=0.4 mm).

Parameter	Value
Layer height [mm]	0.2
Wall thickness [mm]	0.8
Nozzle temperature [°C]	200
Building platform temperature [°C]	50
Print speed [mm·s^{-1}]	20
Print acceleration [mm·s^{-2}]	100

The main morphology of the 3Dobject after shaping is shown in Figure 42a. A detailed view of green is shown in Figure 42b; the homogeneity of the feedstock is obvious.

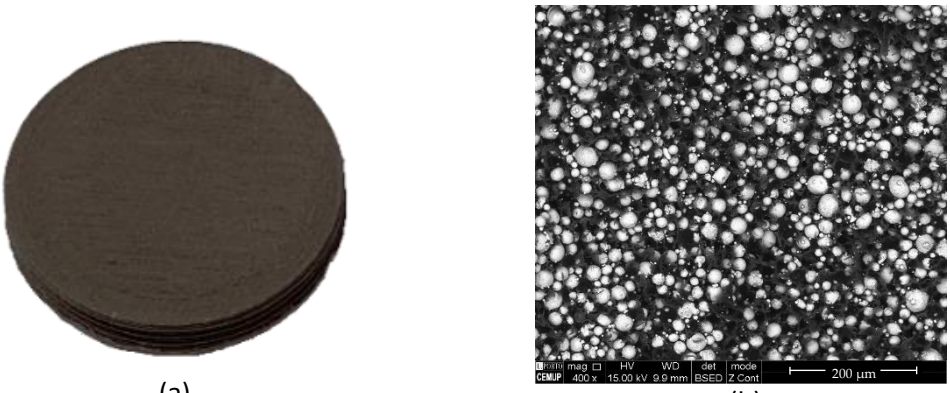

(a) (b)

Figure 42. Green part a) Ø20x3 mm b) detailed micrography (SEM).

3.2.3 Debinding

One of the critical geometrical aspects for debinding and consequently sintering is the dimension of parts (green), in particularly the height or thickness. This is due to the difficulty to eliminate the binder, with or without additives, inside thick specimens. Early works in the process of debinding metallic feedstocks for PEP and PIM, show that the limit for the third dimension of the parts, usually thickness, should be lower than 3 mm. Nevertheless, due to the development of different binders and environmental atmospheres, some works present the critical dimension around 10 mm [15, 131].

The TGA revealed different kinetics for binder M1 and additives (TPE, P) debinding in an argon + hydrogen atmosphere (Figure 43).

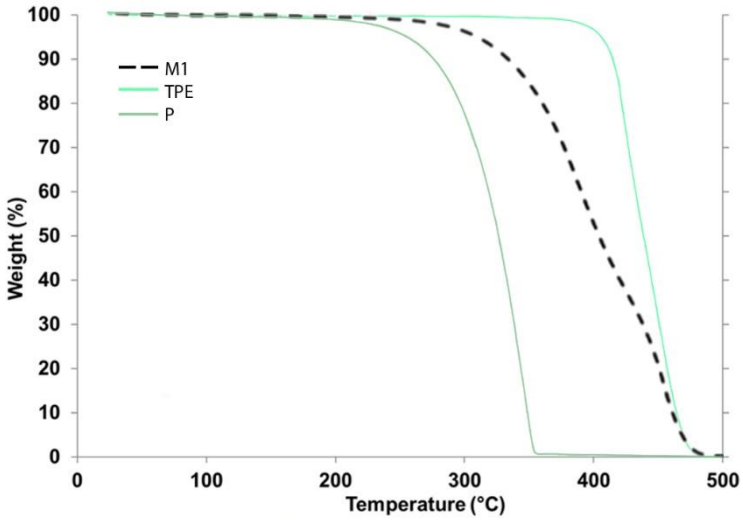

Figure 43. Thermogravimetric curves (TGA) of binder and additives (atmosphere=Ar+H_2).

A N_2 atmosphere induces different kinetics of debinding for binder M1, additives (TPE, P), and the mixtures (M1+TPE and NiTi+M1+TPE+P) (Figure 44). Table 12 summarizes the critical temperatures associated with the degradation of different polymers of the feedstocks in the different atmospheres.

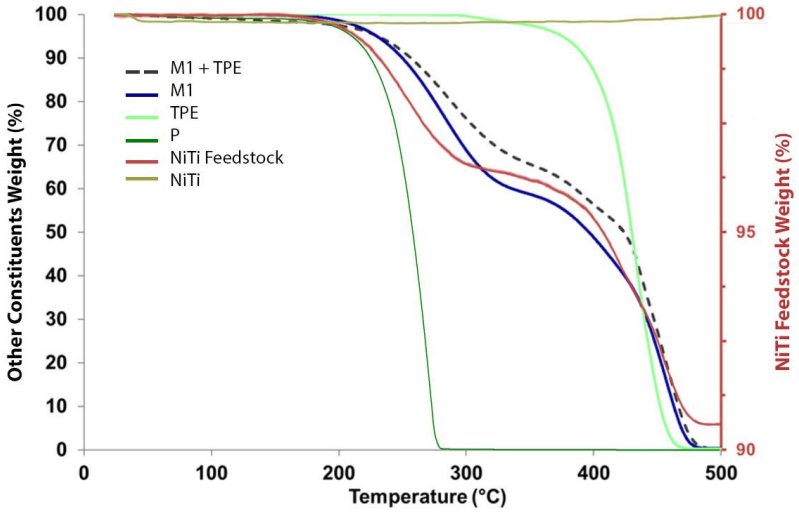

Figure 44. Thermogravimetric curves (TGA) of binder, additives and NiTi mixed and unmixed (Atmosphere=N_2).

Table 12. Start and finish temperatures of different stages of debinding function of different environmental atmospheres.

Feedstock components	1st stage		2nd stage	
	Ti (°C)	Tf (°C)	Ti (°C)	Tf (°C)
M1 (N_2)	200	325	360	485
M1 (Ar+H_2)	250	450	450	485
TPE (N_2)	300	470	-	-
TPE (Ar+H_2)	365	485	-	-
P (N_2)	175	285	-	-
P (Ar+H_2)	185	355	-	-
M1+TPE (N_2)	200	305	370	490
NiTi (N_2)	-	-	>300	Low oxidation
NiTi+M1+TPE+P (Feedstock) (N_2)	150	300	330	490

The kinetics of the debinding process is influenced by the atmosphere, particularly the binder. For TPE and P (additives) the behaviour is similar for both atmospheres, with a well-defined start and end point of degradation, but at very different temperatures (one stage). The binder M1, presents a similar behaviour in both atmospheres with two stages. In N_2 atmosphere the degradation temperatures are different, and the middle stage is much more pronounced,

but a total ustulation occurs at same temperature. The NiTi powder presents a slight decrease in its weight due to dehydration and above 300°C a light rise is registered due to oxidation. The kinetics of the feedstock present a degradation in two stages. The ustulation starts at 150°C and continues up to 300°C. The second sage starts at 330°C and finishes at 490°C, which is the highest temperature needed for complete ustulation of binder and additive constituents.

From the TGA (Figure 43 and Figure 44) it is possible to establish the debinding thermal cycle, in which four stages involving temperatures of 100°C (1 h 30 min), 300°C (4 h), 500°C (4 h 30 min), and 600°C (3 h) must be applied (heating rate=1°Cmin^{-1}) (Figure 45)), to attain the optimization of the debinding stage.

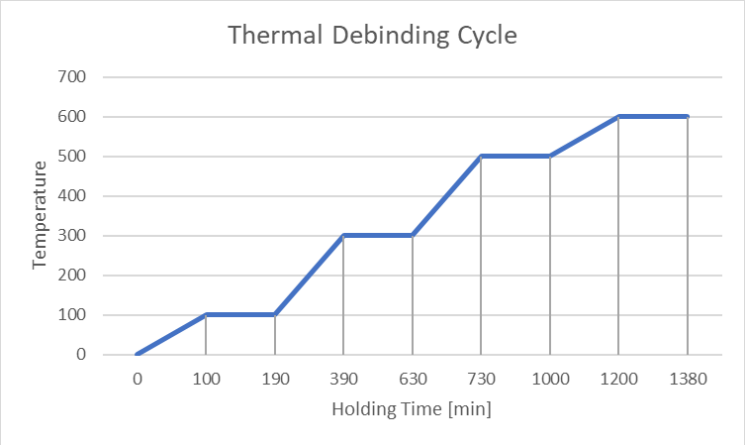

Figure 45. Thermal cycle for debinding (heating rate 1°Cmin^{-1}).

Figure 46 shows NiTi powder after debinding. The chemical ratio of Ni:Ti (Table 13) powder particles of the brown material (Z1, Z2 and Z3) was nearly constant and similar to the virgin powder.

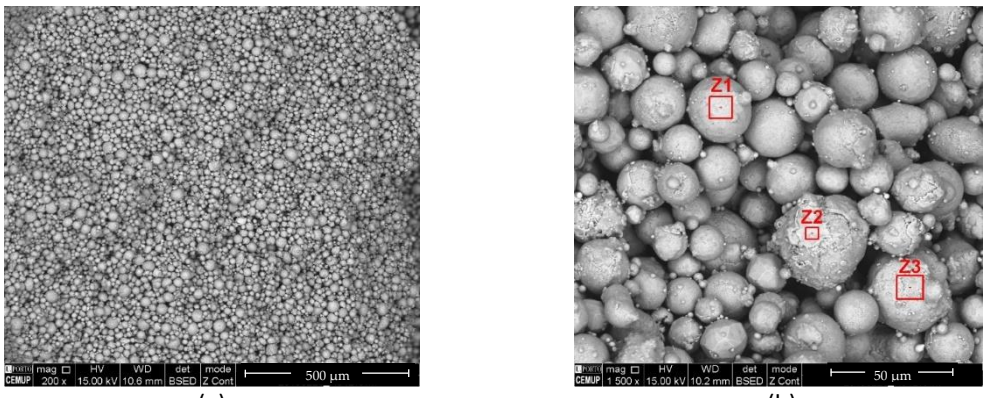

(a) (b)

Figure 46. Powder micrographies a) after debinding (SEM) b) selected zones (Z1, Z2 and Z3) for chemical composition evaluation (EDS).

Table 13. Ni:Ti of powder after debinding in the selected zones.

Ni:Ti (at%)		
Z1	Z2	Z3
0.9	1.0	1.0

3.2.4 Sintering

The sintering was performed under a H_2 atmosphere, with a heating and cooling rate of 5°Cmin^{-1} up to 1165°C (5 hours).

After debinding, the consolidation step, was performed to attain the maximum density of NiTi from prealloyed powder. However, other phases could be present after sintering.

The densities of the possible main phases that can be present after sintering are NiTi=6450 kgm^{-3}, $NiTi_2$=5640 kgm^{-3}, Ni_3Ti=7950 kgm^{-3}, Ni=8908 kgm^{-3} and Ti= 4506 kgm^{-3}.

The specific surface area of the selected powder was lower than that of conventionally used in PIM, which always involves sintering as the primary step in the consolidation process. In MEX technology, the lack of injection pressure must be overcome. Thus, the pressure should be high enough to promote diffusion between powder particles, suitable for increasing sintering kinetics, and prevent significant agglomeration and chemical surface modifications [55, 102].

The most used environmental atmospheres are those resulting for vacuum (low N_2 and O_2 atmosphere), and argon with or without previous vacuum (Table 3, Table 4). During processing, as pores close, the pores lose gas pressure and shrink until completely removed. The use of argon as the atmosphere is proved to be ineffective because it stays trapped inside the matrix creating pores [109]. Similarly, the use of vacuum is not convenient since it may lead to an increase in evaporation of one or more elements within the mixture [132] and also, due to the MEX process, could lead to layers detachment. Thus, and as an innovative aspect of the sintering of NiTi powders, an environment of hydrogen was used in the present study.

Production costs and the formation of undesired phases could be overcome by sintering at temperatures and holding times lower than the selected by other authors (Table 4). Thus, 1100°C (1h), 1165°C (1h) and 1165°C (5h) were the thermal cycles selected in the present work for preliminary studies. The results revealed that at the lowest temperature (1100°C) and a holding time of 1 h, sintering was not accomplished. This low-heat thermal cycle produced no sign of pre-sintering (Figure 47). However, when the maximum temperature was 1165°C for the same holding time (1h), sintering was performed efficiently (Figure 48). Nevertheless, for a holding time of 5h, the effectiveness of sintering is more evident, and almost full densification is observed (Figure 49). Therefore, in a H_2 environmental atmosphere, the best parameter set for the sintering thermal cycle is a maximum temperature of 1165°C, holding time of 5h and

heating and cooling rates of 5°Cmin^{-1}. Other sintering studies on NiTi applied high sintering temperatures and holding times from 5h [19, 20, 55] to 10h [19, 22, 56], depending on the size and geometry of the 3Dobject.

The Ni:Ti (at%) ratio of sintered 3Dobjects (Table 14, Table 15 and Table 16) besides the NiTi phase suggests the formation of other phases from prealloyed powder particles. Sintering obliges to high temperatures to promote diffusion. During slow cooling, $NiTi_2$ and Ni_3Ti intermetallic compounds could be formed at the peritectic (984°C) and eutectic (1116°C) temperatures [28], respectively. However, it must be highlighted the presence of $NiTi_2$ as a pristine phase in the prealloyed powder (LPW). In accordance with the results of other authors, as summarized in Table 4, there is no optimal thermal route that is able to produce only a single phase of the NiTi, whatever the primordial composition of powder. The specimens heat treated at the lowest temperature of 1100°C (1h), a Ni:Ti (at%) ratio of 0.6 suggests the presence of $NiTi_2$, as another phase. 3Dobjects sintered at 1165°C from 1h to 5h in addition to NiTi presents $NiTi_2$ (Figure 48 (Z2b and Z7)) and also Ni_3Ti (Figure 49 (Z6 and Z7)). The presence of the above-mentioned phases is confirmed by the X-ray diffractograms (Figure 54) of 3Dobjects sintered at 1165°C (5h). Phases NiTi and $NiTi_2$ are similar to those obtained by other authors after debinding and sintering prealloyed powder (Table 4). The presence of Ni_3Ti was also observed by authors [20] and its presence is due to different atmospheres and/or other heat treatments after sintering.

The micrography (SEM) (Figure 47) of prealloyed powder, after shaping and debinding, during heat treatment at 1100°C (1h) highlights the absence of powder sintering. In fact, the powder particles do not show an evident bonding among them. Moreover, the phases detected in EDS analysis (Figure 47, Z1, Z2 and Z3) show the presence of $NiTi_2$. This phase already present in the virgin powder (LPW) could also result from phase evolution of NiTi during heat treatment. Some authors, using elemental powder and the same sintering temperature, showed the formation of other phases than NiTi, such as $NiTi_2$ and Ni_3Ti [133].

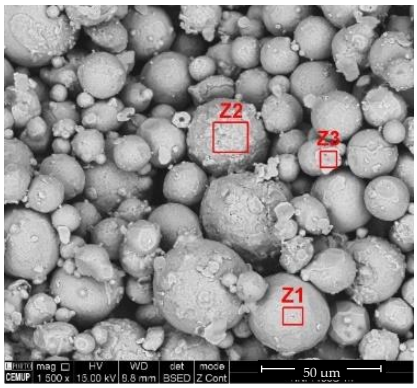

Figure 47. 3Dobject after heat treatment at 1100°C (1h).

Table 14. Ni:Ti after heat treatment at 1100°C (1h).

Ni:Ti (at %)		
Z1	Z2	Z3
0.6	0.6	0.6

However, when the maximum temperature was 1165°C, with the same holding time (1h), it is already visible the sintering of same particles powder (Figure 48).

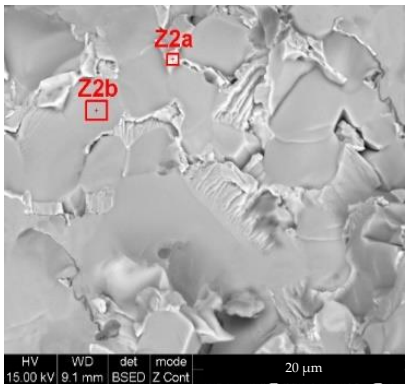

Figure 48. 3Dobject sintered at 1165°C (1h).

Table 15. Ni:Ti after sintering at 1165°C (1h).

Ni:Ti (at %)	
Z2a	Z2b
2.6	0.6

Moreover, for the same maximum temperature and a holding time of 5h the sintering effect is evident and the densification is significant (Figure 49).

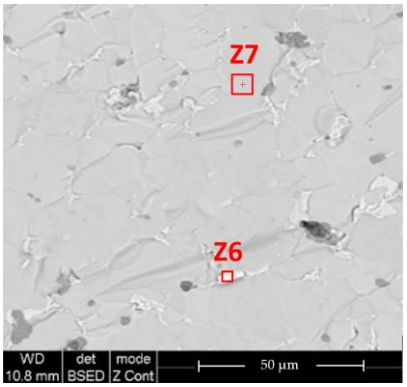

Figure 49. 3Dobject sintered at 1165°C (5h).

Table 16. Ni:Ti after sintering at 1165°C (5h).

Ni:Ti (at %)	
Z6	Z7
2.9	0.6

According to the results from debinding (TGA) and micrographies of the sintered 3Dobjects, the complete thermal cycle was defined (Figure 50).

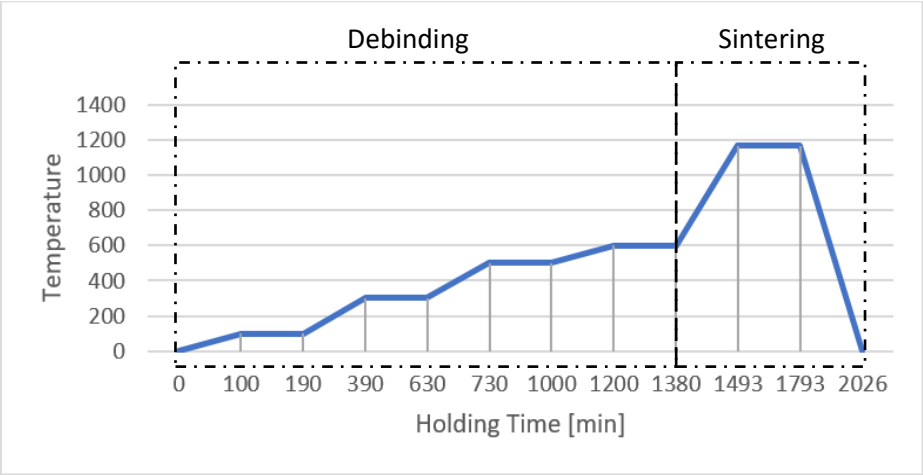

Figure 50. Thermal debinding and sintering cycle.

A detailed analysis of the sintered morphology, in the optimized conditions described above, is evident in Figure 51. This means that sintering could be promoted by other approaches, without increasing temperature and holding time. For instance, adding other metallic elements, that could be significant to the atmosphere inside the 3Dobject and/or suppliers of metallic elements like Ti and/or Ni.

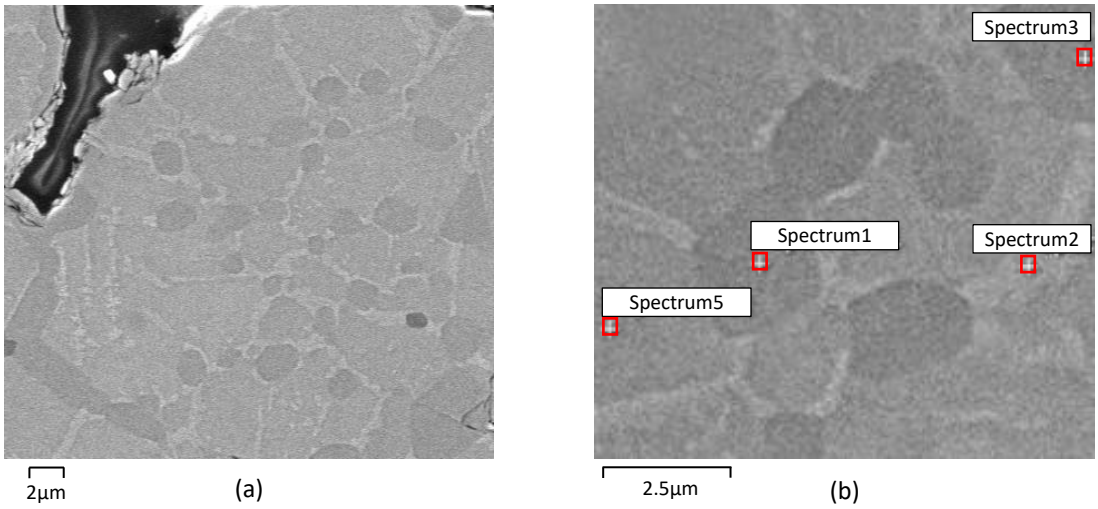

Figure 51. Micrographies of 3Dobject from filament A a) after sintering (SEM) b) selected zones for evaluation of Ni:Ti (S1, S2, S3 and S5) (EDS).

Table 17. Ni:Ti of 3Dobject phases from filament A after sintering (Spectra 1, 2, 3 and 5, Figure 51b)

Ni:Ti (at%)			
S1	S2	S3	S5
0.7	2.9	0.7	1.4

3.2.5 Defects

The main defects that can be present on filament A (green) must be highlighted, in order to evaluate their role in the future stages of MEX. In fact, in indirect technologies, like PIM and extrusion, a defect in green, in general continuous to be a problem in other stages [97], that means in final 3Dobject.

Filament		Strand
Green	Sintered 1165°C (5h)	Green

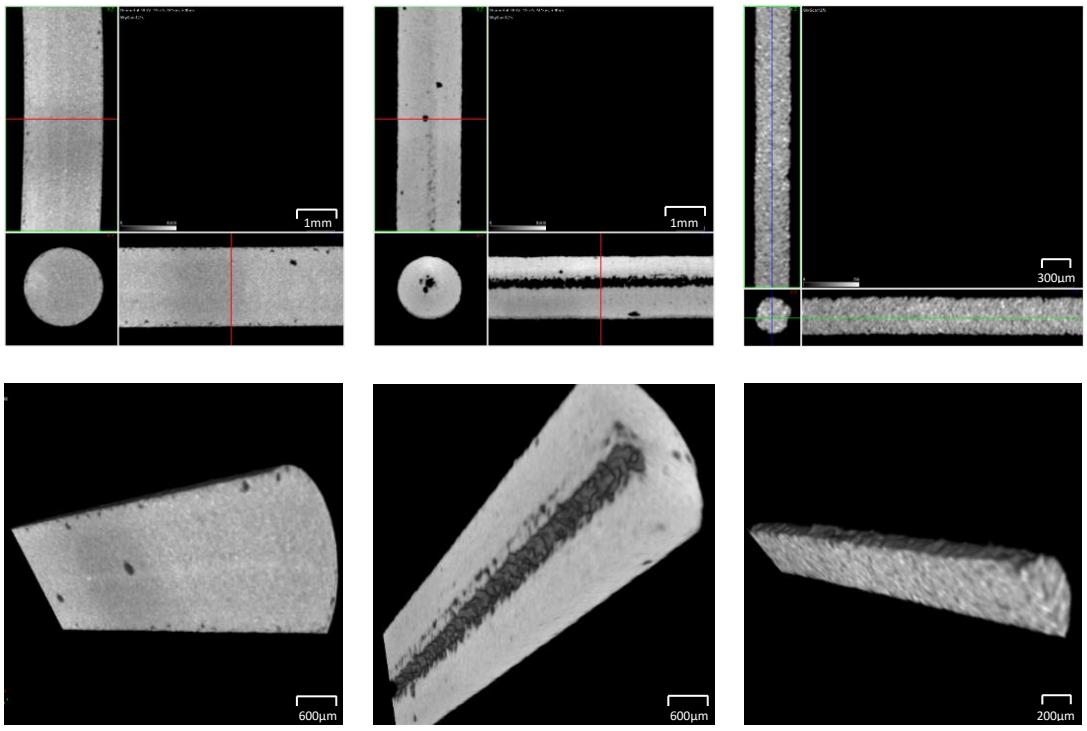

Figure 52. Tomographies of filament A (green and sintered at 1165°C during 5h) and strand A (green).

The effect of IP in the filament quality as green seems to contribute to a better surface quality and reduction of porosity (Figure 53).

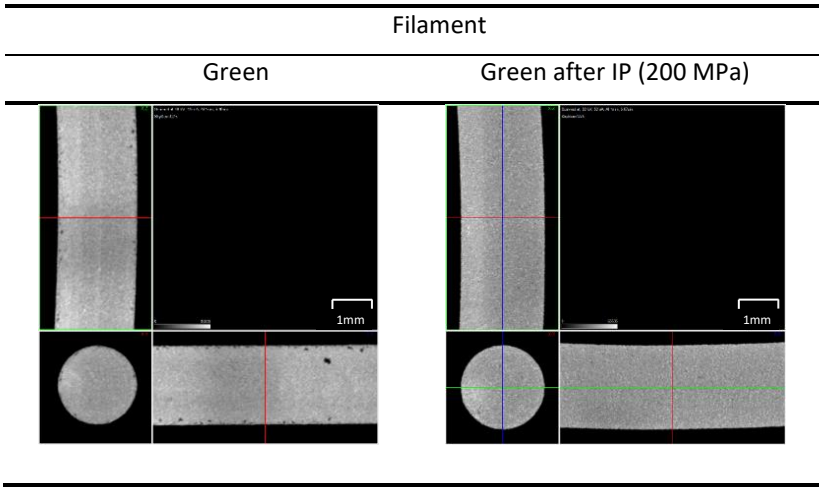

Figure 53. Tomographies of filament A green and green after IP.

3.2.6 Phase composition and defects versus hardness

The typical temperatures and holding times used by other authors to sinter Ni-Ti (SMA) prealloyed powder were 1200°C (5h) [20]; 1250°C (10h) [19-22]; 1260°C (4h) [23]; 1265°C (10h) [22]; 1270°C (5h) [19, 20]. Although, one of the targets of the present study was to decrease significantly maximum sintering temperature for NiTi.

The sintering temperature selected in the present study was 1165°C (5h). The sintering of the prealloyed powder based on prealloyed NiTi, must be enough to guarantee the consolidation of the powder particles, without formation of other intermetallic phases, different from the existent in virgin powder (Figure 21).

However, X-ray diffraction of sintered 3Dobject shows as phase composition: NiTi (master phase, $NiTi_2$ (essentially from powder) and Ni_3Ti resulting from the diffusion of Nickel present in virgin prealloyed powder into NiTi and $NiTi_2$ (Figure 54). Moreover, a detail analyses of diffractogram seems to show yet Ni without reaction.

It is also clear that the contact with the sintering platform is not important to the occurrence of different phases. In fact, top and base of 3Dobject show a similar phase composition meaning that all binder and additives were effectively removed, and the sintered phases are comparable.

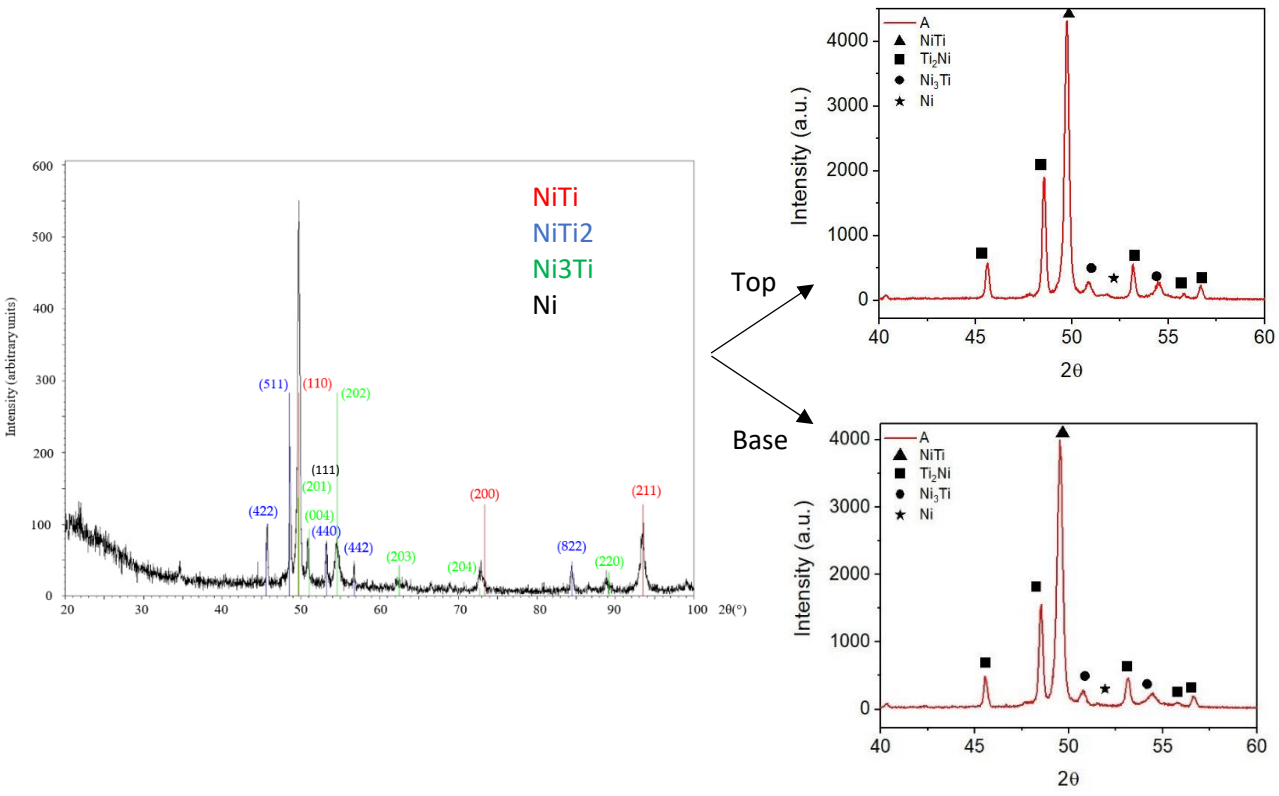

Figure 54. X-ray diffractogram of Ni-Ti (SMA) sintered 3Dobjects at 1165°C (5h).

The occurrence of the new phase Ni_3Ti and the no disappearance of Ni from the virgin powder is obvious. The presence of $NiTi_2$ could be related to its occurrence already in virgin prealloyed powder (NiTi+$NiTi_2$+Ni). The excess of free Ni (Figure 21) in powder particles, could be the responsible for the formation during heat treatments of debinding and sintering, of the new Ni_3Ti phase. In fact, during heating the contact between Ni and NiTi induces Ni_3Ti development, as already observed in other processing technologies, like coatings and powder pressing [134, 135].

The Ni_3Ti could be also observed in micrographies (SEM (EBS)), (Figure 51), as white phase around pristine phases: Ni_3Ti (white) (spectrum 2), $NiTi_2$ (grey) (spectra 1 and 3) and NiTi (light grey) (spectra 5). A detail analyses of the phases NiTi and $NiTi_2$ reveal the presence of a sub-metric and/or nanometric precipitates of Ni_3Ti.

Microhardness values measured in a section, particularly far from the centre, are higher than the typical hardness of NiTi (B2) (275 HV), NiTi (B19) (112 HV), $NiTi_2$ (163 HV) and Ni_3Ti (1071 HV) [133]. The Young moduli (E) of Ni–Ti intermetallic compounds decrease in the following order: Ni_3Ti > B2_NiTi > B19'_NiTi > $NiTi_2$ [136].

The values measured after same sintering conditions (1165°C, 5h) were 887±58 HV. This hardness value is similar to the measured by microhardness for the similar phase composition of NiTi based coating (laser cladding) of 800 HV [134]. This is not attributed to the low load applied during the indentation (present study, 2000 mN), but to the presence of

nanointermetallic phases, in particular Ni_3Ti, which can potentially increase hardness values to higher than 800 HV. Other authors have measured 700 HV [137, 138] and 742 HV [139], respectively. The small grain size and Ni_3Ti nanoprecipitates can explain the values of hardness measured.

Up to now, the conclusion is that the low temperature of sintering (1165°C 5h) can be essential to a good sintering, contributing to a significant decrease in energetical consumption. However, it was expected the non-formation of undesired phases other than NiTi, particularly Ni_3Ti that is a hardening but fragile phase.

3.3 Ni-Ti with additions (TiH_2, Ni)

The main target proposed in the present study was to attain as final phase composition only NiTi. The presence of other phases due to the powder phase composition oblige to search a start composition that could contribute to decrease the Ni in excess, by producing NiTi from $NiTi_2$ and to avoid the occurrence of Ni_3Ti. TiH_2 addition in different percentages, during sintering can contribute to this target, particularly by the disappearance of Ni_3Ti. The use of TiH_2 instead of Ti is to protect Ti from oxidation, contributing also to create inside of the brown a reducing atmosphere (temperature of TiH_2 decomposition assumes its maximum value lower than the temperature of debinding heat treatment defined for NiTi)[140].

Different authors studied the effect of TiH_2 addition, but in the formation of NiTi, from its reaction with powder particles of Ni and processed by pressing and gel casting (Table 18). Studies concerning prealloyed NiTi powder, with addition of TiH_2 and shaped by an additive process is not yet deep studied.

Table 18. Sintering and post-processing conditions of elemental Ni-TiH_2 powder and final phases.

Temp [°C]	Holding Time [h]	Atmosphere [Pa]	Process. Tech.	Porosity after sintering (%)	Post-processing	Phases	Ref
950	1	Vacuum (1.33×10^{-2})	-	33.9-37.6	-	• NiTi • $NiTi_2/Ni_2Ti_4O_x$ • Ni_3Ti	[141, 142]
920	14	Vacuum	Pressing	29-34	• Aged (Ar) 500°C (1h) • Not polished	• NiTi • $Ni_2Ti_4O_x$ • Ni_4Ti_3 • Ni_3Ti • $N_{0.3}TiC_{0.7}$	[34]
					• HIP (Ar) 180MPa 1050°C (3h) • Aged (Ar) 500°C (1h) • Not polished	• NiTi • $Ni_2Ti_4O_x$ • Ni_3Ti • $N_{0.3}TiC_{0.7}$	
					• Aged (Ar) 500°C (1h) • Polished	• NiTi • $Ni_2Ti_4O_x$ • Ni_4Ti_3	
					• HIP (Ar) 180MPa 1050°C (3h) • Aged (Ar) 500°C (1h) • Polished		
					• HIP (Ar) 180MPa 1050°C (3h) • Annealed (Ar) 1100°C (1h) • Aged (Ar) 500°C (1h) • Polished		
1000 1100 1200	2	Vacuum (3×10^{-3})	Pressing	10-33.8	-	• NiTi • $NiTi_2$ • Ni_3Ti	[143]
900 950 1000 1100 1200	2	Vacuum (3×10^{-5})	Pressing	19 (>900°C)	-	• Ni • Ti • NiTi • $NiTi_2$ • Ni_3Ti	[110]
1100 1200					1000°C 6h vacuum	• NiTi • $NiTi_2$	
1000	2	Vacuum (1×10^{-3})	Gel Casting	40-46	-	• NiTi • $NiTi_2$ • Ni_4Ti_3	[144]

Although impurity pickup and the consequent formation of intermetallic phases could occur in both cases, elemental and prealloyed virgin powder. However, elemental powder particles are more susceptible to react with the environmental atmosphere. Elemental Ni and specially Ti which is highly reactive, when in contact with C or O_2 resulting from the debinding step, could easily react and lead to the formation of undesired phases and make difficult the formation of NiTi and the sintering process. The strategy is to reduce oxidation of Ti by adding TiH_2. Nevertheless, during heating, dehydrogenation of TiH_2 also let Ti free suitable to react with Ni and to promote the formation of NiTi [143]. This process is achieved during a stage between debinding and sintering at temperatures up to 600°C [144] to 650°C [143, 145] or 700°C [140, 146]. All the temperatures referred are lower than the sintering temperature (1165°C) used in this work. Thus, total dehydrogenation is expected before sintering. Another advantage of using TiH_2 to obtain Ti in powder metallurgy is that before sintering, the dehydrogenation will expose activated Ti enhancing the sintering process, meaning higher density, also, the oxygen pick up is expected to be lower [147, 148]. However, when used as a substitute of Ti in NiTi alloys, some authors state that porosity size is reduced but with more occurrence and consistently distributed.

Different studies may be highlighted concerning Ni and TiH_2 in the formation of NiTi. Li *et al*, studied the influence of TiH_2 in porosity and shrinkage of NiTi 3Dobjects. The general porosity and open-pore ratio tend to decrease, porosity size also decreases, and the number of pores increases and become more uniform, meaning a reduction in shrinkage. With the increase of TiH_2 vol%, due to the high reactivity of the Ti, together with high temperature, sintering is enhanced, contributing to the formation of Kirkendall pores and the shrinkage of the big ones, that is also associated with the enhancement of the SME [141, 142]. Kirkendall pores are formed when two kinds of metallic atoms diffuse into each other, the main diffusion current is composed of the element with low evaporation energy. In the NiTi, Ni has a lower evaporation energy, and the diffusion coefficient is higher than Ti. Consequently, during the sintering process the diffusion rate of Ni is higher than Ti [149]. Berthevillet *et al*, synthetized NiTi and produced 3Dobject using pressing technology. Surface characterization (not polished) showed the presence of NiTi (B2), Ni_4Ti_3, Ni_3Ti, $Ni_2Ti_4O_x$, and $N_{0.3}TiC_{0.7}$, the last resulting from contamination of the virgin powders during processing. After post-processing, the most prominent phases were NiTi (B2), Ni_4Ti_3, and $Ni_2Ti_4O_x$ [34]. Chen *et al*, used elemental compositions of 51 at% of Ni with Ti or TiH_2 and produced 3Dobjects also by pressing technology. With Ni-Ti powders, after sintering at 1100°C and 1200°C, austenite (B2) was the dominant phase with some minor occurrences of martensite (B19') and intermetallics $NiTi_2$ and Ni_3Ti. However, when sintering at 1000°C α-Ti was also present. Using Ni-TiH_2, a reduction of pore size and an increasing of their number associated to a uniform distribution was observed. Another major difference is that Ni-Ti 3Dobjects present swelling, and in Ni-TiH_2 shrinkage was observed. The most prominent phase

was NiTi (B2) and the occurrences of $NiTi_2$ and Ni_3Ti was lower than in Ni-Ti virgin powder [143]. Bohua *et al*, used gel casting technology to produce also Ni-Ti and Ni-TiH_2 3D objects. After sintering, with Ni-Ti powder, among the NiTi as main phase, $NiTi_2$, Ni_4Ti_3, TiO_2 and TiC were detected. When using Ni-TiH_2 the phases TiO_2 and TiC were absent, due to the reducing environment formed by the release of hydrogen from TiH_2. Regarding porosity, when using Ni-TiH_2 powder, 3Dobject presents a much smaller mean pore size and a homogeneous pore distribution [144].

The use of TiH_2 could point the solution for some encountered problems when processing NiTi from prealloyed powder, promoting sintering kinetics and reduction of secondary phases. The use of TiH_2 combined with an H_2 atmosphere was intended to create a reducing atmosphere both outside and inside the 3Dobjects. Within the sample, H_2 was intended to replace O_2 so that it would not bind to Ti, as Ti has more affinity to O_2 than to Ni. Due to the high temperatures involved in the process, the H_2 after separation from Ti should promote the outflow of O_2 and upon cooling the remaining H_2 would reconnect to Ti preventing the formation of $Ni_2Ti_4O_x$. Although is known that this mechanism could lead to the formation of $NiTi_2$ due to the free Ti, and to the increase of pores in number (but less in size), it was expected that this procedure could prevent the formation of Ti oxides which are well known to be extremely brittle. Also, as said before, activated Ti resulting from dehydrogenation can promote the sintering kinetics. It is also important to highlight, that studies where no binder is used, could be the explanation for the low presence of oxides and carbides.

In conclusion, all the studies concerning the role of TiH_2 powder in sintered NiTi from Ni, point to a uniform distribution of pores, a decrease of pores dimension associated to an increase in number. This also contributes to an increase of shrinkage compared with 3Dobjects made from Ni and Ti powder. The contamination of powder during processing and sintering is significantly lower than the 3D object produced from Ni-Ti.

In present study two solutions will be assumed, the virgin prealloyed powder of NiTi has Ni free, resulting from atomization process, enough to react with TiH_2 added, or the addition of TiH_2 will oblige to a supplementary Ni powder content. The answer to these challenges will be the target of the research, in the present subchapter.

Henceforth, NiTi resulting from prealloyed powder (as feedstock, filament, debinding and sintering) will be designated by A; the NiTi resulting from prealloyed powder and supplementary addition of 1 and 5 wt% TiH_2 by B and C, respectively; and NiTi after addition of 5 wt% TiH_2 + 6.2 wt% Ni by D. All mixings were performed in a ball milling equipment (200 rpm, during 5 min).

3.3.1 Fabrication of Filament

a. Feedstock production

The CPVC selected for B, C and D was the same of A (60 vol%). In fact, the value of the torques in the steady state for all the compositions studied, were between 4.0 and 5.0 Nm (Figure 55).

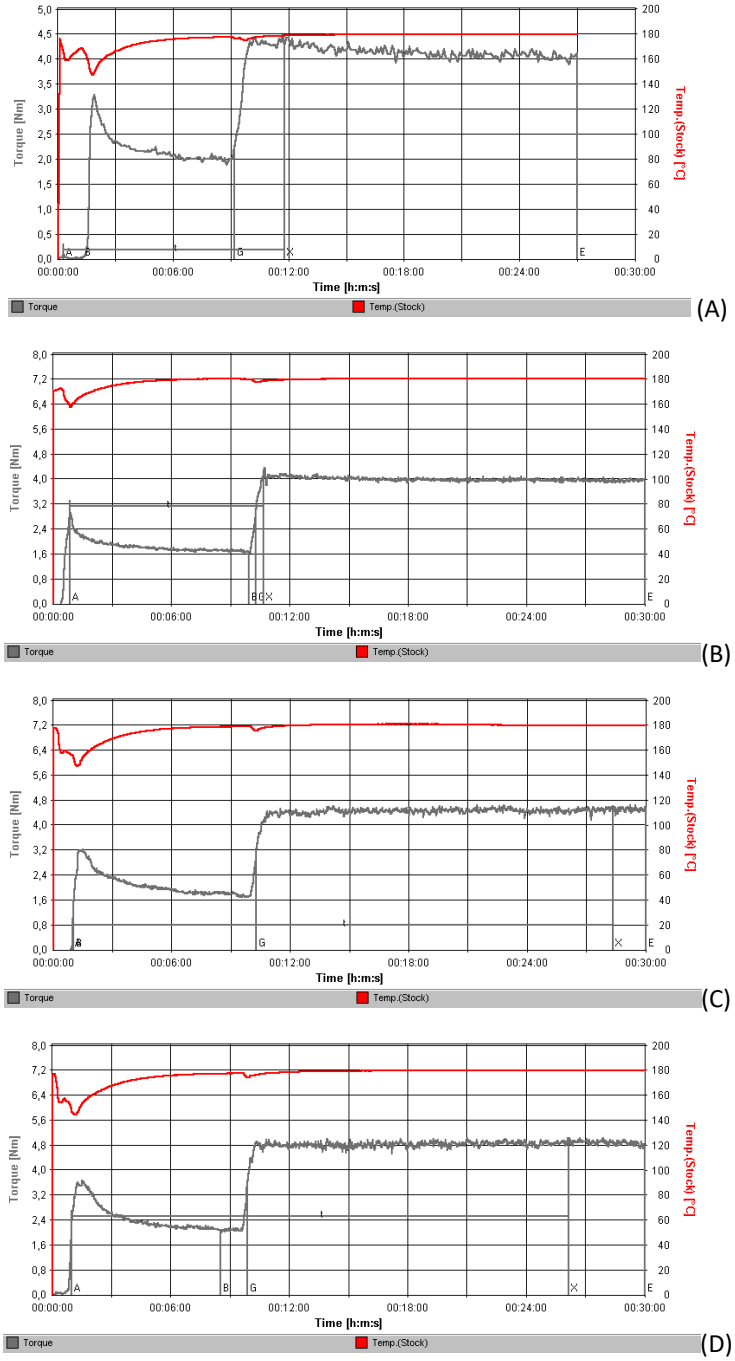

Figure 55. Mixing of binder with NiTi based powder (A)(standard)+ TiH_2 (B,C)+ Ni (D)(wt%).

In the four mixtures a steady state occurred, meaning that the mixtures were homogeneous and have similar rheological behavior (Table 19). Homogeneity in the mixtures is crucial to prevent the formation of secondary phases where the ratio of Ni:Ti is unbalanced. The values of torque for A, B, C and D are quite similar.

Table 19. Steady state torque.

	A	B	C	D
Steady state torque [Nm]	4.2	4.0	4.6	4.8

b. Filament extrusion

SEM analysis of cross sections of the green filaments B, C and D, show the multiplicity of sizes from its constituents. All filaments are similar, showing good distribution of the multiple particles sizes which is a good promoter of compaction. In filaments B and C the particles have a shape factor close to 1. However, in filament with addition of Ni (D) some sharpened particles are observed (Figure 56).

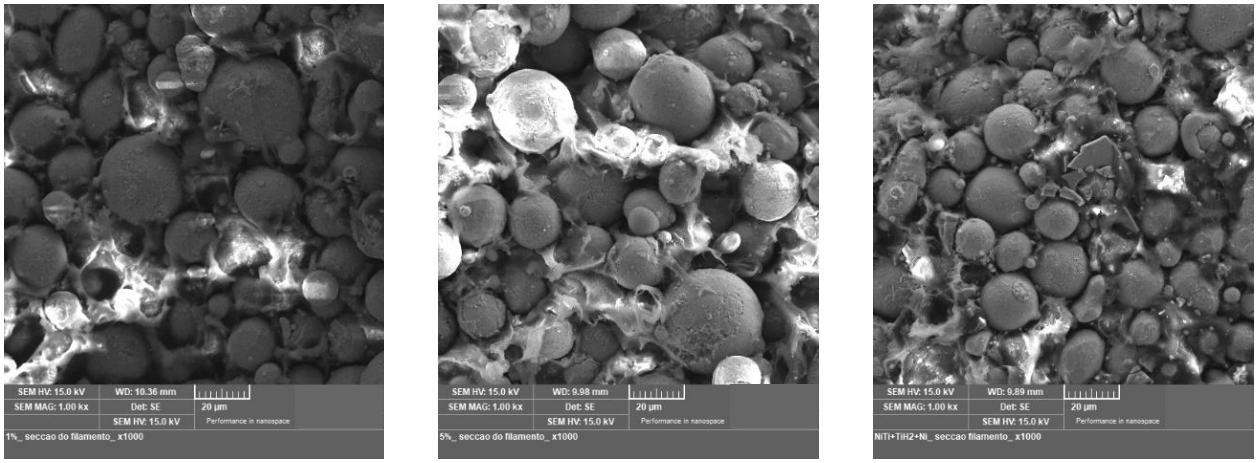

(a) (b) (c)

Figure 56. Micrographies of the green filaments a) B b) C c) D.

Weibull modulus (*m*) in filament B, C and D of the tensile tests are similar to A (Figure 57, Table 20).

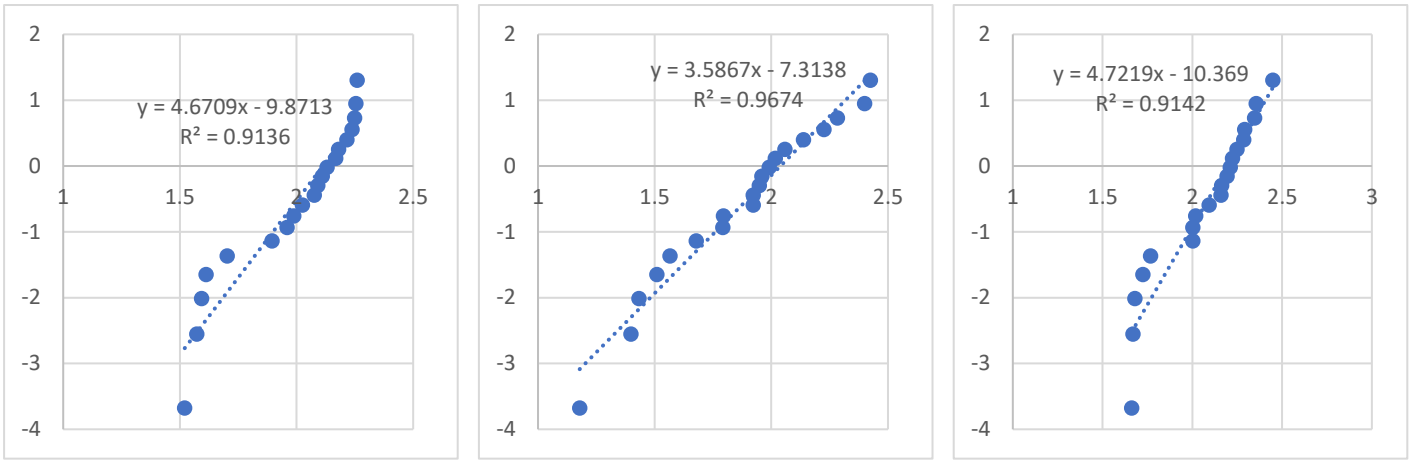

(a) (b) (c)

Figure 57. Weibull modulus plots from tensile test a) B b) C c) D.

Table 20. Weibull modulus from tensile test.

	A	B	C	D
Weibull modulus	7	5	4	5

The Weibull modulus from the 3-point bending test show significative difference between filaments A, B and C to the filament D, that has a value almost the double of the other ones (Figure 58, Table 21). This fact can be attributed to the multiplicity of particles size of the different added powder.

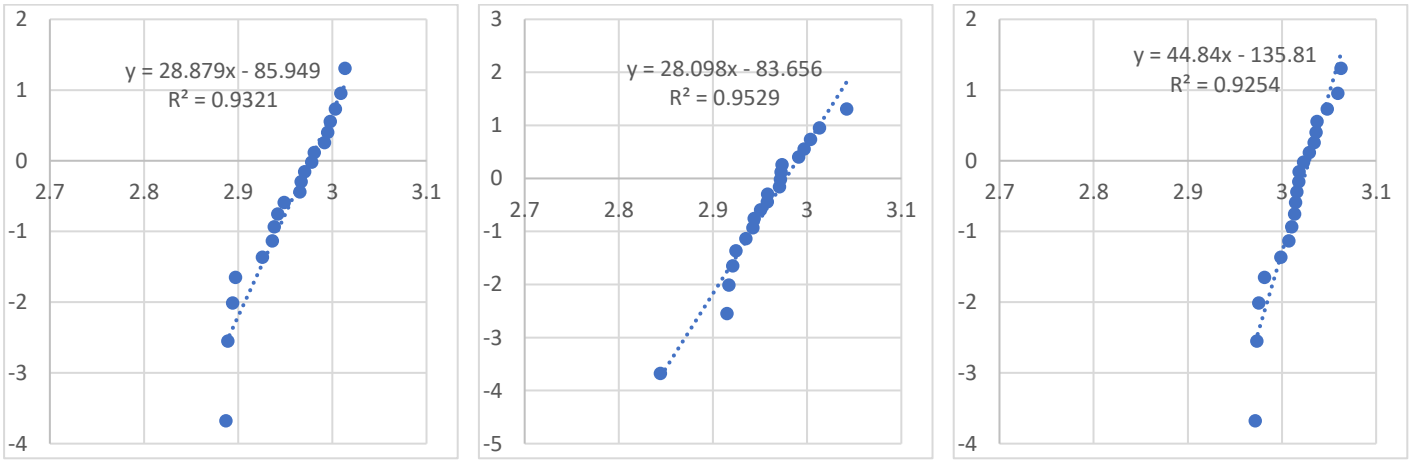

(a) (b) (c)

Figure 58. Weibull modulus plots from 3-point bending a) B b) C c) D.

Table 21. Weibull modulus from 3-point bending.

	A	B	C	D
Weibull modulus	23	29	28	45

In what concerns the Young modulus, the values are very similar for all compositions (Table 22). The values of Young Modulus reveal a similar behaviour on elastic domain, whatever the composition selected, to filament based on NiTi prealloyed powder.

Table 22. Young modulus of the green filaments.

	A	B	C	D
Young modulus [MPa]	258±11	277±15	273±14	249±28

3.3.2 Shaping, Debinding and Sintering

The SDS of 3Dobjects from compositions B, C and D were processed in the same conditions of A (Table 11, Figure 45).

After sintering, based on the colour of the phases, the SEM micrographies (EBS), show like A three different phases. This suggests that the phase composition is constituted by NiTi, $NiTi_2$ and Ni_3Ti (Figure 51, Table 17). This could be attributed to the equipment limitation, to dimension of phases and/or to the presence of other phases, finely dispersed in the master one.

The semi-quantitative analysis of the phases of A shows a significant difference between NiTi and $NiTi_2$ weight percentage (85:15). The white phase attributed to Ni_3Ti is distributed around the different grains of NiTi and $NiTi_2$. A close observation inside the grains of these phases seems also to reveal low precipitation of the Ni_3Ti phase.

No notorious difference is observed with the addition of 1 wt% of TiH_2 to NiTi virgin powder (Figure 59, Table 23). The x-ray diffractogram analysis in what concerns phases, corroborates the presence of the phases detected in micrographies (NiTi, $NiTi_2$ and Ni_3Ti) more Ni from virgin powder (Figure 60). Concerning the percentages of NiTi and $NiTi_2$ from A and B, the tendency is a light increasing of $NiTi_2$ percentage of B.

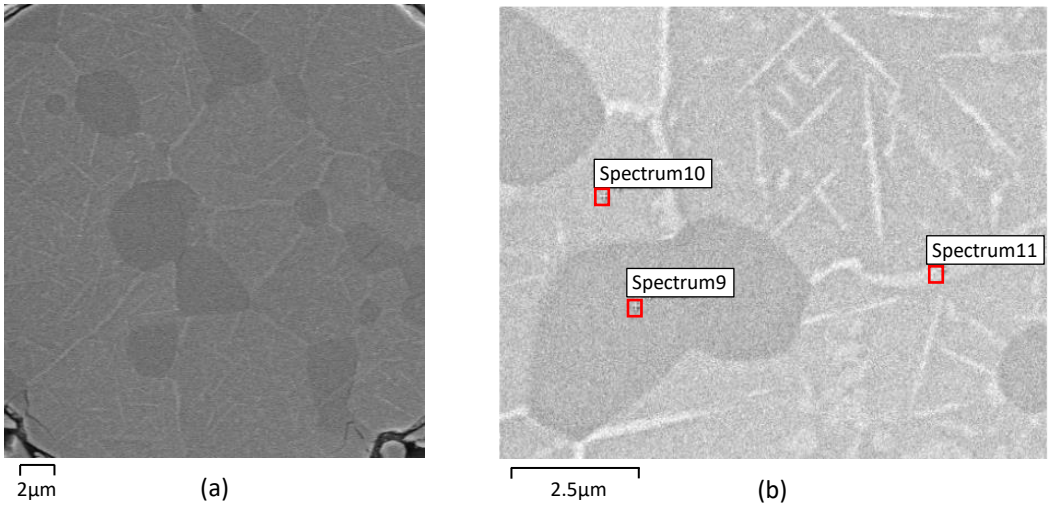

Figure 59. Micrographies of 3Dobject from filament B a) after sintering (SEM) b) selected zones for evaluation of Ni:Ti (S9, S10 and S11) (EDS).

Table 23. Ni:Ti of 3Dobject from filament B phases after sintering (Spectra 9, 10 and 11, Figure 59b).

Ni:Ti (at%)		
S9	S10	S11
0.7	1.4	1.6

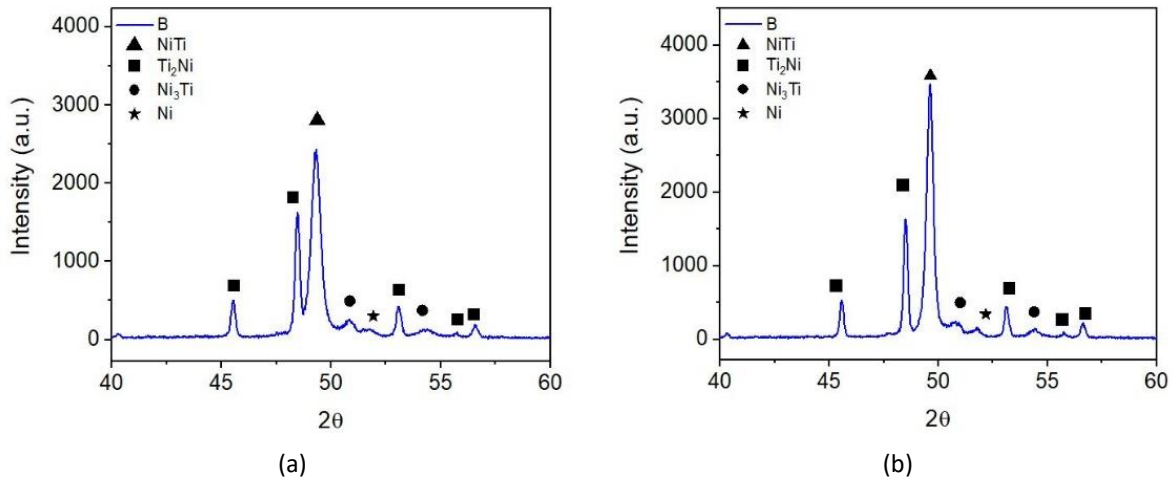

Figure 60. X-ray diffractograms of 3Dobject from filament B a) top b) base.

The micrographies of 3Dobject from C filament (NiTi virgin powder + 5 wt% TiH_2) shows a significant difference from A and B 3Dobjects: the disappearance of the white phase, attributed to Ni_3Ti. Moreover, it is also evident a light increase of $NiTi_2$ content. Similar to the other compositions, the Ni:Ti suggest also the formation of phases constituted by Ni and Ti, although enriched in Ni, like Ni_3Ti_2 and/or Ni_4Ti_3 [20, 23, 55, 56] (Table 24, Figure 61). However,

this must be demonstrated by the use of other characterization techniques (*i.e.* TEM). Nevertheless, these disaccords could be also attributed to the reasons refereed above.

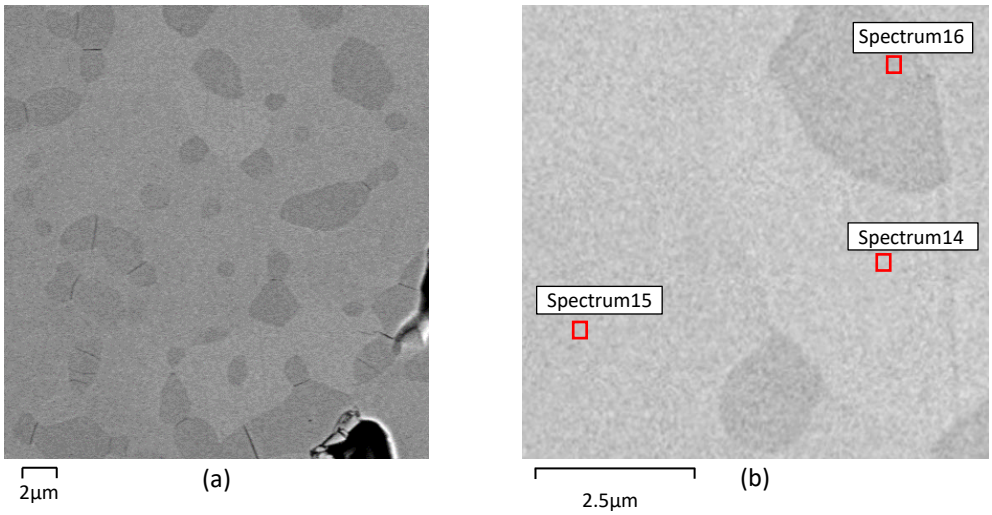

Figure 61. Micrographies of 3Dobject from filament C a) after sintering (SEM) b) selected zones for evaluation of Ni:Ti (S14, S15 and S16) (EDS).

Table 24. Ni:Ti of 3Dobject phases from filament C after sintering (Spectra 14, 15 and 16, Figure 61b).

Ni:Ti (at%)		
S14	S15	S16
1.3	1.4	0.7

X-ray diffractograms show the apparent disappear of Ni_3Ti phase (white phase (SEM)), associated to the pristine free Ni. Moreover, it suggests the possibility of Ti resulting from dehydrogenation, from a higher content of TiH_2 (5 wt%) than the added to the 3Dobject B, contributed for the improvement of NiTi phase instead of other intermetallic compounds. The possibility of a reaction of free Ti with pristine free Ni is supported by this test. Top and base of the sintered 3Dobject present the same phases as the previous compositions.

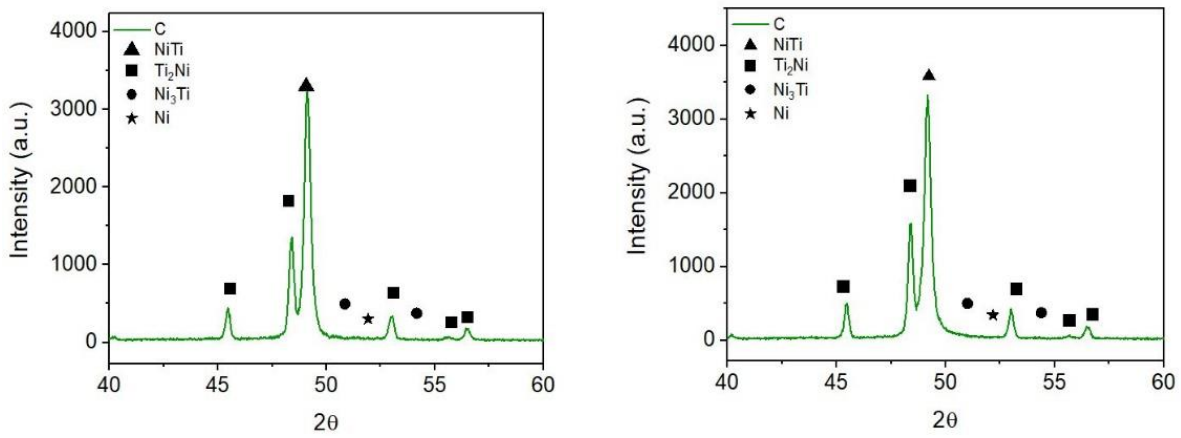

Figure 62. X-ray diffractograms of 3Dobject from filament C a) top b) base.

Other 3Dobject was manufactured using a supplementary Ni content, that was added to virgin powder (NiTi+$NiTi_2$+Ni) mixed with 5 wt% TiH_2. The objective was, by one hand to contribute to highlight the role of Ni in the excess of Ni_3Ti phase formed during processing. By other hand, to analyse the role of the excess of Ni in the disappearance of $NiTi_2$ resulting from NiTi powder fabrication. In fact, it was observed with addition of Ni a drastic decrease of $NiTi_2$ patent in the SEM images of B (Figure 59) and C (Figure 61) when compared to D (Figure 63) 3Dobjects. Thus, Ni powder content in excess, could be a solution for the disappearance of $NiTi_2$ in order obtain only NiTi.

The micrographies and diffractogram from 3Dobject resulting from filaments with Ni in excess (other than the pristine one) shows again the formation of a white phase attributed to Ni_3Ti (Figure 63 and Figure 64), like in the sintered 3Dobjects from filaments with TiH_2 lower than 5 wt%. Although, the addition of Ni shows an occurrence of a “new phase” almost depleted of Ni, suggesting the presence of Ti without any reaction with other metal present (Figure 63, Table 25). Nevertheless, the x-ray diffractogram do not reveal the Ti phase (Figure 64). Similar to the previous compositions, there are no difference in the phases formed during sintering, between the top and the base of 3Dobject.

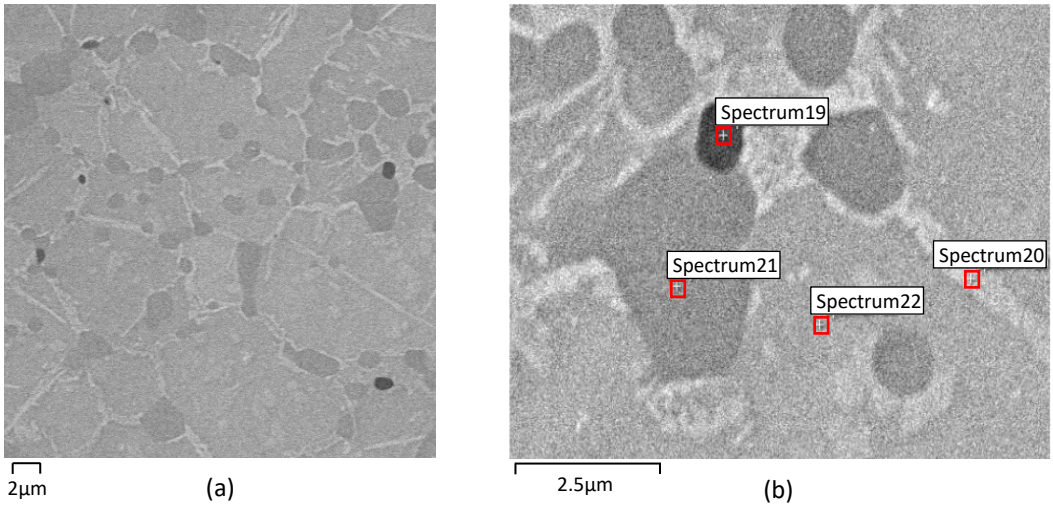

Figure 63. Micrographies of 3Dobject from filament D a) after sintering (SEM) b) selected zones for evaluation of Ni:Ti (S19, S20, S21 and S22) (EDS).

Table 25. Ni:Ti of 3Dobject phases from filament D after sintering (Spectra 19, 20, 21 and 22, Figure 63).

Ni:Ti (at%)			
S19	S20	S21	S22
0.1	2.8	0.7	1.4

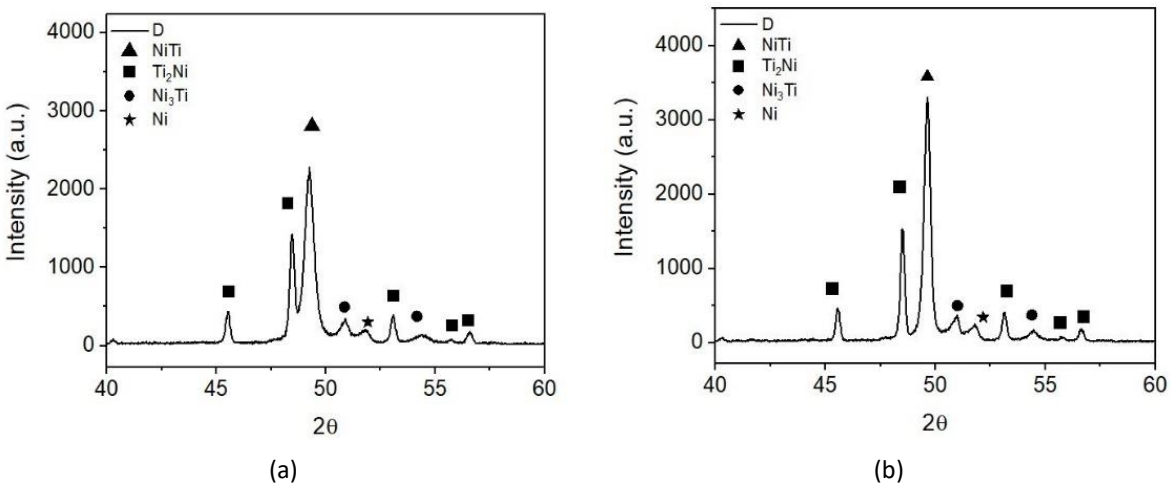

Figure 64. X-ray diffractograms of 3Dobject from filament D a) top b) base.

3.3.3 Defects

Tomographies of filaments is of enormous importance to detect failures inside the green, brown and sintered 3Dobjects, as referred. The detailed analysis on the defects in the

filaments before and after debinding and sintering, processed with the same conditions selected to manufacture the 3Dobjects, for some additions reveal a significative presence of porosity, inside and at the surface. These defects are mainly associated to the filament D. This could explain the odd values of Ni:Ti observed in the “dark phase”, since the evaluation of metallic ratio depends on surface defects.

Filaments of the four compositions studied, sintered at 1165°C during 5h, show that sintered filaments B and C had low quantity of defects. Against D, that show great content of porosity (Figure 65).

The strands (400 µm) were also analysed in order to detect defects in green that can be present inside each layer during the shaping of 3Dobject. This could be also significant to study the effect of layer interface against inside strand defects. Figure 65 also shows the possible relationship between filament defects (green) and strands ones.

	Filament		Strand
	Green	Sintered 1165°C (5h)	Green
B	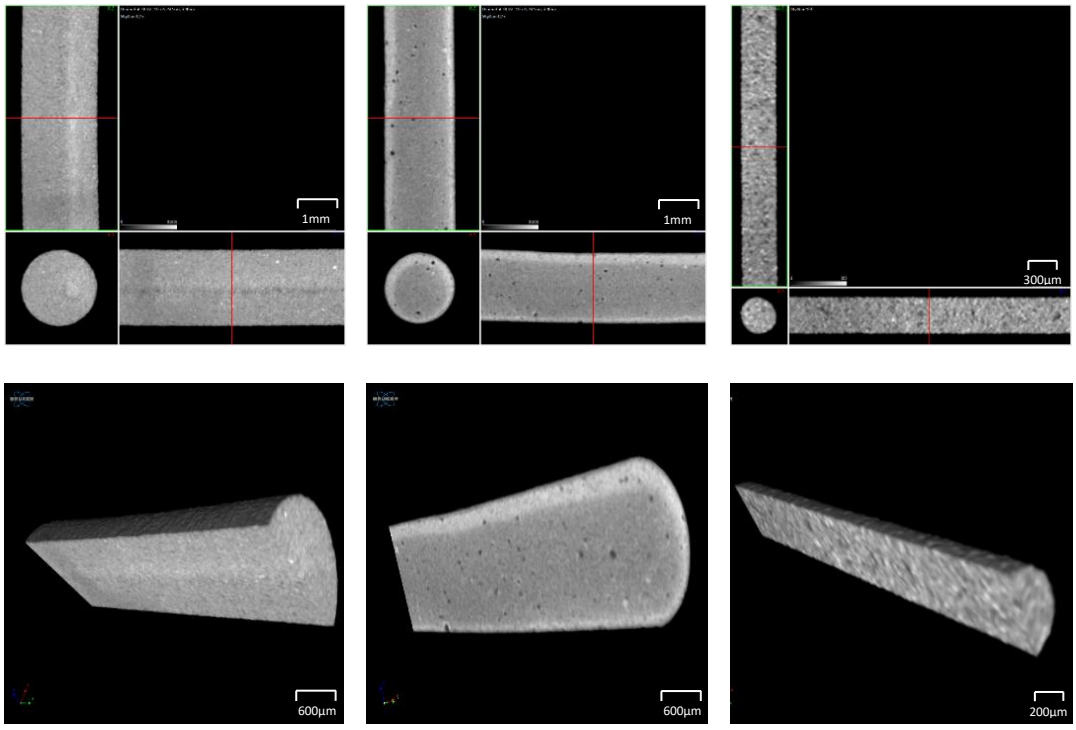		

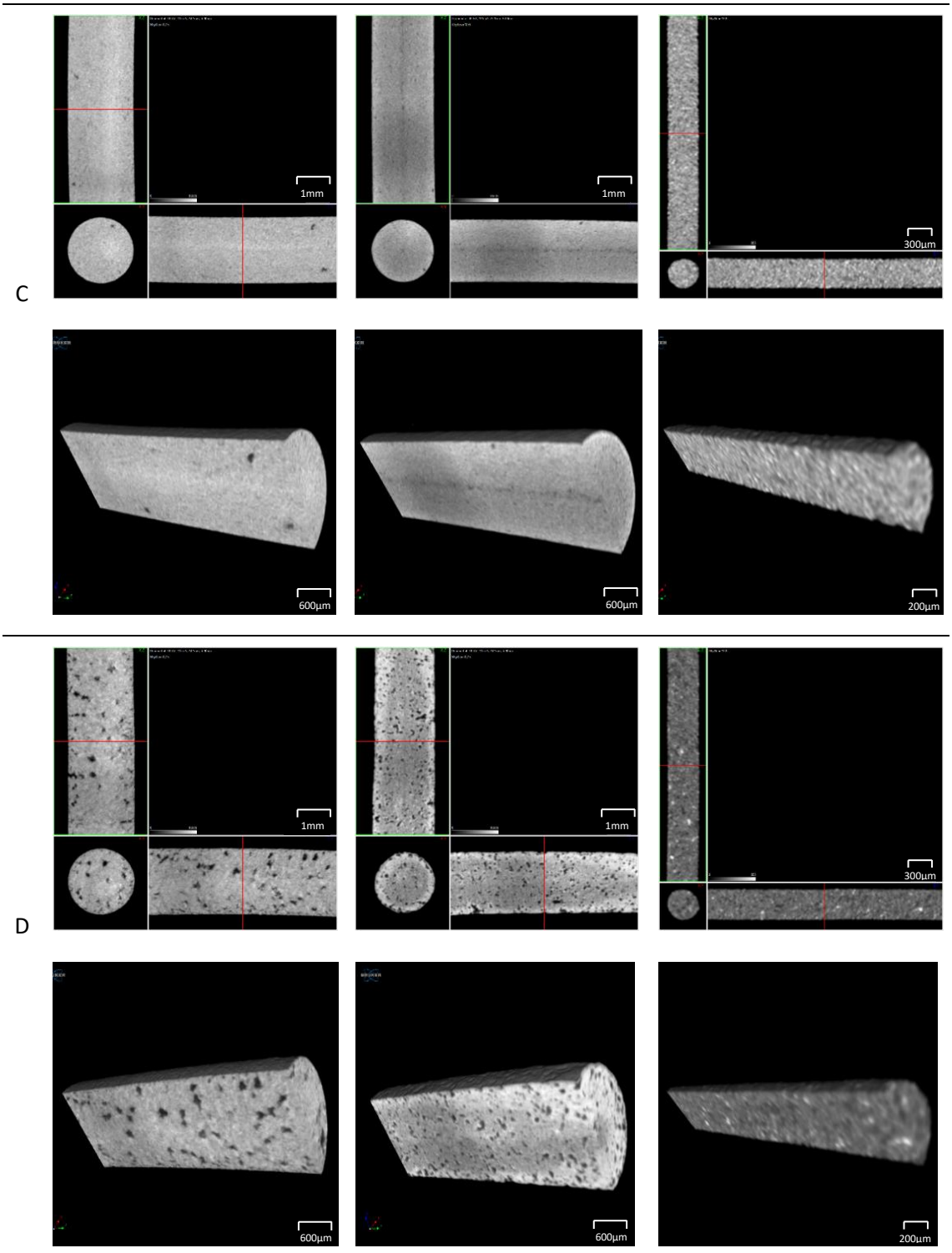

Figure 65. Tomographies of B, C and D filaments (green and sintered at 1165°C during 5h) and strands B, C and D (green).

To complement the study, a post shaping treatment was analysed using tomography. One of the most significative treatments to decrease porosity, in filaments/3Dobjects in the green state, is IP. Tomography results and dimensional variation for all powder compositions

studied are present in Figure 66. The most significant observation is the reduction of porosity in Filament D.

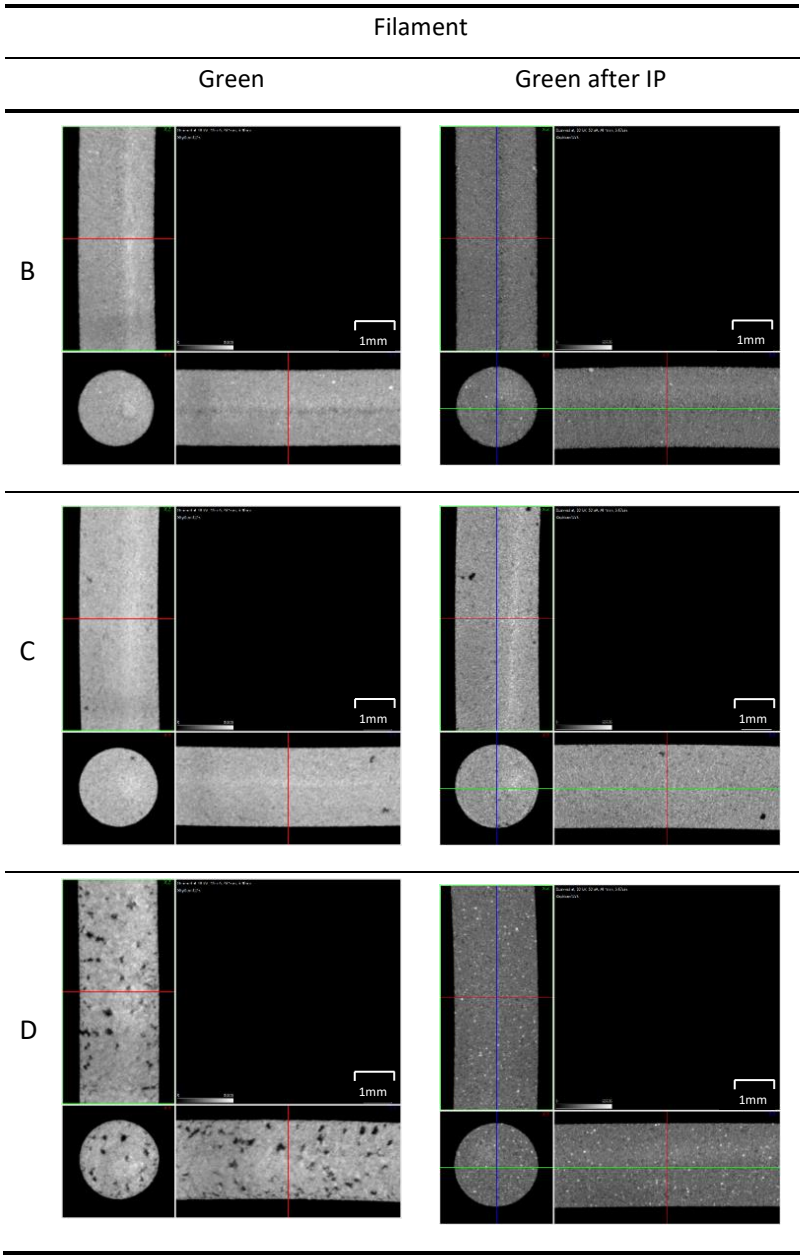

Figure 66. Tomographies of green vs IP green filaments B, C and D.

3.3.4 Phase composition and defects versus hardness

Figure 67 show the different phases resulting from all the chemical compositions of powder studied. As it is clear in Table 26, the best phase composition having in mind the disappear of Ni_3Ti and Ni, is the sintered designated by C.

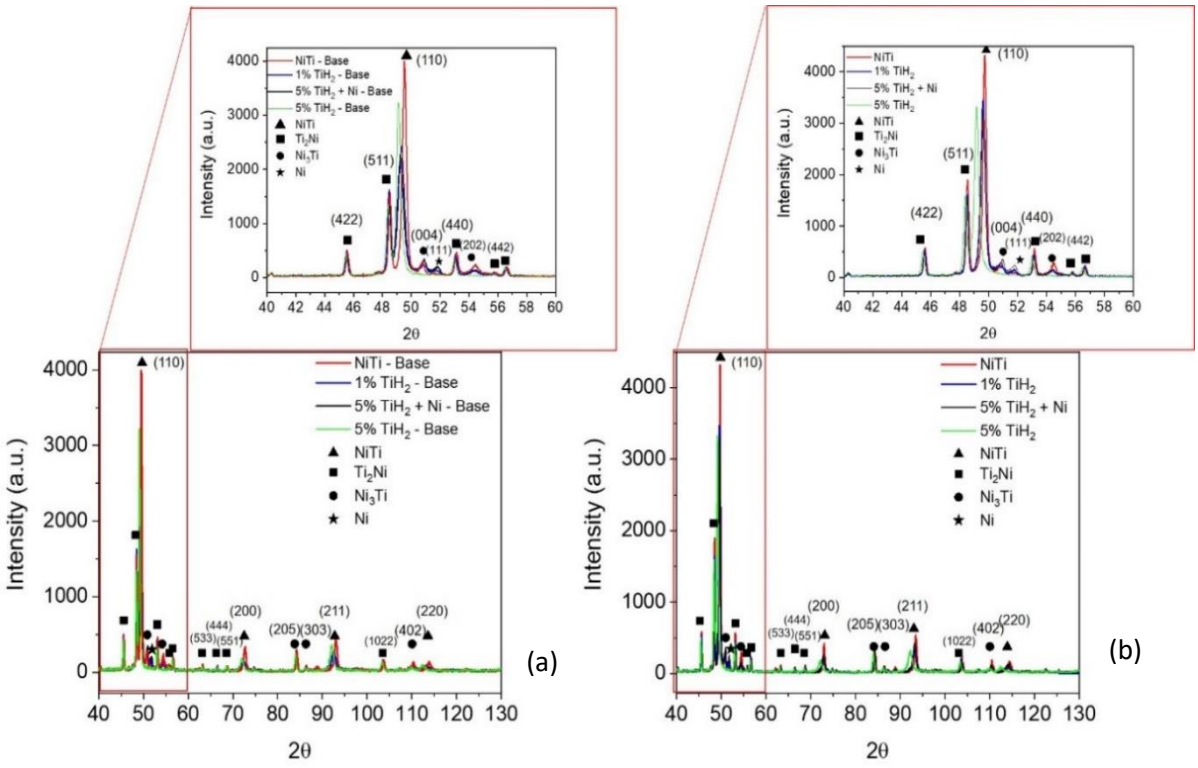

Figure 67. X-ray diffractogram of sintered 3Dobjects with different compositions at 1165°C(5h) a) base b) top.

Table 26. Phases after sintering function of chemical composition (Figure 67).

	Base				Top			
	NiTi	$NiTi_2$	Ni_3Ti	Ni	NiTi	$NiTi_2$	Ni_3Ti	Ni
A	X	X	X	X	X	X	X	X
B	X	X	X	X	X	X	X	X
C	X	X	-	-	X	X	-	-
D	X	X	X	X	X	X	X	X

One clear conclusion is the efficiency of the sintering process. The same phases are observed in both top and base, meaning that the sintering process was performed in the entire sample. All the phases registered before (NiTi, $NiTi_2$, Ni_3Ti and Ni) are still present in samples A, B and D. In the structural analysis of Sample C (NiTi + 5 wt% TiH_2) only NiTi and $NiTi_2$ are observed. It can be concluded that with the addition of 5 wt% of TiH_2 all the loose Ni reacted with the new Ti and formed NiTi and/or $NiTi_2$. An intermediate value, between 1 and 5 wt% could have been the precise amount of TiH_2 not to exceed the amount of Ti and not to form $NiTi_2$.

Table 27 summarizes microhardness and standard deviation (SD) measured for different compositions. Microhardness values are still higher than the hardness of NiTi [132, 133, 150, 151] confirming the presence yet of harder phases (*i.e.*, Ni_3Ti).

Table 27. Microhardness of the sintered samples (1165°C, 5 h).

	Mixture A	Mixture B	Mixture C	Mixture D
Hardness [HV] (MH+SD)	887 ± 58	773 ± 68	715 ± 39	677 ± 59

A possible reason for the decrease in hardness is the increase in the amount of the NiTi phase, from $NiTi_2$. By other hand, the Ni_3Ti formed again, have a morphology that could not be suitable to significantly increase the hardness.

The main conclusion of the present study can be described as a possibility to process, by MEX, NiTi as the master phase. However, the total disappearance of $NiTi_2$ during sintering is not yet achieved. There is a significant decrease of $NiTi_2$, although in conditions where Ni_3Ti is present. The solution envisaged must be studied for more percentages of TiH_2 and Ni highlighting the role of $NiTi_2$ in NiTi SMA behavior.

CHAPTER IV

Injection Moulding Case Study

The moulds industry has always been a pioneer in technological development, and to keep competitivity needs constant improvement and optimization of their processes and tools. As a major driver of technological development, machinery and tools are constantly being developed. Since its beginnings in the 1940s, it has undergone constant improvement and optimization at the expense of empirical knowledge. As a result of world competition, excellent quality tools are increasingly required, to obtain parts with high dimensional, structural and surface finish quality. Nowadays, even the simplest part is bought by the common person not only for its utility but also by its aesthetics, demanding from the production brands a constant changing of their products. Competitive markets, as the automobile, are always evolving to motivate buyers and restyling of its products are constantly being made. Plastic parts are everywhere, and with the grow in quantity also grows its complexity in order to offer quality and functionality (Figure 68a).

Most of the times, plastic parts interact with other parts either from plastic or other materials, and a typical connection used are the “snap fits” (Figure 68b). As many other solutions, these features cause a negative to the extraction direction, that needs to be moulded with special mechanical elements.

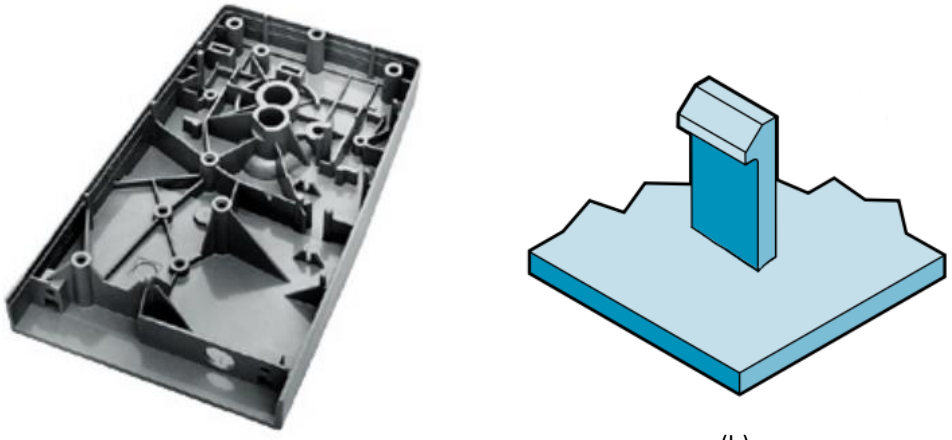

(a) (b)

Figure 68. Plastics parts a) Complex plastic part b) Snap fit connection (Adapted from [152]).

A mould tool is a very complex machine, that can reach thousands of parts and is by nature a mechanical machine. To mould a single undercut a mechanical system must be created that is formed by several parts (Figure 69). Two common solutions are used depending on the location of the undercut in the plastic part. When located at the edge of the part sliders are commonly used (Figure 69a) because they are easy to build, are robust and require less maintenance. When the undercuts are located far from the edge of the plastic part, angle ejectors must be used (Figure 69b). Angle ejectors are not so reliable as sliders, but still the most

used solution. These parts are always produced in steel, require milling and most of them, must be thermal treated to achieve hardness enough to withstand thousands of cycles, which brings costs. Another issue is the volume that these systems require. To produce a single undercut, a complete set of parts is required, and a plastic part can have dozens of undercuts, meaning that a system must be produced for each one.

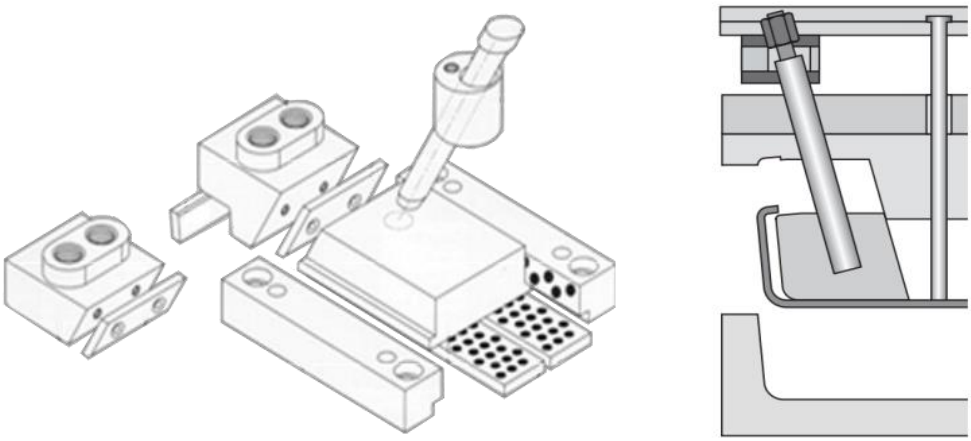

(a) (b)

Figure 69. Undercut moulding system a) Sliders b) Angle ejector (Adapted from [153]).

In Figure 70 is the schematic movement of a slider. With the mould closed, during the injection step, the cavity is filled, creating the plastic part (Figure 70a). After cooling of the part, with the movement of the mould opening, the angle pin pushes the slider back (Figure 70b), creating space for the undercut to be extracted (Figure 70c). The opposite movement pushes the slider back to the injection position. This simple step requires all the parts from Figure 69a.

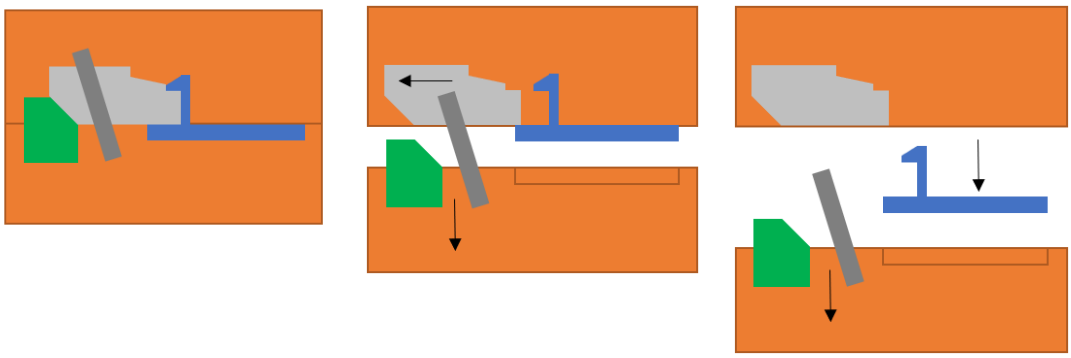

(a) (b) (c)

Figure 70. Slider movement illustration a) Injection step b) mould opening c) extraction.

Although this system is quite robust, and the most used in the injection moulding industry, it can only be used at the edge of the plastic parts because it depends on the interaction between the two parts of the mould to create movement. Also, because the angle pin is located directly under the slider it would damage the plastic part.

Angle sliders are a more complex mechanical system and far more fragile. After injection and cooling (Figure 71a), the mould is opened (Figure 71b) and the ejection plates move forward. With this movement, the angle slider is forced to move down and backwards (Figure 71c).

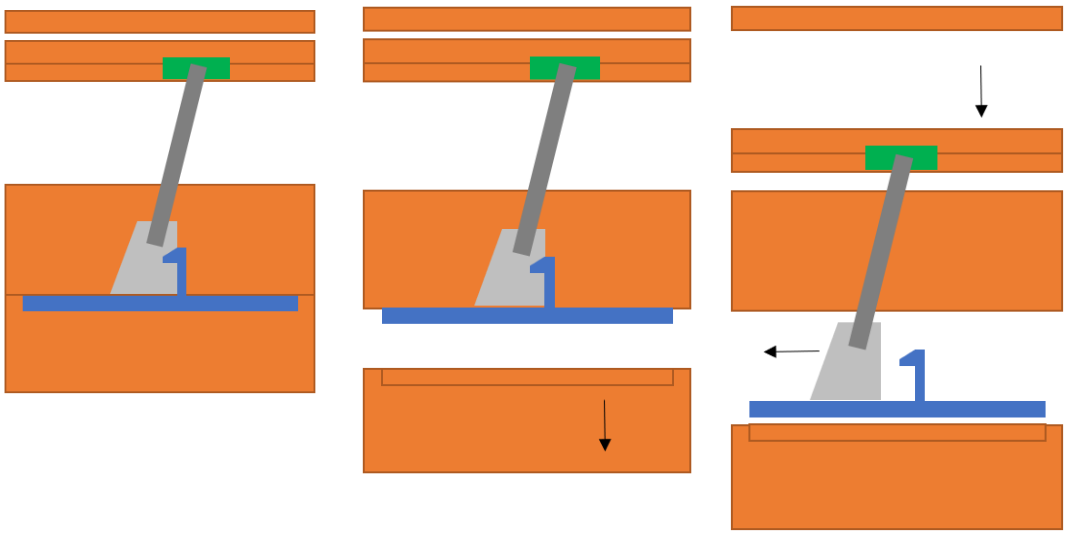

Figure 71. Angle ejector movement illustration a) Injection step b) mould opening c) extraction.

This system is very difficult to set, because it interacts with many other parts to create movement, also, is very fragile because the rod is always very thin and long and breaks many of the times. The rod is submitted to high forces that causes it to buckle and consequently failure. For both systems there is also the limitation of the angle of both pin and rod. These systems are not used for angles higher than 12 degrees to the direction of extraction. This causes a limitation in the travel of the systems, that is tuned by this angle and by the length of the angle pin in the case of sliders and by the high of the ejection size in the case of the angle ejectors. In fact, the angle by itself is not the limitation, the limitation comes by the sum of the angle with the linear forces that both pin and rod are submitted that can cause them to buckle or even to break.

SMAs could be a solution for the complex mechanical systems used to mould undercuts, by using the control temperature of the mould, to activate the transformation temperatures of the NiTi alloy.

The shape setting temperature of Nitinol is usually around 500°C [154-156]. The most used polymers in injection moulding are processed around 200°C which is below the shape setting temperature, and should have no influence in the properties of the alloy. The (Mf) should be set to a temperature close to 50°C (Figure 4), which is also a recommended temperature to

extract plastic parts, and because the transformation hysteresis (composition 49-51 at% Ni) of NiTi is around 30°C [30], the (Af) should be in a temperature below the processing temperature.

Figure 72 illustrates how SMAs can be used to demould an undercut. During injection, with the temperature of the mould above (Af), the NiTi insert is stiff, and will be used to mould the undercut (Figure 72a). After injection (Figure 72b), the cooling system of the mould will drop the temperature below (Mf), and the alloy will become ductile. The plastic part when extracted, should deform the NiTi insert, allowing it to be removed from inside the mould. Heating up the mould above (Af), should make the NiTi insert to recover its initial shape, allowing a new injection cycle (Figure 72c).

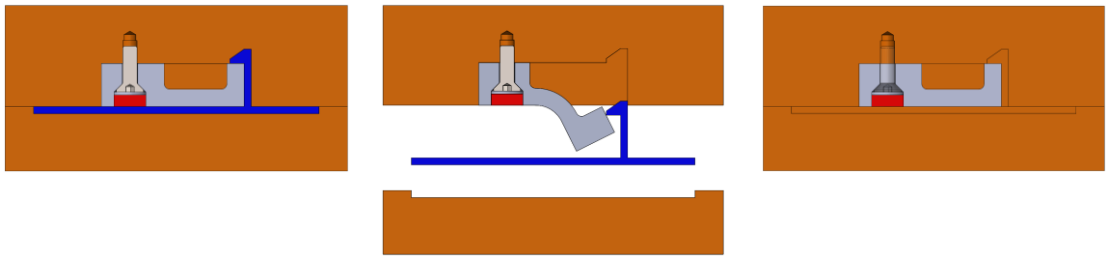

(a) (b) (c)

Figure 72. Undercut demoulding using SMA a) Injection step b) extraction c) recovery of SMA.

The freedom of shape of the parts produced by AM allows the production of inserts and demoulding parts, without milling operations, that is prejudicial to SMA. Using AM to produce parts from NiTi is expected to be of great advantage for the injection moulding industry.

CONCLUSIONS

For several years AM has been recognized to solve major production problems in processing 3Dobjects. Some of the limitations of AM applications are related to cost reasons, but also in selecting the adequate technology suitable to the geometry of the 3Dobject, without loss of feedstock material or excessive finishing procedures. However, the main limitation of AM application is attributed to the material selected to attain the final properties of parts/systems/devices. Although, a significant type of materials used in AM, have the microstructure desired to the application envisaged, with or without post processing treatment. Nevertheless, in some materials is very difficult to attain the desired target, whatever the AM technology selected.

NiTi (SMA) is one material with excellent properties, but up to know has been difficult to attain by conventional processing in liquid and/or solid phase (casting, subtractive and replicative technologies) from bulk material or powder feedstocks.

The study had two thresholds, as follows:

- to study the AM new technology (SLM versus MEX),
- to optimize the powder composition,

to attain NiTi, as main final phase.

According to the bibliography about SLM, the preferable powder selection is prealloyed NiTi. This type of powder contributes to yield a more uniform microstructure, and is susceptive to form, during processing, lower Ni_3Ti and $NiTi_2$ content than Ni-Ti elemental powder. Nevertheless, this behaviour is always associated with pure powder (free of impurities or secondary phases), however, the major of the research published, does not show NiTi prealloyed powder characteristics, despite of the occurrence of $NiTi_2$ and Ni to be a common result from atomization process. Moreover, $NiTi_2$ powder can be a helpful aiding in milling and mechanical alloying of Ni-Ti elemental powder, as a promoter of the process.

In prealloyed powder, $NiTi_2$ could have a significant role in AM, where the sintering is the consolidation technique. One of the most promising indirect technologies for AM is MEX, which uses maximum processing temperatures, lower than the melting temperatures of the powder particles. The present research work shows that $NiTi_2$ intermetallic, in prealloyed powder, can contribute to the uniformization of the final microstructure in indirect additive processes like MEX. Due to its low melting temperature (984°C), according to diffusion-controlled nature of sintering. However, the content of $NiTi_2$ in the feedstock must be considered, not to significantly change the mechanical behaviour of NiTi after consolidation. Although, the presence of $NiTi_2$ in the prealloyed powder associated to free Ni, could be suitable

to promote, in liquid phase during sintering, the formation of NiTi. After sintering, free Ni disappearance, could be attributed to its vapour pressure and/or reaction with $NiTi_2$ and/or formation of Ni_3Ti at sintering temperatures. In the present study the Ni_3Ti formation assumes the main role. This behaviour approaches prealloyed powder to elemental powder, like the results in SLM, resulting in the formation of Ni_3Ti and the presence of $NiTi_2$ after consolidation.

According to the available literature, no study has investigated the application of MEX technology to intermetallic NiTi powder particles. Therefore, it is crucial to have a complete understanding of all five steps involved in the manufacturing process: mixing the constituents of filaments feedstock (NiTi prealloyed powder, binder and additives), extrusion (filament fabrication), shaping (conforming the 3Dobject), debinding (binder removal) and sintering (part consolidation).

A methodology developed to evaluate the CPVC for PIM was adapted to prealloyed NiTi powder filament mixing, and the maximum value of 60 vol% including other additives than binder (as in PIM) was attained with suitable rheological properties. This value is higher than the filaments, with other metallic powder particles, available in the market. The filament developed in the present study was successfully extruded with a homogeneous distribution of the powder particles, binder and additives. The filaments have an excellent level of reproducibility, as evidenced by the high Weibull modulus (m) for the filament flexural strength (m=23). Moreover, it is necessary to consider the absence of pressure when shaping, in contrast to PIM, where the injection pressure can reach high values. For the first time, microtomography was used to evaluate the integrity inside the NiTi based filaments and porosity was detected for some compositions, although it was not an obstacle for successful shapping.

After shaping several geometries, thermal debinding allows the total elimination of binder and additives (Tmax = 600°C) in a H_2 atmosphere. Sintering in a hydrogen atmosphere at $T_{optimal}$=1165°C during 5h, similar to sintering at higher temperatures, also produces Ni_3Ti and $NiTi_2$ phases.

In order to highlight the role of Ni in the virgin powder, different contents of TiH_2 were added to NiTi prealloyed powder. This procedure highlighted that Ti after dehydrogenation could contribute together with free Ni to the formation of NiTi instead of Ni_3Ti. During dehydrogenation the released H_2 was effective in the removal of O_2 preventing the formation of oxides. The composition with 5 wt% TiH_2 showed the best results in the final phases. The new Ti reacted with the loose Ni and formed only NiTi and $NiTi_2$ avoiding the formation of Ni-rich phases and total depletion of loose Ni. The gap of 4 wt% of TiH_2 (1 wt% and 5 wt%) allowed the formation of Ti-rich phases meaning that a lower amount in wt% of TiH_2 would probably be effective in the avoidance of $NiTi_2$ formation.

In consequence, the hardness registered was lower than the consolidation of initial NiTi prealloyed powder. The sintering process was total in all the conditions and the phases formed, in both the top and base, were the same.

For future perspectives and being the MEX technology composed of so many stages, all of them with its own particularities, there are some issues that still can be improved. The correct choice of additives was effective in the production of the feedstock with the correct CPVC. No changes were detected in the phases formed and homogeneity was achieved.

During shaping the correct set of parameters allowed to print the geometries selected. Nevertheless, the layers were visible, meaning that gaps and porosity can be formed inside the parts, that can compromise total sintering and the structural integrity of the parts produced. New parameters can be studied to allow the use of a sprue with a small diameter and consequently allowing shaping with smaller increments.

Due to the temperatures reached and the slow cooling, secondary phases can be formed, that completely modify the properties of the main phase. It is also known that post-processing can influence the formation of phases, especially the metastable ones. Being NiTi sensible to composition changes and its composition dependent on the stages involving temperature, heating and cooling procedures and post-processing approaches must be optimized.

Although secondary phases were formed besides NiTi, MEX appears to be a promising technology for processing NiTi prealloyed powder particles by AM. Given this approach, is expected in the near future a good solution for NiTi manufacturing with the best results.

BIBLIOGRAPHY

1. Buehler, W.J., J.V. Gilfrich, and R.C. Wiley, Effect of Low-Temperature Phase Changes on the Mechanical Properties of Alloys near Composition TiNi *Journal of Applied Physics*, **1963**. 34(1475).
2. Hodgson, D.E., M.H. Wu, and R.J. Biermann, *ASM Handbook-Properties and Selection: Nonferrous Alloys and Special-Purpose Materials*. Shape Memory Alloys. Vol. 2. 1990: ASM International.
3. Cederstrom, J. and J.V. Humbeeck, Relationship Between Shape Memory Material Properties and Applications. *Journal de Physique IV Proceedings*, **1995**. 5: p. 335-341.
4. Walker, J., M. Elahinia, and C. Haberland, An investigation of process parameters on selective laser melting of nitinol, in ASME 2013 Conference on Smart Materials, Adaptive Structures and Intelligent Systems. 2013, American Society of Mechanical Engineers: Snowbird, Utah, USA.
5. Meier, H., C. Haberland, and J. Frenzel, Structural and functional properties of NiTi shape memory alloys produced by selective laser melting, in Innovative developments in design and manufacturing: advanced research in virtual and rapid prototyping. 2011, Taylor & Francis Group: Leiria, Portugal. p. 291–296.
6. Frenzel, J., E.P. George, A. Dlouhy, C. Somsen, M.F.X. Wagner, and G. Eggeler, Influence of Ni on martensitic phase transformations in NiTi shape memory alloys. *Acta Materialia*, **2010**. 58(9): p. 3444-3458.
7. Ortega, A., J. Tyber, C. Frick, K. Gall, and H. Maier, Cast NiTi Shape-Memory Alloys. *Advanced Engineering Materials*, **2005**. 7: p. 492-507.
8. Meier, H., C. Haberland, J. Frenzel, and R. Zarnetta, Selective Laser Melting of NiTi Shape Memory Components, in Innovative Developments in Design and Manufacturing – Advanced Research in Virtual and Rapid Prototyping. 2009, CRC Press Balkema: Leiria, Portugal. p. 233-238.
9. Bormann, T., R. Schumacher, B. Muller, M. Mertmann, and M. Wild, Tailoring selective laser melting process parameters for NiTi implants. *Journal of Materials Engineering and Performance*, **2012**. 21(12): p. 447-454.
10. Bormann, T., B. Müller, M. Schinhammer, A. Kessler, P. Thalmann, and M. Wild, Microstructure of selective laser melted nickel–titanium. *Materials Characterization*, **2014**. 94: p. 189-202.
11. Haberland, C., M. Elahinia, and J. Walker, Additive manufacturing of shape memory devices and pseudoelastic components, in ASME 2013 conference on smart materials, adaptive structures and intelligent systems. 2013, New York: ASME.
12. Elahinia, M., N.S. Moghaddam, M.T. Andani, A. Amerinatanzi, B.A. Bimber, and R.F. Hamilton, Fabrication of NiTi through additive manufacturing: A review. *Progress in Materials Science*, **2016**. 83: p. 630-663.
13. Dudziak, S., M. Gieseke, H. Haferkamp, S. Barcikowski, and D. Kracht, Functionality of laser-sintered shape memory micro-actuators. *Physics Procedia*, **2010**. 5: p. 607-615.
14. Shishkovsky, I.V., L.T. Volova, M.V. Kuznetsov, Y.G. Morozov, and I.P. Parkin, Porous biocompatible implants and tissue scaffolds synthesized by selective laser sintering from Ti and NiTi. *Journal of Materials Chemistry*, **2008**. 18(12): p. 1309-1317.
15. Heaney, D.F., *Handbook of Metal Injection Molding*. Second Edition ed. Metals and Surface Engineering, ed. W.P. Series. 2019: Elsevier.
16. ASTM52900:2021, I., Standard Terminology for Additive Manufacturing, General Principles, Terminology. *ASTM International*, **2021**.
17. Crump, S., Apparatus and Method for Creating Three-Dimensional Objects. 1992: United States.
18. Krone, L., J. Mentz, M. Bram, H. Buchkremer, D. Stöver, M. Wagner, G. Eggeler, D. Juhre, S. Reese, D. Bogdanski, M. Köller, S. Esenwein, G. Muhr, O. Prymak, and M. Epple, The Potential of Powder Metallurgy for the Fabrication of Biomaterials on the Basis of Nickel-

Titanium: A Case Study with a Staple Showing Shape Memory Behaviour. *Advanced Engineering Materials.*, **2005**. 7: p. 613-619.
19. Krone, L., E. Schüller, M. Bram, O. Hamed, H. Buchkremer, and D. Stöver, Mechanical behaviour of NiTi parts prepared by powder metallurgical methods. *Materials Science and Engineering*, **2003**. 378(1-2): p. 185-190.
20. Schöller, E., L. Krone, M. Bram, H. Buchkremer, and D. Ståaver, Metal injection molding of shape memory alloys using prealloyed NiTi powders. *Journal of Materials Science*, **2005**. 40: p. 4231-4238.
21. Köhl, M., T. Habijan, M. Bram, H. Buchkremer, D. Stöver, and M. Köller, Powder Metallurgical Near-Net-Shape Fabrication of Porous NiTi Shape Memory Alloys for Use as Long-Term Implants by the Combination of the Metal Injection Molding Process with the Space-Holder Technique. *Advanced Engineering Materials.*, **2009**. 11: p. 959 - 968.
22. Köhl, M., M. Bram, M. Moser, H. Buchkremer, T. Beck, and D. Stöver, Characterization of porous, net-shaped NiTi alloy regarding its damping and energy-absorbing capacity. *Materials Science and Engineering*, **2011**. 528(6): p. 2454-2462.
23. Bidaux, J.E., H.A. Amherd, H. Girard, A.M. Rodríguez, L. Reynard, J. Chevallier, F. Aeby, G.J. Charles, and M.E. Carreño, Metal injection moulding of superelastic TiNi parts. *Key Engineering Materials*, **2016**. 704: p. 173-182.
24. Buehler, W.J. and F.E. Wang, A Summary of Recent Research on the NITINOL Alloys and their Potential Application in Ocean Engineering. *Ocean Engineering*, **1967**. 1: p. 105-120.
25. Mihálcz, I., Fundamental characteristics and design method for nickel-titanium shape memory alloy. *Periodica Polytechnica Mechanical Engineering* **2001**. 45(1): p. 75-86.
26. Cherian, C.J., R. Groarke, K. O'Toole, and D. Brabazon, Advances in Selective Laser Melting of Nitinol Shape Memory Alloy Part Production. *Materials*, **2019**. 12(809).
27. Kumar, P.K. and D.C. Lagoudlas, *Shape Memory Alloys: Modeling and Engineering Applications*. 2008: Springer: Texas.
28. Otsuka, K. and X. Ren, Physical metallurgy of Ti–Ni-based shape memory alloys. *Progress in Materials Science*, **2005**. 50(5): p. 511-678.
29. Andani, M.T., N.S. Moghaddam, C. Haberland, D. Dean, M.J. Miller, and M. Elahinia, Metals for bone implants. Part 1. Powder metallurgy and implant rendering. *Acta Biomaterialia*, **2014**. 10(10): p. 4058-4070.
30. Fernandes, F.M.B., Ligas com memória de forma, D.d.c.d.M. CENIMAT, Editor. 2003, Universidade Nova de Lisboa: Faculdade de Ciencias e Tecnologia.
31. Duerig, T.W., D. Stockel, K.N. Melton, and C.M. Wayman, *Engineering Aspects of Shape Memory Alloys*. 1990.
32. Horikawa, H., H. Tamura, Y. Okamoto, H. Hamanaka, and F. Miura, *MRS Int. Mtg. Adv. Mater*, **1989**. 9(195).
33. Zhang, J., X. Ren, K. Otsuka, and M. Asai, REVERSIBLE CHANGE IN TRANSFORMATION TEMPERATURES OF A Ti-51at%Ni ALLOY ASSOCIATED WITH ALTERNATING AGING. *Scripta Materialia*, **1999**. 41(10): p. 1109–1113.
34. Bertheville, B., M. Neudenberger, and J.E. Bidaux, Powder sintering and shape-memory behaviour of NiTi compacts synthesized from Ni and TiH2. **2004**. 384(1–2): p. 143-150.
35. Polozov, I. and A. Popovich, Microstructure and Mechanical Properties of NiTi-Based Eutectic Shape Memory Alloy Produced via Selective Laser Melting In-Situ Alloying by Nb. *Materials*, **2021**. 14(10): p. 2696.
36. Khoo, Z.X., Y. Liu, J. An, C.K. Chua, Y.F. Shen, and C.N. Kuo, A Review of Selective Laser Melted NiTi Shape Memory Alloy. *Materials (Basel)*, **2018**. 11(4).
37. Oliveira, R., Y. Lima, E. Sallet, D. Gonçalves, N. Le Sénéchal, E. Melo, R. Teixeira, P. Rodrigues, P. Neto, J. Silva, L.P. Brandao, and A. Paula, Production of Cylindrical Specimens Based on the Ni-Ti System by Selective Laser Melting from Elementary Powders. *Journal of Materials Engineering and Performance*, **2021**. 30.

38. Wang, X., J. Yu, J. Liu, L. Chen, Q. Yang, H. Wei, J. Sun, Z. Wang, Z. Zhang, G. Zhao, and J. Humbeeck, Effect of process parameters on the phase transformation behavior and tensile properties of NiTi shape memory alloys fabricated by selective laser melting. *Additive Manufacturing*, **2020**. 36: p. 101545.
39. Wu, G., N.A. Langrana, S. Rangarajan, R. McCuiston, R. Sadanji, S.C. Danforth, and A. Safari. Fabrication of Metal Components using FDMet: Fused Deposition of Metals. in *Proceedings of the Solid Freeform Fabrication Symposium*. 1999. Austin TX.
40. Wu, G., N.A. Langrana, R. Sadanji, and S.C. Danforth, Solid freeform fabrication of metal components using fused deposition of metals. *Materials & Design*, **2002**. 23(1): p. 97-105.
41. Agarwala, M.K., R.V. Weeren, A. Bandyopadhyay, A. Safari, and S.C. Danforth. Filament feed materials for fused deposition processing of ceramics and metals. in *Proceedings of the Solid Freeform Fabrication Symposium*. 1996. Austin, Texas.
42. Agarwala, M.K., R.V. Weeren, A. Bandyopadhyay, P.J. Whalen, A. Safari, and S.C. Danforth. Fused deposition of ceramics and metals: An overview. in *Proceedings of the Solid Freeform Fabrication Symposium*. 1996. Austin, Texas.
43. Agarwala, M.K., A. Bandyopadhyay, R.V. Weeren, N.A. Langrana, A. Safari, S.C. Danforth, V.R. Jamalabad, P.J. Whalen, D. R., and J. Pollinger. Fused deposition of ceramics (fdc) for structural silicon nitride components. in *Proceedings of the Solid Freeform Fabrication Symposium*. 1996. Austin, Texas.
44. Gutierrez, J.G., D. Godec, C. Kukla, T. Schlauf, C. Burkhardt, and C. Holzer, Shaping, debinding and sintering of steel components via fused filament fabrication, in 16th International Scientific Conference on Production Engineering - Computer Integrated Manufacturing and High Speed Machining. 2017: Zadar, Croatia.
45. Gutierrez, J.G., C. Kukla, S. Schuschnigg, D. Ivica, and H. Clemens, Fused Filament Fabrication for Metallic Parts, in 25. Leobener Kunststoff-Kolloquium 2016: Leoben, Austria.
46. Kukla, C., J.G. Gutierrez, I. Duretek, S. Schuschnigg, and C. Holzer. Effect of Particle Size on the Properties of Highly-Filled Polymers for Fused Filament Fabrication. in *AIP Conference Proceedings*. 2016.
47. Burkhardt, C., F. P., O. Weber, P. Imgrund, and S. Hampel, Fused Filament Fabrication (FFF) of 316L Green Parts for the MIM process, in World PM2016 – AM - Deposition Technologies. 2016.
48. Cruz, N., J. Vasco, and F.M. Barreiros, Binder system for fused deposition of metals, in International Powder Metallurgy Congress and Exhibition, Euro PM 2013. 2013.
49. Gutierrez, J.G., D. Godec, R. Guran, M. Spoerk, C. Kukla, and C. Holzer, 3d printing conditions determination for feedstock used in fused filament fabrication (fff) of 17-4ph stainless steel parts. *Journal Metalurgija*, **2018**. 57(1-2): p. 117-120.
50. Kukla, C., J.G. Gutierrez, S. Cano, S. Hampel, C. Burkhardt, T. Moritz, and C. Holzer, Fused Filament Fabrication (FFF of PIM Feedstock, in VI Congreso Nacional de Pulvimetalurgia y I Congreso Iberoamericano de Pulvimetalurgia. 2017.
51. Elahinia, M., M. Hashemi, M. Tabesh, and S.B. Bhaduri, Manufacturing and processing of NiTi implants: A review. *Progress in Materials Science*, **2012**. 57(5): p. 911-946.
52. Mohammad, H.E., M. Hashemi, M. Tabesh, and B.B. Sarit, Manufacturing and processing of NiTi implants: A review. *Progress in Materials Science*, **2012**. 57(5): p. 911-946.
53. Donald, F.H., *Handbook of Metal Injection Molding*. 2012: Woodhead Publishing Limited. 604.
54. Mulser, M. and F. Petzoldt, Standards for Metal Injection Moulding: Progress to-date and future challenges, in Powder Injection Moulding International. 2017.
55. Bram, M., M. Bitzer, H. Buchkremer, and D. Stöver, Reproducibility Study of NiTi Parts Made by Metal Injection Molding. *Journal of Materials Engineering and Performance*, **2012**.

56. Bram, M., k. M., H. Buchkremer, and D. Stöver, Mechanical Properties of Highly Porous NiTi Alloys. *Journal of Materials Engineering and Performance*, **2010**.
57. Bram, M., A.A. Khanlou, A. Heckmann, B. Fuchs, H. Buchkremer, and D. Stover, *Materials Science Engineering*, **2002**. A337: p. 254.
58. Muhammad, H.I., G. Russell, A.D. Hywel, and T. Iain, Porous NiTi alloy by metal injection moulding/sintering of elemental powders: Effect of sintering temperature. *Materials Letters*, **2012**. 70: p. 142-145.
59. F2792-12a, A., Standard Terminology for Additive Manufacturing Technologies. **2013**.
60. ASTM52900:2015, I., Standard Terminology for Additive Manufacturing, General Principles, Terminology. *ASTM International*, **2015**.
61. Gebhardt, A., *Rapid Prototyping*. 2003: Hanser Gardner Publications.
62. Noorani, R., *Rapid Prototyping - Principles and Applications*. 2006: John Wiley & Sons.
63. Ashley, S., Rapid prototyping systems. *Mechanical Engineering*, **1991**. 113(4).
64. Wohlers, T. and I. Campbell, *Wohlers Report 2017 - 3D Printing and Additive Manufacturing State of the Industry*. 2017: Wohlers Associates, Inc.
65. Frazier, W.E., Metal additive manufacturing: a review. *Mater Eng Perform*, **2014**. 23: p. 1917-1928.
66. Wohlers, T., *Wohlers Report 2019 - 3D Printing and Additive Manufacturing State of the Industry*. 2019.
67. Statistica. Projected global additive manufacturing market growth between 2020 and 2026. 2021; Available online: https://www.statista.com/statistics/284863/additive-manufacturing-projected-global-market-size/ (acessed on: 10/09/2021).
68. KG, A.G.C., Metal additive Manufacturing, G.C. KG, Editor. 2020.
69. Hull, C.W., Apparatus for production of three-dimensional objects by stereolithography. 1986: United States.
70. Thompson, M.K., G. Moroni, T. Vaneker, G. Fadel, R.I. Campbell, I. Gibson, A. Bernard, J. Schulz, P. Graf, B. Ahuja, and F. Martina, Design for Additive Manufacturing: Trends, opportunities, considerations, and constraints. *CIRP Annals*, **2016**. 65(2): p. 737-760.
71. Klahn, C., B. Leutenecker, and M. Meboldt, Design Strategies for the Process of Additive Manufacturing. *CIRP 25th Design Conference Innovative Product Creation*, **2015**. 36: p. 230-235.
72. Yang, L., K. Hsu, B. Baughman, D. Godfrey, F. Medina, M. Menon, and S. Wiener, *Additive Manufacturing Process Chain*, in *Additive Manufacturing of Metals: The Technology, Materials, Design and Production*. 2017. p. 33-43.
73. Wohlers, T., *History of Additive Manufacturing*, in *Wohlers Report 2017*. 2017, Wohlers Associates.
74. Shishkovsky, I., I. Yadroitsev, and I. Smurov, Direct Selective Laser Melting of Nitinol Powder. *Physics Procedia*, **2012**. 39: p. 447-454.
75. Meier, H. and C. Haberland, Experimental studies on selective laser melting of metallic parts. *Materialwissenschaft und Werkstofftechnik*, **2008**. 39(9): p. 665–670.
76. Walker, J., C. Haberland, M.T. Andani, H.E. Karaca, D. Dean, and M. Elahinia, Process development and characterization of additively manufactured nickel–titanium shape memory parts*Journal of Intelligent Material Systems and Structures* **2016**. 27(19): p. 2653 - 2660.
77. Gu, D. and C. Ma, In-situ formation of Ni4Ti3 precipitate and its effect on pseudoelasticity in selective laser melting additive manufactured NiTi-based composites. *Applied Surface Science*, **2018**. 441: p. 862-870.
78. Walker, J., Additive manufacturing towards the realization of porous and stiffness-tailored NiTi implants, in Bioengineering. 2014, University of Toledo.
79. Yang, Y., Y. Huang, and W. Wu. One-step shaping of NiTi biomaterial by selective laser melting. in *SPIE*. 2008.

80. Haberland, C., M. Elahinia, J. Walker, H. Meier, and J. Frenzel, On the development of high quality {NiTi} shape memory and pseudoelastic parts by additive manufacturing. *Smart Materials and Structures*, **2014**.
81. Clare, A.T., P.R. Chalker, S. Davies, C.J. Sutcliffe, and S. Tsopanos, Selective laser melting of high aspect ratio 3D nickel–titanium structures two way trained for MEMS applications. *International Journal of Mechanics and Materials in Design*, **2008**. 4(2): p. 181-187.
82. Saedi, S., A.S. Turabi, M.T. Andani, C. Haberland, H.E. Karaca, and M. Elahinia, The influence of heat treatment on the thermomechanical response of Ni-rich NiTi alloys manufactured by selective laser melting. *Journal of Alloys and Compounds*, **2016**. 677: p. 204-210.
83. Haberland, C., H. Meier, and J. Frenzel, On the properties of Ni-rich NiTi shape memory parts produced by selective laser melting, in ASME 2012 conference on smart materials, adaptive structures and intelligent systems. 2012, American Society of Mechanical Engineers.
84. Boparai, K.S., R. Singh, and H. Singh, Development of rapid tooling using fused deposition modeling: a review. *Rapid Prototyping Journal*, **2016**. 22(2): p. 281-299.
85. Marcincinova, L.N. and I. Kuric. Basic and Advanced Materials for Fused Deposition Modeling Rapid Prototyping Technology. in *Manufacturing and Industrial Engineering*. 2012.
86. Marcincinova, L.N., J.N. Marcincin, J. Barna, and J. Torok. Special materials used in FDM rapid prototyping technology application. in *Proceedings of the 16th International Conference on intelligent engineering system*. 2012.
87. Smith, W.C. and R.W. Dean, Structure characteristics of fused deposition modeling polycarbonate material. *Polymer Testing*, **2013**. 32(8): p. 306-1312.
88. Carreira, P., F. Cerejo, N. Alves, and M.T. Vieira, In Search of the Optimal Conditions to Process Shape Memory Alloys (NiTi) Using Fused Filament Fabrication (FFF). *Materials*, **2020**. 13(21): p. 4718.
89. Cerejo, F., Development of filamentos for 3D printing of steel parts. 2018, University of Coimbra.
90. German, R.M., *Powder Metallurgy Science*. 2 ed. 1994, NJ USA: Metal Powder Industries Federation: Princeton.
91. Kukla, C., D. Ivica, S. Schuschnigg, J.G. Gutierrez, and C. Holzer, Properties for PIM Feedstocks Used in Fused Filament Fabrication, in World PM 2016 Congress and Exhibition. 2016: Hamburg, Germany.
92. Shishkovsky, I., I. Yadroitsev, and I. Smurov, Manufacturing ThreeDimensional Nickel Titanium Articles Using LayerbyLayer LaserMelting Technology. *Technical Physics Letters*, **2013**. 39(12): p. 1081-1084.
93. Barreiros, F.M., M.T. Vieira, and J.M. Castanho, Fine tuning injection feedstock by nano coating SS powder. *Metal Powder Report*, **2009**. 64(9): p. 18-1.
94. Vieira, M.T., A.G. Martins, F.M. Barreiros, M. Matos, and J.M. Castanho, Surface modification of stainless steel powders for microfabrication. *Journal of Materials Processing Technology*, **2008**. 201(1-3): p. 651-656.
95. German, R.M., Powder Injection Molding. *Metal Powder Industries Federation: Princeton*, **1990**.
96. German, R.M. and A. Bose, Injection Molding of Metals and Ceramics. *Metal Powder Industries Federation: Princeton*, **1997**.
97. Barreiros, F.M., Optimização da moldação por injeção de pós de residuos industriais inorgânicos. 2002, University of Coimbra.
98. Brabender, Original Brabender Instruments for Material Research and Quality Control 2017.

99. Mohamed, O.A., S.H. Masood, and J.L. Bhowmik, Optimization of fused deposition modeling process parameters: a review of current research and future prospects. *Advances in Manufacturing*, **2015**. 3(1): p. 42-53.
100. Dassault, S. Solidworks Student Version. 2019; Available online: https://www.3ds.com/products-services/solidworks/ (acessed on: 10/05/2019).
101. Ultimaker, B.V. Ultimaker Cura 4.1. 2019; Available online: https://ultimaker.com/en/products/ultimaker-cura-software (acessed on: 05/03/2019).
102. Heaney, D.F., *Handbook of metal injection molding*. 2012: Ed. Woodhead Publishing in Materials.
103. ELNIK MIM 3002 T-50. Available online: https://elnik.com/products/mim-3000-series/ (acessed on: 26/08/2020).
104. Ferreira, T.J.J., Microinjection Moulding of austenitic stainless steel reinforced with carbon nanotubes. 2018, University of Coimbra.
105. Kothari, N.C., THE EFFECT OF PARTICLE SIZE ON SINTERING KINETICS IN ALUMINA POWDER. *Journal of Nuclear Materials*, **1965**. 17: p. 43-53.
106. Ting, J.M. and R.Y. Lin, Effect of particle size distribution on sintering *JOURNAL OF MATERIALS SCIENCE*, **1995**. 30: p. 2382-2389.
107. Miyake, K., Y. Hirata, T. Shimonosono, and S. Sameshima, The Effect of Particle Shape on Sintering Behavior and Compressive Strength of Porous Alumina. *Materials*, **2018**. 11(1137).
108. Otsuka, K. and T. Kakeshit, Science and Technology of Shape-Memory Alloys: New Developments. *Materials Reseach Society*, **2002**.
109. German, R.M., Carbon control: An important discriminant in Metal Injection Moulding, in Powder Injection Moulding International. 2015.
110. Chen, G., K.L. Liss, and P. Cao, In situ observation and neutron diffraction of NiTi powder sintering. *Acta Materialia*, **2014**. 67: p. 32-44.
111. Laeng, J., Z. Wu, Y. Wang, Y. Liu, and H. Yang, Phase Formation in Ti–Ni Binary System during Solid-State Synthesis. *Shape Memory and Superelasticity*, **2018**. 4(3): p. 351-359.
112. Khanlari, K., M. Ramezani, P. Kelly, P. Cao, and T. Neitzert, Mechanical and microstructural characteristics of as-sintered and solutionized porous 60NiTi. *Intermetallics*, **2018**. 100: p. 32-43.
113. Wei, L., X. Zhang, and L. Geng, Microstructure and properties of NiTi foams with 69% porosity. *Vacuum*, **2019**. 162.
114. LPW, C.A.U., Test certificate, in LPW-NITI-AZAR. 2018.
115. Elements, A. 2020; Powder Suplier]. Available online: www.americanelements.com (acessed on: 2020
116. Kadir, R.A.A., R. Razali, N. Nor, I. Subuki, and M. Ismail, The Effect of Particles Shape and Size on Feedstock Flowibility and Chemical content of As-sintered NiTi Alloys. 2018, Materials Science and Engineering.
117. Lim, T.J., B. Smith, and D.L. McDowell, Behavior of a random hollow sphere metal foam. *Acta Materialia*, **2002**. 50(11): p. 2867-2879.
118. Ou, S.-F., B.-Y. Peng, Y.-C. Chen, and M.-H. Tsai, Manufacturing and Characterization of NiTi Alloy with Functional Properties by Selective Laser Melting. *Metals*, **2018**. 8(5): p. 342.
119. Ashby, M.F., A.G. Evans, N.A. Fleck, L.J. Gibson, J.W. Hutchinson, and H.N.G. Wadley, *Metal Foams, A Design Guide*. 2000.
120. Liu, P.S. and G.F. Chen, *Porous Materials: Processing and Applications*. 2014: Elsevier.
121. Ferreira, T.J.J. and M.T. Vieira. Behavior of feedstocks reinforced with nanotubes for micromanufacturing. in *Euro PM 2014*. 2014.

122. Gutierrez, J.G., S. Cano, S. Schuschnigg, C. Kukla, J. Sapkota, and H. Clemens, Additive Manufacturing of Metallic and Ceramic Components by the Material Extrusion of Highly-Filled Polymers: A Review and Future Perspectives. *Materials*, **2018**. 11.
123. Chen, B., J. Shen, X. Ye, L. Jia, S. Li, J. Umeda, M. Takahashi, and K. Kondoh, Length effect of carbon nanotubes on the strengthening mechanisms in metal matrix composites. *Acta Materialia*, **2017**. 140: p. 317-325.
124. Belgacem, M., B. Thierry, and G.J. Claude, Investigations on thermal debinding process for fine 316L stainless steel feedstocks and identification of kinetic parameters from coupling experiments and finite element simulations. *Powder Technology*, **2013**. 235: p. 192-202.
125. Gutierrez, J.G., G.B. Stringari, and I. Emri, *Powder Injection Molding of Metal and Ceramic Parts*, in *Some Critical Issues for Injection Molding*. 2012, IntechOpen.
126. Kohli, R. and K.L. Mittal, *Developments in Surface Contamination and Cleaning*. 2012, William Andrew Publishing. p. 107-178.
127. Weissleder, R., J. Wittenberg, M.J. Harisinghani, and J.C. Chen, *Imaging Physics*, in *Primer of Diagnostic Imaging*. 2011. p. 690-746.
128. How does a micro-CT scanner work. 2015; Available online: https://www.microphotonics.com/how-does-a-microct-scanner-work/ (acessed on: 2021 15/09).
129. Abel, J., A. Mannschatz, R. Teuber, B. Müller, O. Al Noaimy, S. Riecker, J. Thielsch, B. Matthey, and T. Weißgärber, Fused Filament Fabrication of NiTi Components and Hybridization with Laser Powder Bed Fusion for Filigree Structures. *Materials*, **2021**. 14(16): p. 4399.
130. Liu, B., Y.X. Wang, Z.W. Lin, and T. Zhang, Creating metal parts by Fused Deposition Modeling and Sintering. *Materials Letters*, **2020**. 263.
131. Optimising your design for MIM production. Available online: https://www.pim-international.com/metal-injection-molding/optimising-your-design-for-mim-production/ (acessed on: 01/08/2020).
132. Alnomani, S.A., E.Z. Fadhel, and A.A. Mehatlaf, Prepare Nitinol Alloys and Improve their Hardness Using Copper as an Alloying Element. *International Journal of Applied Engineering Research*, **2017**. 12(14): p. 4299-4308.
133. Akbarpour, M.R., S. Alipour, M. Najafi, T. Ebadzadeh, and H.S. Kim, Microstructural characterization and enhanced hardness of nanostructured Ni3Ti– NiTi (B2) intermetallic alloy produced by mechanical alloying and fast microwave-assisted sintering process. *Intermetallics*, **2021**. 131: p. 107119.
134. Feng, Y., Z. Du, and Z. Hu, Study on the Effect of Ni Addition on the Microstructure and Properties of NiTi Alloy Coating on AISI 316 L Prepared by Laser Cladding. *Materials*, **2021**. 14(16).
135. Ye, D., S.F. Li, R.D.K. Misra, R. Zheng, and Y.F. Yang, Ni-loss compensation and thermomechanical property recovery of 3D printed NiTi alloys by pre-coating Ni on NiTi powder. *Additive Manufacturing*, **2021**. 47: p. 102344.
136. Li, Y.F., S.L. Tang, Y.M. Gao, S.Q. Ma, Q.L. Zheng, and Y.H. Cheng, Mechanical and thermodynamic properties of intermetallic compounds in the Ni–Ti system. *International Journal of Modern Physics B*, **2017**. 31(22).
137. Yoshida, M., H. Shiraishi, and N. Ikk, Microstructure and Mechanical Properties of NiTi2-TiB Composite Fabricated by Spark Plasma Sintering. *World Journal of Engineering and Technology*, **2015**. 3: p. 84-88.
138. Wang, H.M. and Y.F. Liu, Microstructure and wear resistance of laser clad Ti5Si3/NiTi2 intermetallic composite coating on titanium alloy. *Materials Science and Engineering*, **2002**. A338: p. 126-132.
139. Mokgalaka, M.N., A.P.I. Popoola, and S.L. Pityana, In situ laser deposition of NiTi intermetallics for corrosion improvement of Ti−6Al−4V alloy. *ScienceDirect*, **2015**.

140. Chen, G., K.-D. Liss, G. Auchterlonie, H. Tang, and P. Cao, Dehydrogenation and Sintering of TiH2: An In Situ Study. *Metallurgical and Materials Transactions A*, **2017**. 48.
141. Li, B.Y., L.J. Rong, and Y.Y. Li, The influence of addition of TiH 2 in elemental powder sintering porous Ni–Ti alloys. *Materials Science and Engineering A-structural Materials Properties Microstructure and Processing*, **2000**. 281: p. 169-175.
142. Li, B.Y., L.J. Rong, and Y.Y. Li, Anisotropy of dimensional change and its corresponding improvement by addition of TiH2 during elemental powder sintering of porous NiTi alloy. *Materials Science and Engineering: A*, **1998**. 255: p. 70-74.
143. Chen, G., P. Cao, and N. Edmonds, Porous NiTi alloys produced by press-and-sinter from Ni/Ti and Ni/TiH2 mixtures. *Materials Science and Engineering: A.*, **2013**. 582: p. 117-125.
144. Bohua, D., Z. Yasong, W. Dezhi, Z. Yingrui, and X. Chunge, Fabrication and Properties of Porous NiTi Alloy by Gel-Casting with TiH2 Powders. *Journal of Materials Engineering and Performance*, **2017**. 26(10): p. 5118–5125.
145. Bhosle, V., E.G. Baburaj, M. Miranova, and K. Salama, Dehydrogenation of TiH2. *Materials Science and Engineering: A*, **2003**. 356(1-2): p. 190-199.
146. Chen, G., K.D. Liss, and P. Cao, An in situ Study of NiTi Powder Sintering Using Neutron Diffraction *Metals - Open Access Journal*, **2015**. 5: p. 530-546.
147. Peng, Q., B. Yang, and B. Friedrich, Porous Titanium Parts Fabricated by Sintering of TiH2 and Ti Powder Mixtures. *Journal of Materials Engineering and Performance*, **2017**. 27.
148. Sun, P., H. Wang, M. Lefler, Z. Fang, T. Lei, S. Fang, W. Tian, and H. Li. Sintering of TiH2 - A new approach for powder metallurgy titanium. in *World Powder Metallurgy Congress and Exhibition*. 2010.
149. Zhu, S.L., X.J. Yang, F. Hu, S.H. Deng, and Z.D. Cui, Processing of porous TiNi shape memory alloy from elemental powders by Ar-sintering. *Materials Letters,*, **2004**. 58(19): p. 2369-2373.
150. Xu, W., P.E.J. Rivera-Díaz-del-Castillo, W. Wang, K. Yang, V. Bliznuk, L.A.I. Kestens, and S. van der Zwaag, Genetic design and characterization of novel ultra-high-strength stainless steels strengthened by Ni3Ti intermetallic nanoprecipitates. *Acta Materialia*, **2010**. 58(10): p. 3582-3593.
151. Verdian, M.M., K. Raeissi, M. Salehi, and S. Sabooni, Characterization and corrosion behavior of NiTi–Ti2Ni–Ni3Ti multiphase intermetallics produced by vacuum sintering. *Vacuum*, **2011**. 86(1): p. 91-95.
152. *Part and mold design*. Bayer Material Science LLC. 2000: Bayer Corporation.
153. Centimfe, *Manual do projetista para moldes de injeção de plásticos*. 2003.
154. Gilbert, H.B. and R.J. Webster, 3rd, Rapid, Reliable Shape Setting of Superelastic Nitinol for Prototyping Robots. *IEEE robotics and automation letters*, **2016**. 1(1): p. 98-105.
155. Components, J.M. Nitinol shape setting. Available online: https://matthey.com/en/products-and-services/medical-components/resource-library/nitinol-shape-setting (acessed on: 2021 11 November).
156. Confluent. NITINOL FACTS. Available online: https://confluentmedical.com/tech-center/nitinol-facts/ (acessed on: 2021 11 November).

ANNEX I

Characteristics of Powder LPW

LED&MAT

Created by: Win7
Last edited: 23-10-2018 14:26:52

Malvern

Measurement Details

IPN/LED&MAT/2018/	A1681	**Operator Name**	Vitor Redondo
Sample Name	NiTi Comercial	**Analysis Model**	General Purpose
Client	DEM	**Dispersant Name**	Water
Scattering Model	Fraunhofer	**Dispersant Refractive Index**	1,330
		Result Source	Averaged

Measurement Details

Instrument Type	Mastersizer3000	**Laser Obscuration**	3,81 %
Instrument Firmware Version	5.02		
Accessory Name	Hydro MV	**D [3;2]**	20,5 µm
Dv (10)	13,4 µm	**D [4;3]**	23,2 µm
Dv (50)	22,1 µm	**Specific Surface Area**	293,4 m²/kg
Dv (90)	34,7 µm		

Frequency (compatible)

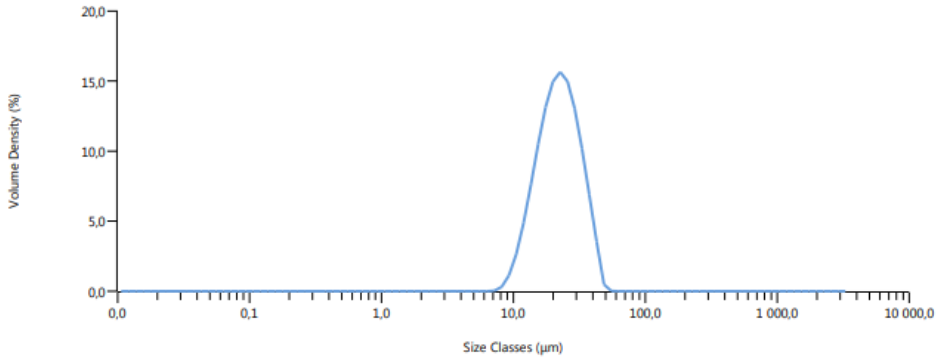

Size (µm)	% Volume In	Size (µm)	% Volume In	Size (µm)	% Volume In	Size (µm)	% Volume In	Size (µm)	% Volume In	Size (µm)	% Volume In	Size (µm)	% Volume In
0,0100	0,00	0,0679	0,00	0,460	0,00	3,12	0,00	21,2	13,13	144	0,00	976	0,00
0,0114	0,00	0,0771	0,00	0,523	0,00	3,55	0,00	24,1	12,58	163	0,00	1110	0,00
0,0129	0,00	0,0876	0,00	0,594	0,00	4,03	0,00	27,4	10,94	186	0,00	1260	0,00
0,0147	0,00	0,0995	0,00	0,675	0,00	4,58	0,00	31,1	8,51	211	0,00	1430	0,00
0,0167	0,00	0,113	0,00	0,767	0,00	5,21	0,00	35,3	5,74	240	0,00	1630	0,00
0,0189	0,00	0,128	0,00	0,872	0,00	5,92	0,00	40,1	2,95	272	0,00	1850	0,00
0,0215	0,00	0,146	0,00	0,991	0,00	6,72	0,00	45,6	0,19	310	0,00	2100	0,00
0,0244	0,00	0,166	0,00	1,13	0,00	7,64	0,22	51,8	0,00	352	0,00	2390	0,00
0,0278	0,00	0,188	0,00	1,28	0,00	8,68	0,89	58,9	0,00	400	0,00	2710	0,00
0,0315	0,00	0,214	0,00	1,45	0,00	9,86	2,16	66,9	0,00	454	0,00	3080	0,00
0,0358	0,00	0,243	0,00	1,65	0,00	11,2	4,02	76,0	0,00	516	0,00	3500	
0,0407	0,00	0,276	0,00	1,88	0,00	12,7	6,33	86,4	0,00	586	0,00		
0,0463	0,00	0,314	0,00	2,13	0,00	14,5	8,79	98,1	0,00	666	0,00		
0,0526	0,00	0,357	0,00	2,42	0,00	16,4	11,00	111	0,00	756	0,00		
0,0597	0,00	0,405	0,00	2,75	0,00	18,7	12,55	127	0,00	859	0,00		

Software Version: 3.10
Instrument Serial Number: MAL1062507 Measurement File: C:\Clientes\2018\Universidade de Coimbra\DEM\Outubro\NiTi Comercial.mmes
Malvern Instruments Ltd - www.malvern.com
Page 1 of 2

Malvern

Figure 73. Differential distribution of powder LPW.

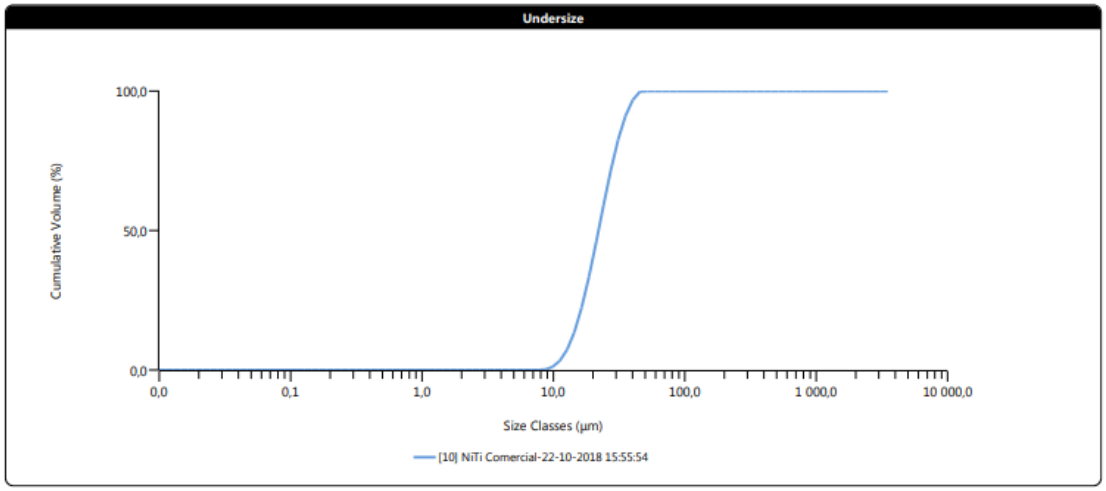

Size (µm)	% Volume Under	Size (µm)	% Volume Under	Size (µm)	% Volume Under	Size (µm)	% Volume Under	Size (µm)	% Volume Under	Size (µm)	% Volume Under
0,0100	0,00	0,0876	0,00	0,767	0,00	6,72	0,00	58,9	100,00	516	100,00
0,0114	0,00	0,0995	0,00	0,872	0,00	7,64	0,00	66,9	100,00	586	100,00
0,0129	0,00	0,113	0,00	0,991	0,00	8,68	0,22	76,0	100,00	666	100,00
0,0147	0,00	0,128	0,00	1,13	0,00	9,86	1,11	86,4	100,00	756	100,00
0,0167	0,00	0,146	0,00	1,28	0,00	11,2	3,27	98,1	100,00	859	100,00
0,0189	0,00	0,166	0,00	1,45	0,00	12,7	7,29	111	100,00	976	100,00
0,0215	0,00	0,188	0,00	1,65	0,00	14,5	13,62	127	100,00	1110	100,00
0,0244	0,00	0,214	0,00	1,88	0,00	16,4	22,41	144	100,00	1260	100,00
0,0278	0,00	0,243	0,00	2,13	0,00	18,7	33,41	163	100,00	1430	100,00
0,0315	0,00	0,276	0,00	2,42	0,00	21,2	45,96	186	100,00	1630	100,00
0,0358	0,00	0,314	0,00	2,75	0,00	24,1	59,09	211	100,00	1850	100,00
0,0407	0,00	0,357	0,00	3,12	0,00	27,4	71,67	240	100,00	2100	100,00
0,0463	0,00	0,405	0,00	3,55	0,00	31,1	82,61	272	100,00	2390	100,00
0,0526	0,00	0,460	0,00	4,03	0,00	35,3	91,12	310	100,00	2710	100,00
0,0597	0,00	0,523	0,00	4,58	0,00	40,1	96,86	352	100,00	3080	100,00
0,0679	0,00	0,594	0,00	5,21	0,00	45,6	99,81	400	100,00	3500	100,00
0,0771	0,00	0,675	0,00	5,92	0,00	51,8	100,00	454	100,00		

Figure 74. Cumulative distribution of powder LPW.

PANalytical

Quantification of sample SE154_A992 MTV

R.M.S.:	0.050
Result status:	
Sum before normalization:	88.3 %
Normalised to:	100.0 %
Sample type:	Solid
Correction applied for medium:	Yes
Correction applied for film:	Yes
Results database:	omnian 37 he
Results database in:	c:\panalytical\superq\userdata

	Compound Name	Conc. (%)
1	Ni	57.141
2	Ti	41.602
3	Al	0.746
4	Mg	0.261
5	Si	0.102
6	Cr	0.065
7	Co	0.044
8	Fe	0.035
9	Zr	0.004

Figure 75. Chemical analysis of powder LPW.

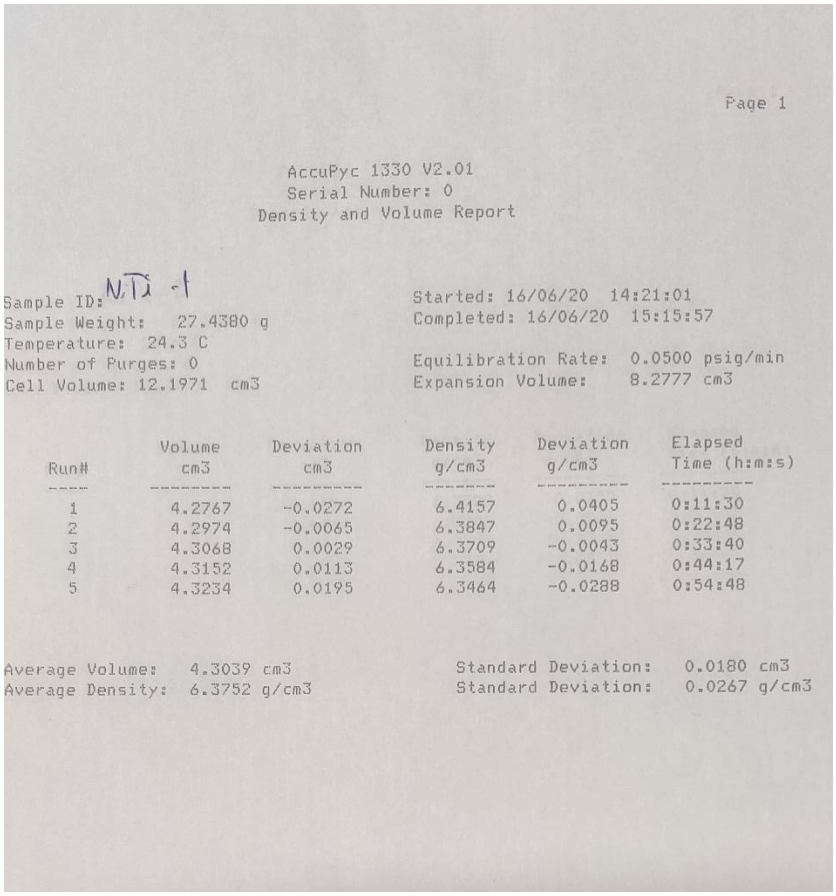

Page 1

AccuPyc 1330 V2.01
Serial Number: 0
Density and Volume Report

Sample ID: NTi -1
Sample Weight: 27.4380 g
Temperature: 24.3 C
Number of Purges: 0
Cell Volume: 12.1971 cm3

Started: 16/06/20 14:21:01
Completed: 16/06/20 15:15:57

Equilibration Rate: 0.0500 psig/min
Expansion Volume: 8.2777 cm3

Run#	Volume cm3	Deviation cm3	Density g/cm3	Deviation g/cm3	Elapsed Time (h:m:s)
1	4.2767	-0.0272	6.4157	0.0405	0:11:30
2	4.2974	-0.0065	6.3847	0.0095	0:22:48
3	4.3068	0.0029	6.3709	-0.0043	0:33:40
4	4.3152	0.0113	6.3584	-0.0168	0:44:17
5	4.3234	0.0195	6.3464	-0.0288	0:54:48

Average Volume: 4.3039 cm3 Standard Deviation: 0.0180 cm3
Average Density: 6.3752 g/cm3 Standard Deviation: 0.0267 g/cm3

Figure 76. Density analysis of powder LPW.

ANNEX II

Characteristics of Powder AE

LED&MAT

Created by: Win7
Last edited: 06-04-2021 11:37:58

Malvern

Measurement Details

IPN/LED&MAT/2021/	A857	**Operator Name**	Vitor Redondo
Sample Name	NiTi	**Analysis Model**	General Purpose
Client	DEM	**Dispersant Name**	Water
Scattering Model	Fraunhofer	**Dispersant Refractive Index**	1,330
		Result Source	Averaged

Measurement Details

Instrument Type	Mastersizer3000	**Laser Obscuration**	8,59 %
Instrument Firmware Version	5.02		
Accessory Name	Hydro MV	**D [3;2]**	1,65 µm
Dv (10)	0,752 µm	**D [4;3]**	3,58 µm
Dv (50)	2,70 µm	**Specific Surface Area**	3633 m²/kg
Dv (90)	7,61 µm		

Frequency (compatible)

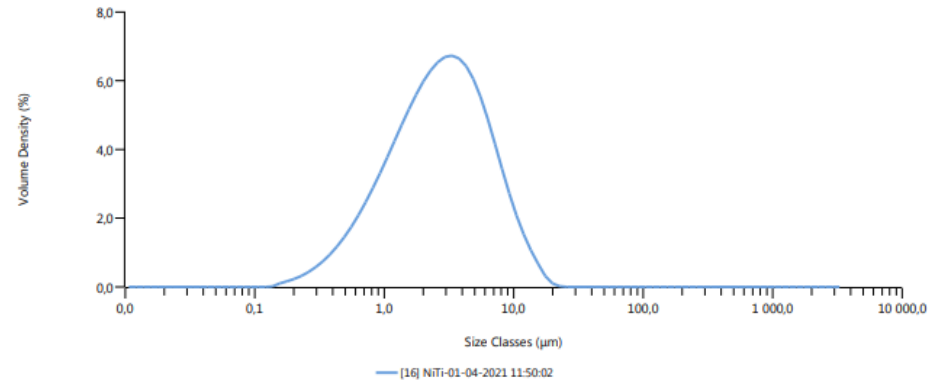

Size (µm)	% Volume In	Size (µm)	% Volume In	Size (µm)	% Volume In	Size (µm)	% Volume In	Size (µm)	% Volume In	Size (µm)	% Volume In	Size (µm)	% Volume In
0,0100	0,00	0,0679	0,00	0,460	1,20	3,12	5,62	21,2	0,01	144	0,00	976	0,00
0,0114	0,00	0,0771	0,00	0,523	1,46	3,55	5,55	24,1	0,00	163	0,00	1110	0,00
0,0129	0,00	0,0876	0,00	0,594	1,74	4,03	5,37	27,4	0,00	186	0,00	1260	0,00
0,0147	0,00	0,0995	0,00	0,675	2,06	4,58	5,05	31,1	0,00	211	0,00	1430	0,00
0,0167	0,00	0,113	0,00	0,767	2,40	5,21	4,62	35,3	0,00	240	0,00	1630	0,00
0,0189	0,00	0,128	0,00	0,872	2,76	5,92	4,08	40,1	0,00	272	0,00	1850	0,00
0,0215	0,00	0,146	0,09	0,991	3,14	6,72	3,48	45,6	0,00	310	0,00	2100	0,00
0,0244	0,00	0,166	0,13	1,13	3,54	7,64	2,86	51,8	0,00	352	0,00	2390	0,00
0,0278	0,00	0,188	0,19	1,28	3,93	8,68	2,26	58,9	0,00	400	0,00	2710	0,00
0,0315	0,00	0,214	0,26	1,45	4,31	9,86	1,73	66,9	0,00	454	0,00	3080	0,00
0,0358	0,00	0,243	0,36	1,65	4,67	11,2	1,27	76,0	0,00	516	0,00	3500	
0,0407	0,00	0,276	0,47	1,88	4,98	12,7	0,88	86,4	0,00	586	0,00		
0,0463	0,00	0,314	0,61	2,13	5,25	14,5	0,56	98,1	0,00	666	0,00		
0,0526	0,00	0,357	0,78	2,42	5,46	16,4	0,25	111	0,00	756	0,00		
0,0597	0,00	0,405	0,98	2,75	5,58	18,7	0,07	127	0,00	859	0,00		

Malvern

Figure 77. Differential distribution of powder AE.

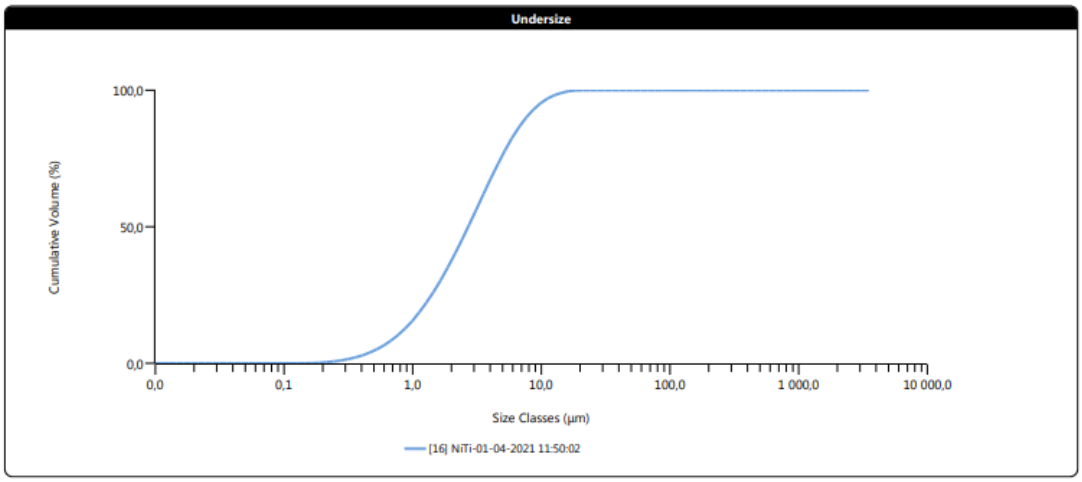

Size (µm)	% Volume Under	Size (µm)	% Volume Under	Size (µm)	% Volume Under	Size (µm)	% Volume Under	Size (µm)	% Volume Under	Size (µm)	% Volume Under
0,0100	0,00	0,0876	0,00	0,767	10,33	6,72	86,63	58,9	100,00	516	100,00
0,0114	0,00	0,0995	0,00	0,872	12,72	7,64	90,11	66,9	100,00	586	100,00
0,0129	0,00	0,113	0,00	0,991	15,48	8,68	92,97	76,0	100,00	666	100,00
0,0147	0,00	0,128	0,00	1,13	18,63	9,86	95,23	86,4	100,00	756	100,00
0,0167	0,00	0,146	0,00	1,28	22,16	11,2	96,95	98,1	100,00	859	100,00
0,0189	0,00	0,166	0,09	1,45	26,09	12,7	98,22	111	100,00	976	100,00
0,0215	0,00	0,188	0,22	1,65	30,40	14,5	99,10	127	100,00	1110	100,00
0,0244	0,00	0,214	0,41	1,88	35,07	16,4	99,66	144	100,00	1260	100,00
0,0278	0,00	0,243	0,67	2,13	40,05	18,7	99,91	163	100,00	1430	100,00
0,0315	0,00	0,276	1,03	2,42	45,30	21,2	99,99	186	100,00	1630	100,00
0,0358	0,00	0,314	1,50	2,75	50,76	24,1	100,00	211	100,00	1850	100,00
0,0407	0,00	0,357	2,12	3,12	56,34	27,4	100,00	240	100,00	2100	100,00
0,0463	0,00	0,405	2,90	3,55	61,96	31,1	100,00	272	100,00	2390	100,00
0,0526	0,00	0,460	3,87	4,03	67,52	35,3	100,00	310	100,00	2710	100,00
0,0597	0,00	0,523	5,07	4,58	72,88	40,1	100,00	352	100,00	3080	100,00
0,0679	0,00	0,594	6,53	5,21	77,94	45,6	100,00	400	100,00	3500	100,00
0,0771	0,00	0,675	8,27	5,92	82,55	51,8	100,00	454	100,00		

Figure 78. Cumulative distribution of powder AE.

PANalytical

Quantification of sample Teste NiTi pó MTV

R.M.S.:	0.042
Result status:	
Sum before normalization:	84.9 %
Normalised to:	100.0 %
Sample type:	Loose powder
Correction applied for medium:	Yes
Correction applied for film:	Yes
Results database:	omnian 37 he
Results database in:	c:\panalytical\superq\userdata

	Compound Name	Conc. (%)
1	Ni	55.957
2	Ti	43.065
3	Al	0.724
4	Si	0.104
5	Cr	0.066
6	Co	0.047
7	Fe	0.033
8	Zr	0.004

Figure 79. Chemical analysis of powder AE.

Page 1

AccuPyc 1330 V2.01
Serial Number: 0
Density and Volume Report

Sample ID: NiTi
Sample Weight: 9.5500 g
Temperature: 24.4 C
Number of Purges: 0
Cell Volume: 12.1971 cm3

Started: 31/03/21 22:06:18
Completed: 31/03/21 23:04:09

Equilibration Rate: 0.0500 psig/min
Expansion Volume: 8.2777 cm3

Run#	Volume cm3	Deviation cm3	Density g/cm3	Deviation g/cm3	Elapsed Time (h:m:s)
1	1.5386	-0.0034	6.2071	0.0133	0:11:40
2	1.5499	0.0080	6.1617	-0.0321	0:23:29
3	1.5545	0.0125	6.1436	-0.0502	0:35:09
4	1.5415	-0.0004	6.1951	0.0013	0:46:29
5	1.5252	-0.0168	6.2616	0.0678	0:57:42

Average Volume: 1.5419 cm3
Average Density: 6.1938 g/cm3

Standard Deviation: 0.0113 cm3
Standard Deviation: 0.0456 g/cm3

Figure 80. Density analysis of powder AE.

ANNEX III

Characteristics of Additives and Thermal Cycle Atmosphere

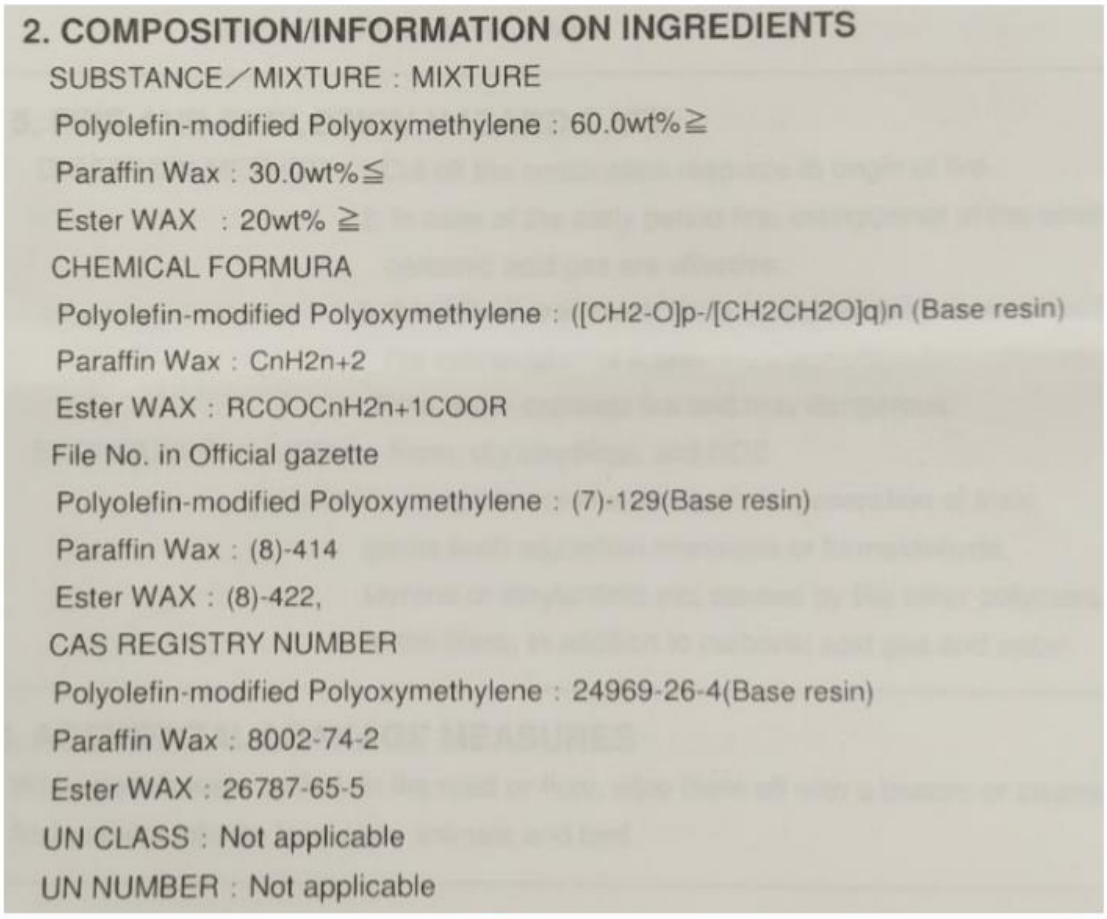

2. COMPOSITION/INFORMATION ON INGREDIENTS

SUBSTANCE／MIXTURE : MIXTURE

Polyolefin-modified Polyoxymethylene : 60.0wt%≧

Paraffin Wax : 30.0wt%≦

Ester WAX : 20wt% ≧

CHEMICAL FORMURA

Polyolefin-modified Polyoxymethylene : ([CH2-O]p-/[CH2CH2O]q)n (Base resin)

Paraffin Wax : CnH2n+2

Ester WAX : RCOOCnH2n+1COOR

File No. in Official gazette

Polyolefin-modified Polyoxymethylene : (7)-129(Base resin)

Paraffin Wax : (8)-414

Ester WAX : (8)-422,

CAS REGISTRY NUMBER

Polyolefin-modified Polyoxymethylene : 24969-26-4(Base resin)

Paraffin Wax : 8002-74-2

Ester WAX : 26787-65-5

UN CLASS : Not applicable

UN NUMBER : Not applicable

Figure 81. Composition of master binder M1.

LED&MAT

Created by: Win7
Last edited: 29-10-2021 17:16:37

Malvern

Measurement Details

IPN/LED&MAT/2021/	A2888	**Operator Name**	Vítor Redondo
Sample Name	Ni	**Analysis Model**	General Purpose
Client	DEM	**Dispersant Name**	Water
Scattering Model	Fraunhofer	**Dispersant Refractive Index**	1,330
		Result Source	Averaged

Measurement Details

Instrument Type	Mastersizer3000	**Laser Obscuration**	2,27 %
Instrument Firmware Version	5.02		
Accessory Name	Hydro MV	**D [3;2]**	28,9 µm
Dv (10)	21,4 µm	**D [4;3]**	30,7 µm
Dv (50)	30,0 µm	**Specific Surface Area**	207,7 m^2/kg
Dv (90)	41,2 µm		

Frequency (compatible)

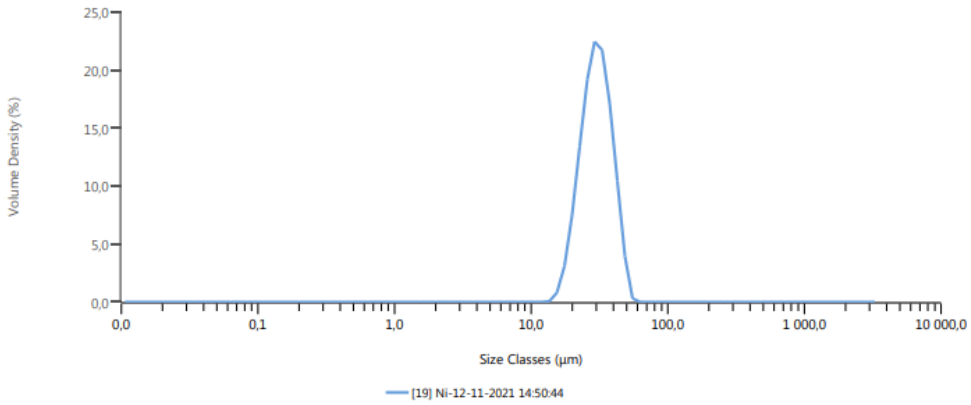

Size (µm)	% Volume In	Size (µm)	% Volume In	Size (µm)	% Volume In	Size (µm)	% Volume In	Size (µm)	% Volume In	Size (µm)	% Volume In	Size (µm)	% Volume In
0,0100	0,00	0,0679	0,00	0,460	0,00	3,12	0,00	21,2	11,18	144	0,00	976	0,00
0,0114	0,00	0,0771	0,00	0,523	0,00	3,55	0,00	24,1	16,14	163	0,00	1110	0,00
0,0129	0,00	0,0876	0,00	0,594	0,00	4,03	0,00	27,4	19,01	186	0,00	1260	0,00
0,0147	0,00	0,0995	0,00	0,675	0,00	4,58	0,00	31,1	18,40	211	0,00	1430	0,00
0,0167	0,00	0,113	0,00	0,767	0,00	5,21	0,00	35,3	14,40	240	0,00	1630	0,00
0,0189	0,00	0,128	0,00	0,872	0,00	5,92	0,00	40,1	8,68	272	0,00	1850	0,00
0,0215	0,00	0,146	0,00	0,991	0,00	6,72	0,00	45,6	3,07	310	0,00	2100	0,00
0,0244	0,00	0,166	0,00	1,13	0,00	7,64	0,00	51,8	0,01	352	0,00	2390	0,00
0,0278	0,00	0,188	0,00	1,28	0,00	8,68	0,00	58,9	0,00	400	0,00	2710	0,00
0,0315	0,00	0,214	0,00	1,45	0,00	9,86	0,00	66,9	0,00	454	0,00	3080	0,00
0,0358	0,00	0,243	0,00	1,65	0,00	11,2	0,00	76,0	0,00	516	0,00	3500	
0,0407	0,00	0,276	0,00	1,88	0,00	12,7	0,00	86,4	0,00	586	0,00		
0,0463	0,00	0,314	0,00	2,13	0,00	14,5	0,55	98,1	0,00	666	0,00		
0,0526	0,00	0,357	0,00	2,42	0,00	16,4	2,44	111	0,00	756	0,00		
0,0597	0,00	0,405	0,00	2,75	0,00	18,7	6,12	127	0,00	859	0,00		

Malvern

Figure 82. Differential distribution of Ni powder.

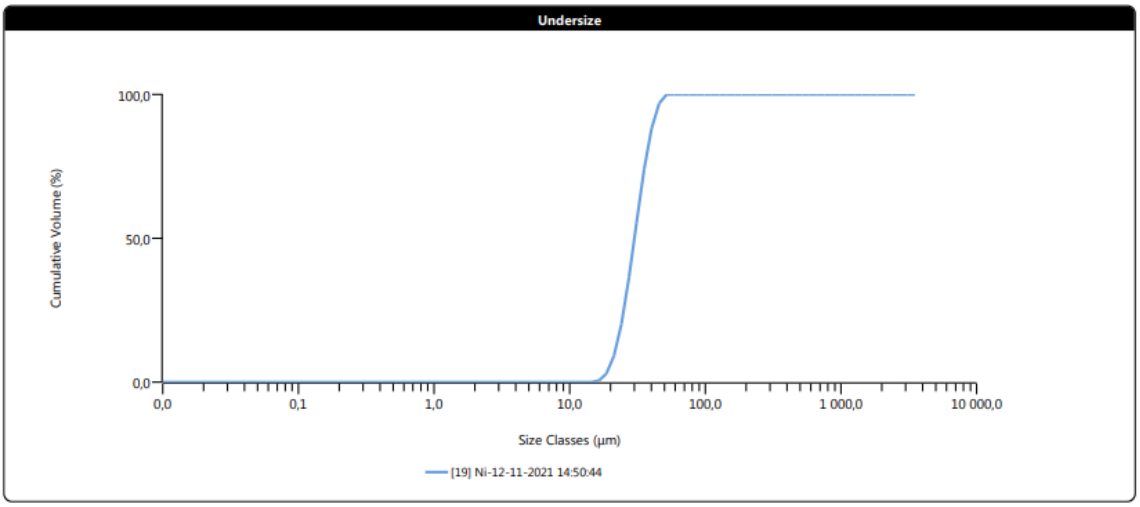

Size (µm)	% Volume Under	Size (µm)	% Volume Under	Size (µm)	% Volume Under	Size (µm)	% Volume Under	Size (µm)	% Volume Under	Size (µm)	% Volume Under
0,0100	0,00	0,0876	0,00	0,767	0,00	6,72	0,00	58,9	100,00	516	100,00
0,0114	0,00	0,0995	0,00	0,872	0,00	7,64	0,00	66,9	100,00	586	100,00
0,0129	0,00	0,113	0,00	0,991	0,00	8,68	0,00	76,0	100,00	666	100,00
0,0147	0,00	0,128	0,00	1,13	0,00	9,86	0,00	86,4	100,00	756	100,00
0,0167	0,00	0,146	0,00	1,28	0,00	11,2	0,00	98,1	100,00	859	100,00
0,0189	0,00	0,166	0,00	1,45	0,00	12,7	0,00	111	100,00	976	100,00
0,0215	0,00	0,188	0,00	1,65	0,00	14,5	0,00	127	100,00	1110	100,00
0,0244	0,00	0,214	0,00	1,88	0,00	16,4	0,56	144	100,00	1260	100,00
0,0278	0,00	0,243	0,00	2,13	0,00	18,7	2,99	163	100,00	1430	100,00
0,0315	0,00	0,276	0,00	2,42	0,00	21,2	9,11	186	100,00	1630	100,00
0,0358	0,00	0,314	0,00	2,75	0,00	24,1	20,29	211	100,00	1850	100,00
0,0407	0,00	0,357	0,00	3,12	0,00	27,4	36,43	240	100,00	2100	100,00
0,0463	0,00	0,405	0,00	3,55	0,00	31,1	55,44	272	100,00	2390	100,00
0,0526	0,00	0,460	0,00	4,03	0,00	35,3	73,84	310	100,00	2710	100,00
0,0597	0,00	0,523	0,00	4,58	0,00	40,1	88,24	352	100,00	3080	100,00
0,0679	0,00	0,594	0,00	5,21	0,00	45,6	96,92	400	100,00	3500	100,00
0,0771	0,00	0,675	0,00	5,92	0,00	51,8	99,99	454	100,00		

Software Version: 3.10
Instrument Serial Number: MAL1062507 Measurement File: C:\Clientes\2021\Universidade de Coimbra\FCTUC\DEM\Teresa Vieira\Novembro\Ni.mmes
Malvern Instruments Ltd - www.malvern.com
Page 2 of 2

Malvern

Figure 83. Cumulative distribution of Ni powder.

LED&MAT

Created by: Win7
Last edited: 29-10-2021 17:16:37

Malvern

Measurement Details

IPN/LED&MAT/2021/	A2889	**Operator Name**	Vítor Redondo
Sample Name	TiH2	**Analysis Model**	General Purpose
Client	DEM	**Dispersant Name**	Water
Scattering Model	Fraunhofer	**Dispersant Refractive Index**	1,330
		Result Source	Averaged

Measurement Details

Instrument Type	Mastersizer3000	**Laser Obscuration**	15,28 %
Instrument Firmware Version	5.02		
Accessory Name	Hydro MV	**D [3;2]**	8,00 µm
Dv (10)	3,44 µm	**D [4;3]**	17,7 µm
Dv (50)	15,3 µm	**Specific Surface Area**	750,2 m^2/kg
Dv (90)	35,7 µm		

Frequency (compatible)

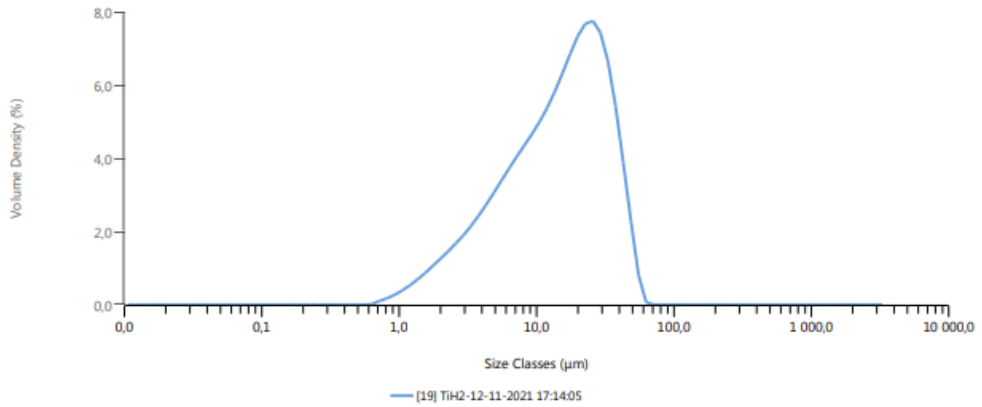

Size (µm)	% Volume In	Size (µm)	% Volume In	Size (µm)	% Volume In	Size (µm)	% Volume In	Size (µm)	% Volume In	Size (µm)	% Volume In	Size (µm)	% Volume In
0,0100	0,00	0,0679	0,00	0,460	0,00	3,12	1,79	21,2	6,44	144	0,00	976	0,00
0,0114	0,00	0,0771	0,00	0,523	0,00	3,55	2,02	24,1	6,51	163	0,00	1110	0,00
0,0129	0,00	0,0876	0,00	0,594	0,00	4,03	2,28	27,4	6,25	186	0,00	1260	0,00
0,0147	0,00	0,0995	0,00	0,675	0,09	4,58	2,55	31,1	5,59	211	0,00	1430	0,00
0,0167	0,00	0,113	0,00	0,767	0,15	5,21	2,83	35,3	4,55	240	0,00	1630	0,00
0,0189	0,00	0,128	0,00	0,872	0,22	5,92	3,11	40,1	3,25	272	0,00	1850	0,00
0,0215	0,00	0,146	0,00	0,991	0,32	6,72	3,38	45,6	1,92	310	0,00	2100	0,00
0,0244	0,00	0,166	0,00	1,13	0,44	7,64	3,64	51,8	0,62	352	0,00	2390	0,00
0,0278	0,00	0,188	0,00	1,28	0,58	8,68	3,90	58,9	0,00	400	0,00	2710	0,00
0,0315	0,00	0,214	0,00	1,45	0,73	9,86	4,18	66,9	0,00	454	0,00	3080	0,00
0,0358	0,00	0,243	0,00	1,65	0,89	11,2	4,49	76,0	0,00	516	0,00	3500	
0,0407	0,00	0,276	0,00	1,88	1,05	12,7	4,86	86,4	0,00	586	0,00		
0,0463	0,00	0,314	0,00	2,13	1,22	14,5	5,28	98,1	0,00	666	0,00		
0,0526	0,00	0,357	0,00	2,42	1,40	16,4	5,73	111	0,00	756	0,00		
0,0597	0,00	0,405	0,00	2,75	1,58	18,7	6,14	127	0,00	859	0,00		

Software Version: 3.10
Instrument Serial Number: MAL1062507 Measurement File: C:\Clientes\2021\Universidade de Coimbra\FCTUC\DEM\Teresa Vieira\Novembro\TiH2.mmes
Malvern Instruments Ltd - www.malvern.com
Page 1 of 2

Malvern

Figure 84. Differential distribution of TiH_2 powder.

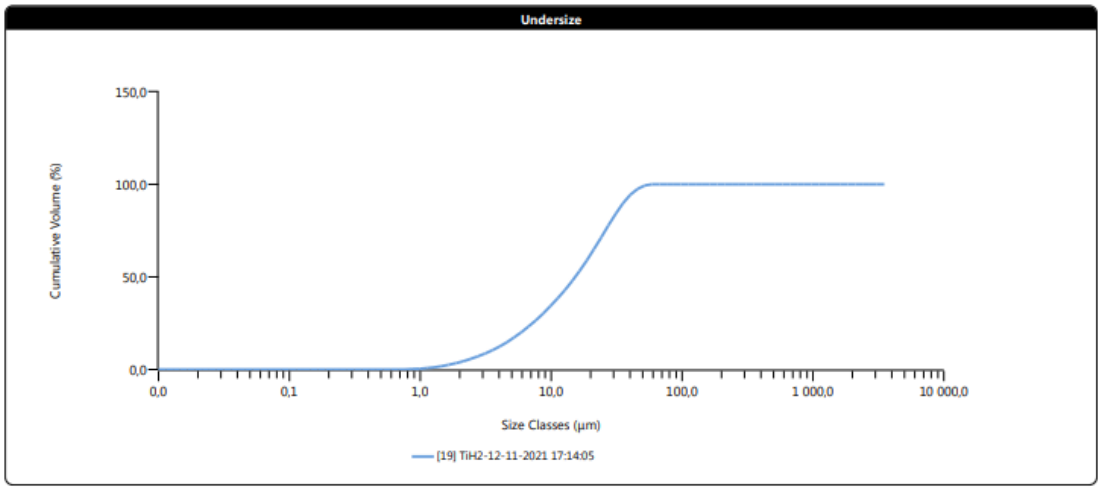

Size (µm)	% Volume Under	Size (µm)	% Volume Under	Size (µm)	% Volume Under	Size (µm)	% Volume Under	Size (µm)	% Volume Under	Size (µm)	% Volume Under
0,0100	0,00	0,0876	0,00	0,767	0,09	6,72	23,25	58,9	100,00	516	100,00
0,0114	0,00	0,0995	0,00	0,872	0,23	7,64	26,63	66,9	100,00	586	100,00
0,0129	0,00	0,113	0,00	0,991	0,46	8,68	30,26	76,0	100,00	666	100,00
0,0147	0,00	0,128	0,00	1,13	0,78	9,86	34,16	86,4	100,00	756	100,00
0,0167	0,00	0,146	0,00	1,28	1,22	11,2	38,34	98,1	100,00	859	100,00
0,0189	0,00	0,166	0,00	1,45	1,80	12,7	42,83	111	100,00	976	100,00
0,0215	0,00	0,188	0,00	1,65	2,53	14,5	47,70	127	100,00	1110	100,00
0,0244	0,00	0,214	0,00	1,88	3,41	16,4	52,98	144	100,00	1260	100,00
0,0278	0,00	0,243	0,00	2,13	4,46	18,7	58,71	163	100,00	1430	100,00
0,0315	0,00	0,276	0,00	2,42	5,68	21,2	64,85	186	100,00	1630	100,00
0,0358	0,00	0,314	0,00	2,75	7,07	24,1	71,29	211	100,00	1850	100,00
0,0407	0,00	0,357	0,00	3,12	8,66	27,4	77,80	240	100,00	2100	100,00
0,0463	0,00	0,405	0,00	3,55	10,45	31,1	84,05	272	100,00	2390	100,00
0,0526	0,00	0,460	0,00	4,03	12,48	35,3	89,65	310	100,00	2710	100,00
0,0597	0,00	0,523	0,00	4,58	14,76	40,1	94,20	352	100,00	3080	100,00
0,0679	0,00	0,594	0,00	5,21	17,31	45,6	97,45	400	100,00	3500	100,00
0,0771	0,00	0,675	0,00	5,92	20,14	51,8	99,38	454	100,00		

Figure 85. Cumulative distribution of TiH_2 powder.

Table 28. Debinding and sintering atmosphere.

Element	Purity	Composition
Hydrogen Extra pure 3X	>99.999 % H_2	< 5 ppm H_2O
		< 2 ppm O_2
		< 0.2 ppm THC (has methane)
		< 5 ppm N_2